# OFFICE OF CIVILIAN RADIOACTIVE WASTE MANAGEMENT
## ANALYSIS/MODEL COVER SHEET
*Complete Only Applicable Items*

1. QA: QA

Page: 1 of 147

2. ☐ Analysis — Check all that apply

| | |
|---|---|
| Type of Analysis | ☐ Engineering<br>☐ Performance Assessment<br>☐ Scientific |
| Intended Use of Analysis | ☐ Input to Calculation<br>☐ Input to another Analysis or Model<br>☐ Input to Technical Document |
| Describe use: | |

3. ☒ Model — Check all that apply

| | |
|---|---|
| Type of Model | ☐ Conceptual Model ☐ Abstraction Model<br>☐ Mathematical Model ☐ System Model<br>☒ Process Model |
| Intended Use of Model | ☐ Input to Calculation<br>☒ Input to another Model or Analysis<br>☐ Input to Technical Document |
| Describe use: | This model currently provides bounding arguments which are intended for use as input to other AMRs. |

4. Title:
Aging and Phase Stability of Waste Package Outer Barrier

5. Document Identifier (including Rev. No. and Change No., if applicable):
ANL-EBS-MD-000002 REV 00

6. Total Attachments:
N/A

7. Attachment Numbers - No. of Pages in Each:
N/A

| | Printed Name | Signature | Date |
|---|---|---|---|
| 8. Originator | Tammy S. Edgecumbe Summers | Tammy Summers | 3/20/00 |
| 9. Checker | R. Daniel McCright | R Daniel McCright | 3/20/2000 |
| 10. Lead/Supervisor | Allan C. Lingenfelter | A C Lingenfelter | 3/20/00 |
| 11. Responsible Manager | David Stahl | David Stahl | 3/21/00 |

12. Remarks:

INFORMATION COPY

LAS VEGAS DOCUMENT CONTROL



WM-11

Enclosure 1

ADD: Manny Cmar DFD3

# OFFICE OF CIVILIAN RADIOACTIVE WASTE MANAGEMENT
# ANALYSIS/MODEL REVISION RECORD

***Complete Only Applicable Items***



2. Analysis or Model Title:

Aging and Phase Stability of Waste Package Outer Barrier

3. Document Identifier (including Rev. No. and Change No., if applicable):

ANL-EBS-MD-000002 REV 00

| 4. Revision/Change No. | 5. Description of Revision/Change |
|---|---|
| 00 | Initial issue. |

## DISCLAIMER

This contractor document was prepared for the U.S. Department of Energy (DOE), but has not undergone programmatic, policy, or publication review, and is provided for information only. The document provides preliminary information that may change based on new information or analysis, and represents a conservative treatment of parameters and assumptions to be used specifically for Total System Performance Assessment analyses. The document is a preliminary lower level contractor document and is not intended for publication or wide distribution.

Although this document has undergone technical reviews at the contractor organization, it has not undergone a DOE policy review. Therefore, the views and opinions of authors expressed may not state or reflect those of the DOE. However, in the interest of the rapid transfer of information, we are providing this document for your information per your request.

# CONTENTS

Page

## FIGURES

Page

INTENTIONALLY LEFT BLANK

## TABLES

Page

INTENTIONALLY LEFT BLANK

# ABBREVIATIONS AND ACRONYMS

| | |
|---|---|
| AMR | Analysis/Model Report |
| CRWMS | Civilian Radioactive Waste Management System |
| EBS | Engineered Barrier System |
| GTAW | gas-tungsten-arc welding |
| HAZ | heat-affected zone |
| LADS | license application design selection |
| LRO | long-range order |
| M&O | management and operating contractor |
| MGR | monitored geologic repository |
| NRC | Nuclear Regulatory Commission |
| QA | quality assurance |
| SAD | selected area diffraction |
| SCC | stress corrosion cracking |
| SEM | scanning electron microscopy |
| TBV | to be verified |
| TEM | transmission electron microscopy |
| TTT | time-temperature-transformation |
| UNS | unified numbering system |
| WP | waste package |
| WPOB | waste package outer barrier |

INTENTIONALLY LEFT BLANK

# 1. PURPOSE

## 1.1 SUMMARY OF MODEL

This Analysis/Model Report (AMR) was prepared in accordance with the Work Direction and Planning Document, *Aging and Phase Stability of Waste Package Outer Barrier* (CRWMS M&O 1999a). It takes into consideration the Enhanced Design Alternative II (EDA II), which has been selected as the preferred design for the Engineered Barrier System (EBS) by the License Application Design Selection (LADS) program team (CRWMS M&O 1999b). The salient features of the EDA II design for this model are a waste package (WP) consisting of an outer barrier of Alloy 22 and an inner barrier of Type 316L stainless steel. This report provides information on the phase stability of Alloy 22[1], the current waste-package-outer-barrier (WPOB) material. These phase stability studies are currently divided into three general areas:

- Intermetallic and carbide precipitation in the base metal
- Intermetallic and carbide precipitation in welded samples
- Long-range order reactions

Intermetallic and carbide precipitates that form in Alloy 22 are generally rich in chromium (Cr) and/or molybdenum (Mo). Because these elements are responsible for the good corrosion resistance of Alloy 22, precipitation of intermetallics and carbides, especially at grain boundaries, can lead to an increased susceptibility to localized corrosion in the alloy. These phases are brittle and also tend to embrittle the alloy. They are known to form in Alloy 22 at temperatures greater than approximately 600°C. Whether they also form at the lower temperatures expected in the potential repository in times up to approximately 10,000 years must be determined. The kinetics of this precipitation will be determined for both the base metal and the weld heat-affected zone (HAZ). In these analyses, it is assumed that the precipitation kinetics of the various intermetallics and carbides that form can be described by a single equation. A procedure is currently being developed for identifying and measuring the relative amounts of each phase that form after a given aging treatment. If the preceding assumption proves invalid, the analyses can be modified to account for the precipitation of more than one phase.

The intermetallic phases P, $\mu$, and $\sigma$ are present in the weld metal in the as-welded condition. It may be possible to eliminate these phases through heat treatment, but that may not be possible for the closure weld because the spent-nuclear-fuel cladding cannot be heated to more than 350°C. These analyses will determine if the precipitation that occurs during the welding process has a significant effect on weld properties. If the weld properties are found to be adequate, it will be determined whether aging of Alloy 22 welds causes the precipitates to change in such a way that the properties are affected. The effects of any stress mitigation techniques such as laser

[1] The designation Alloy 22 is used in this report to indicate the alloy composition given by the Society of Automotive Engineers (SAE) – American Society of Testing and Materials (ASTM) Unified Numbering System (UNS) N06022. A number of manufacturers produce material within this UNS specification. This alloy is sold and often referred to in the technical literature by names such as Hastelloy Alloy C-22, Inconel Alloy 622, Allegheny Alloy AL-22, and possibly others. The designation Alloy 22 is therefore a generalized designation that covers all of these alloys.

peening or solution heat treating that might be used to reduce the propensity for stress corrosion cracking on the properties and aging response of the welds must also be investigated.

Long-range order (LRO) occurs in nickel (Ni)-Cr-Mo alloys such as Alloy 22 at temperatures less than approximately 600°C. This ordering has been linked to an increased susceptibility of Ni-Cr-Mo alloys to stress corrosion cracking (SCC) and hydrogen embrittlement. These analyses will provide information on the rate at which LRO will occur in Alloy 22 under repository conditions.

Determination of the kinetics of transformations through experimental techniques requires that the transformations being investigated be accelerated, at least in this case in which service life is expected to be 10,000 years. Phase transformations are typically accelerated through an increase in temperature. The rate of transformation is determined at the higher temperature and is extrapolated to the lower temperatures of interest. In performing this extrapolation, two assumptions must be made. First, it must be assumed that the phases forming at the higher temperatures are stable and, therefore, also form at the lower temperatures. Second, it must be assumed that the transformation mechanism operating at the higher temperatures also operates at the lower temperatures. These assumptions must be verified as more data become available.

## 1.2 RELATIONSHIP TO PRINCIPAL FACTORS

The "principal factors" of the "Post-Closure Safety Case" have been identified in *Repository Safety Strategy: Plan to Prepare the Postclosure Safety Case to Support Yucca Mountain Site Recommendation and Licensing Consideration* (CRWMS M&O 2000a). The "performance of the waste package barriers" has been identified as a "principal factor" of the repository system concept for Site Recommendation and License Application considerations. The importance of understanding the phase stability of the WPOB is that phase changes in the material can cause degradation of the mechanical and corrosion properties. Both the mechanical properties (e.g. in rock fall) and the corrosion behavior of the WPOB are used as bases for evaluating the performance of the waste package barriers. This Analysis/Model Report (AMR) addresses the phase stability of the WPOB, Alloy 22.

## 1.3 INTENDED USE OF MODEL

A quantitative model for phase stability of the WPOB is not currently available due to a lack of appropriate data. Thus far, a bounding case has been made for formation of intermetallic phases and for conditions under which LRO might occur in Alloy 22 base metal. The effects of phase changes on the mechanical properties of the alloy are to be addressed by this AMR, but that work is still in progress. Some mechanical property data for Alloy 22 base metal will be available for the next revision of this report. There is also currently an insufficient amount of data on Alloy 22 welds to predict the response of welds to thermal aging under potential repository conditions. It is expected that enough data for making a bounding argument for the welds will become available before the next revision of this report. The effect of phase changes on the corrosion resistance of the WPOB is addressed in the companion AMR on General Corrosion and Localized Corrosion of the WPOB (CRWMS M&O 2000b). The effects of LRO on the SCC and hydrogen embrittlement behavior of Alloy 22 have not yet been accounted for. Should future

versions of this model indicate that LRO could potentially occur, then the effect of this ordering on these degradation modes will be quantified.

Ultimately, it is the goal of this work to provide a quantitative model which can be used in performance assessment to predict the amount of any phases forming as a function of both time and temperature. Because the kinetic data required for creating this type of model do not exist, it is not possible to provide a model directly to performance assessment at this time. The intended use of the current bounding argument is as input to the AMR on General Corrosion and Localized Corrosion of the WPOB (CRWMS M&O 2000b). Corrosion data for fully aged Alloy 22 can be used as a worst case for the effects of phase instability on the corrosion behavior.

The bounding arguments presented in this report are based on a very limited amount of data. Also, the effects of heat-to-heat variability and cold work on the precipitation kinetics have not been accounted for. It is intended that more data be generated and incorporated into future revisions of this report.

## 1.4 RESOLUTION OF COMMENTS IN ISSUE RESOLUTION STATUS REPORT

The Issue Resolution Status Report recently issued by the NRC (1999) provides guidance for the development of process-level models. The key technical issue concerning container life and source term is the adequacy of the EBS design. The Issue Resolution Status Report defines the boundary of the EBS by the walls of the waste package emplacement drifts. Thus, the EBS design must provide assurance that the containers will be adequately long-lived, and radionuclide releases from the EBS will be sufficiently controlled. The container design and packaging of spent nuclear fuel and high-level waste glass are expected to make a significant contribution to the overall repository performance. The Issue Resolution Status Report deems six subissues to be important to the resolution of the key technical issue on the container life and source term. The second subissue, the effects of phase instability of materials and initial defects on the mechanical failure and lifetime of the containers, is specifically relevant to this AMR. The first subissue, the effects of corrosion processes on the lifetime of the containers, is indirectly related to this AMR.

Subissue 2 concerns the long-term phase stability of waste package materials and the effect of any phase transformations on the degradation of mechanical properties of container materials over time. This AMR addresses phase stability issues in Alloy 22 only. The kinetics of precipitation of phases which form in Alloy 22 are determined and extrapolated to the relatively low temperatures expected in the potential repository. Measurement of the effect of these transformations on the mechanical properties of Alloy 22 is in progress. Characterization of weld structures and their response to aging is also in progress.

Subissue 1 is related to failure of container materials due to various corrosion processes. In some cases, phase transformations within Alloy 22 can affect these corrosion processes. In those cases, the degree to which any phase changes occur is addressed in this AMR. The consequent effect on the corrosion processes is addressed in the companion AMR on General Corrosion and Localized Corrosion of the WPOB (CRWMS M&O 2000b). The effect of the segregated weld structure on the corrosion properties of Alloy 22 is addressed in the AMR for corrosion of

WPOB materials (CRWMS M&O 2000b), but any changes in the weld structure during prolonged exposure to elevated temperatures are to be covered by this AMR.

The acceptance criteria for the first subissue above are addressed in the AMR on General Corrosion and Localized Corrosion of the WPOB (CRWMS M&O 2000b). The following paragraphs address each of the acceptance criteria for subissue 2 that are applicable to the scope of this AMR.

1. DOE has identified and considered the relevant mechanical failure processes that may affect the performance of the proposed container materials.

   *Response*: Mechanical failure processes of as-received base metal and welds are covered by other AMRs. The mechanical failure modes considered thus far are SCC, hydrogen embrittlement, and mechanical failure due to rock fall. Discussion of these failure modes is beyond the scope of this AMR.

2. DOE has identified and considered the effect of material stability on mechanical failure processes for the various container materials as a result of prolonged exposure to the expected range of temperatures and stresses, including the effects of chemical composition microstructure, thermal treatments, and fabrication processes.

   *Response*: A preliminary bounding argument has been made for intermetallic formation and LRO in Alloy 22 base metal. The bounding argument for intermetallic formation has been used to define a worst case for corrosion testing. The effects of LRO on the SCC and hydrogen embrittlement behavior of Alloy 22 have not yet been accounted for. Should future versions of this model indicate that LRO could potentially occur, then the effect of this ordering on these degradation modes will be quantified. A limited testing program designed to determine the magnitude of the effect of phase instability on SCC of Alloy 22 base metal and welds has recently been initiated. The effect of phase changes on the mechanical properties of Alloy 22 base metal and welds are currently being investigated, but the data are not available for this version of the report. Alloys 59 and 686 are currently being added to the phase stability test program. The data obtained from these alloys when compared to that from Alloy 22 will provide some insight into the effect of chemical composition on the phase stability of these alloys. Detailed heat-to-heat variability studies, however, have not been done. Work aimed at characterizing the effect of fabrication processes that result in cold work and of weld stress mitigation techniques is planned.

3. DOE has demonstrated that the numerical models used for container materials stability and mechanical failures are effective representations, taking into consideration associated uncertainties, of the expected materials behavior and are not likely to underestimate the actual rate of failure in the repository environment.

   *Response*: The bounding arguments made in this AMR for phase stability of Alloy 22 base metal are believed to be conservative. They are, however, based on a very limited amount of data which do not include possible processing effects such as cold work. The stability of

Alloy 22 welds must also be investigated. Testing is currently being done so that considerably more data should be available for license application.

4. DOE has considered the compatibility of container materials and the variability in container manufacturing processes, including welding, in its WP failure analyses and in the evaluation of radionuclide release.

   *Response*: This AMR applies to phase stability of Alloy 22. A discussion of the compatibility of container materials is beyond the scope of this report. The effect of variability in container manufacturing processes is covered in other AMRs.

5. DOE has identified the most appropriate methods for nondestructive examination of fabricated containers to detect and evaluate fabrication defects in general and, particularly, in seam and closure welds.

   *Response*: A nondestructive examination protocol is under development and will be used for container material inspection. A discussion of these plans is beyond the scope of this AMR.

6. DOE has justified the use of material test results not specifically designed or performed for the YM repository program for environmental conditions (i.e., temperature, stress, and time) expected to prevail at the proposed YM repository.

   *Response*: At expected repository temperatures, the waste containers are required to maintain integrity for at least 10,000 years. Clearly, a phase stability test program must involve acceleration of the transformations that would naturally occur. This acceleration is accomplished through an increase in the temperature. The phases that do form and the rate at which they form are determined at higher temperatures, and these data are fit to theory and extrapolated to lower temperatures to predict if the alloy is expected to be stable at the lower potential repository temperatures. The lower the temperatures used in generating data from which the extrapolation is made, the greater the confidence that the mechanism of transformation and the thermodynamics of the system still apply at the lower temperatures. An extensive aging study has been initiated at LLNL which involves temperatures as low as 400°C. It is intended that this testing continue beyond license application to provide adequate assurance that extrapolations made from test data are appropriate for proposed repository conditions. In addition, theoretical modeling is being initiated with powerful, state-of-the-art software as further assurance that the thermodynamics and transformation mechanisms do not differ at the test temperatures from the lower temperatures.

7. DOE has conducted a consistent, sufficient, and suitable materials testing program at the time of the LA submittal. In addition, DOE has identified specific plans for further testing to reduce any significant area(s) of uncertainty as part of the performance confirmation program.

   *Response*: Only thermal aging and mechanical testing of alloy 22 base metal and welds apply to this AMR. Other test programs involving, for example, SCC and hydrogen embrittlement are discussed in other AMRs. An extensive aging study is currently being initiated. This study includes tension testing, Charpy impact toughness testing, and microstructural

characterization using SEM, TEM, x-ray diffraction, energy dispersive spectroscopy of alloys 22, 59 and 686 aged at temperatures between 400 and 750°C. It is planned that this aging will continue beyond license application. Samples are also being aged for reverse DC SCC crack propagation rate testing and cyclic polarization testing. Characterization of alloy 22 welds including the effects of stress mitigation techniques such as annealing and laser peening has begun. A study of the effect of thermal aging on the microstructure and corrosion resistance of these welds is planned.

A discussion of the plans for the performance confirmation period are beyond the scope of this AMR.

8. DOE has established a defensible program of monitoring and mechanical testing of the engineered subsystems components, during the performance confirmation period, to assure they are functioning as intended and anticipated, in the presence of thermal and stress perturbations.

   *Response*: A discussion of the plans for the performance confirmation period are beyond the scope of this AMR.

## 2. QUALITY ASSURANCE

The Quality Assurance (QA) program applies to this analysis. All types of waste packages were classified (per QAP-2-3 REV 10) as Quality Level-1 in *Classification of the MGR Uncanistered Spent Nuclear Fuel Disposal Container System* (CRWMS M&O 1999c, p. 7). This analysis applies to all of the waste package designs included in the MGR (Monitored Geologic Repository) Classification Analyses. Reference CRWMS M&O (1999c) is cited as an example. The development of this analysis is conducted under activity evaluation *Waste Package Testing and Data Generation* (CRWMS M&O 1999d) which was prepared per QAP-2-0 REV 5. The results of that evaluation were that the activity is subject to the *Quality Assurance Requirements and Description* (DOE 2000) requirements. This report was prepared in accordance with AP-3.10Q REV 2, *Analysis and Models.*

This document may be affected by technical product input information that requires confirmation. Any changes to the document that may occur as a result of completing the confirmation activities will be reflected in subsequent revisions. The status of the input information quality may be confirmed by review of the Document Input Reference System database.

INTENTIONALLY LEFT BLANK

# 3. COMPUTER SOFTWARE AND MODEL USAGE

## 3.1 SOFTWARE REQUIRING APPROVAL FOR QA WORK

No software requiring QA approval has been used in developing this model.

## 3.2 SOFTWARE ROUTINES

KaleidaGraph v3.08d (Synergy Software), loaded on a PowerMac G4 with Macintosh operating system 8.6, was used for graphing data. This graph (Figure 96) is for visual representation of the data only, and all points plotted were checked by visual inspection. The actual table of values plotted rather than the plot is being submitted to the CRWMS M&O databases so that any approved software can be used to plot the data if necessary.

Excel 98 (Microsoft), loaded on a PowerMac G4 with Macintosh operating system 8.6, was used for graphing data, calculating curve fits to the data and for manipulating data through the use of routines. Microsoft Excel is considered industry standard software, and according to AP-SI.1Q REV 2, ICN 4, section 5.1, built-in functions such as plotting and curve fitting do not need to be verified. In some cases, simple spreadsheet calculations were made with the data prior to plotting. These routines (written within Excel) were handled in accordance with AP-SI.1Q section 5.1. Equations used for data manipulation are provided in the text and all calculations were verified by hand. Other data analyses done in Excel spreadsheets with routines and/or macros were verified in the scientific notebook through the use of sample calculations.

INTENTIONALLY LEFT BLANK

# 4. INPUTS

## 4.1 DATA AND PARAMETERS

### 4.1.1 Transmission Electron Microscopy Micrographs Used in Preliminary Intermetallic and Carbide Phase Identification

This section contains transmission electron microscopy (TEM) images and electron-selected area diffraction (SAD) patterns used to identify the phases that form in Alloy 22 base metal after aging in the temperature range of 600 to 760°C (Figures 1 through 39). Because of the structural similarity of the μ and P phases, some diffraction patterns could be indexed as either phase. For this reason, the phases forming in some cases are only tentatively identified. Several carbides form in Alloy 22, but they all have very similar structures. Although they are significantly different chemically, it is not possible to distinguish them in the work reported here. They are, therefore, simply called carbide.

TS_AMR_fig4-1

NOTE: This phase was identified as P phase. (TS393-049b, Image S0244, 8/23/99, SN #442, p. 19)

Figure 1. Grain Boundary Precipitation in Alloy 22 Aged for 1000 hr at 593°C [DTN # LL000115905924.113]

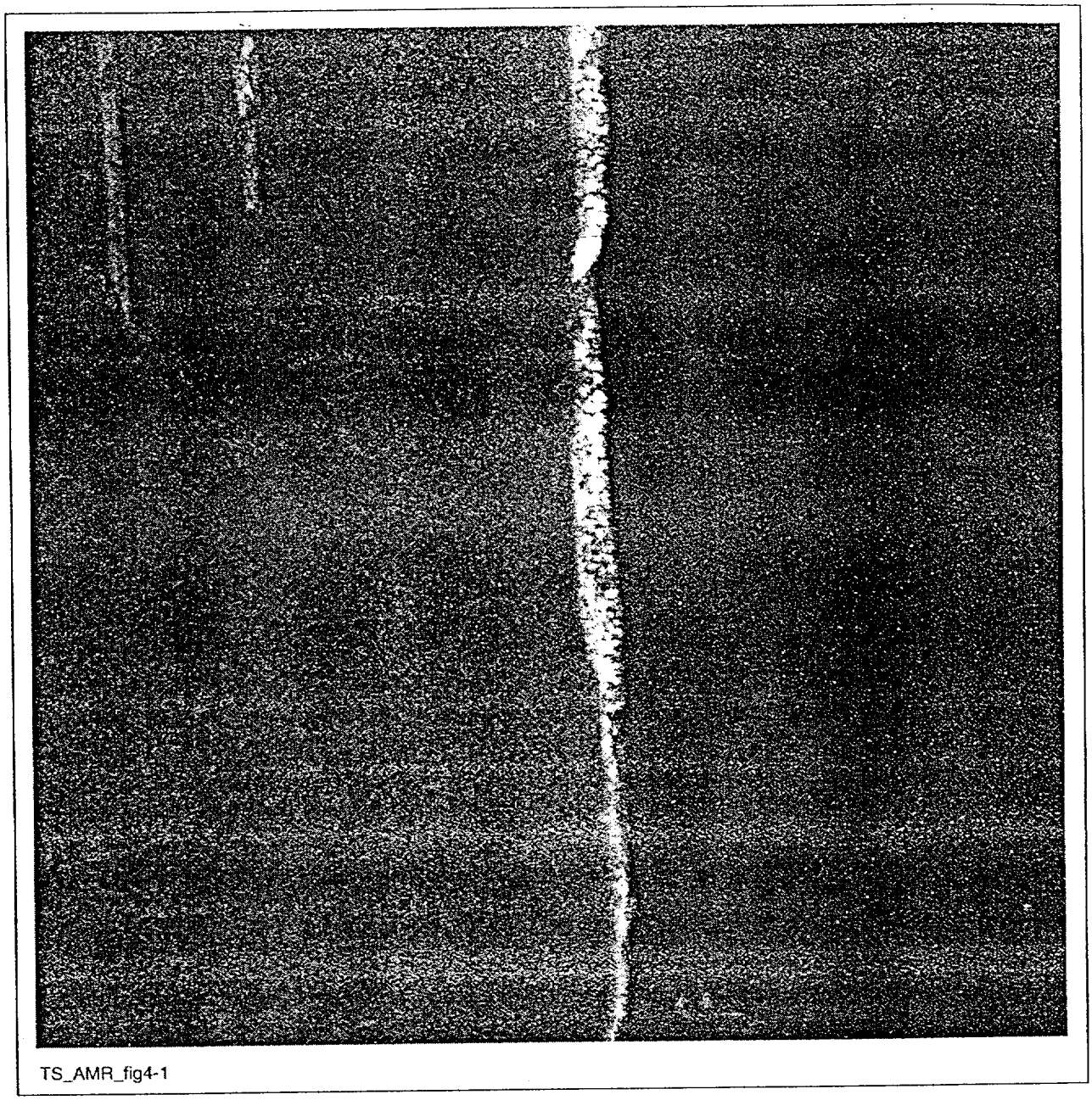

TS_AMR_fig4-1

NOTE: The grain boundary precipitate identified as P appears light. (TS393-049b, Image S0245, 8/23/99, SN #442, p. 19)

Figure 2. Dark-Field Image Corresponding to Figure 1 [DTN # LL000115905924.113]

TS_AMR_fig1-3

NOTE: This pattern was indexed as P phase. (TS393-049b, Image S0246, 8/23/99, SN #442, p. 20)

Figure 3. SAD Pattern from the Grain Boundary Precipitate Shown in Figures 1 and 2 [DTN # LL000115905924.113]

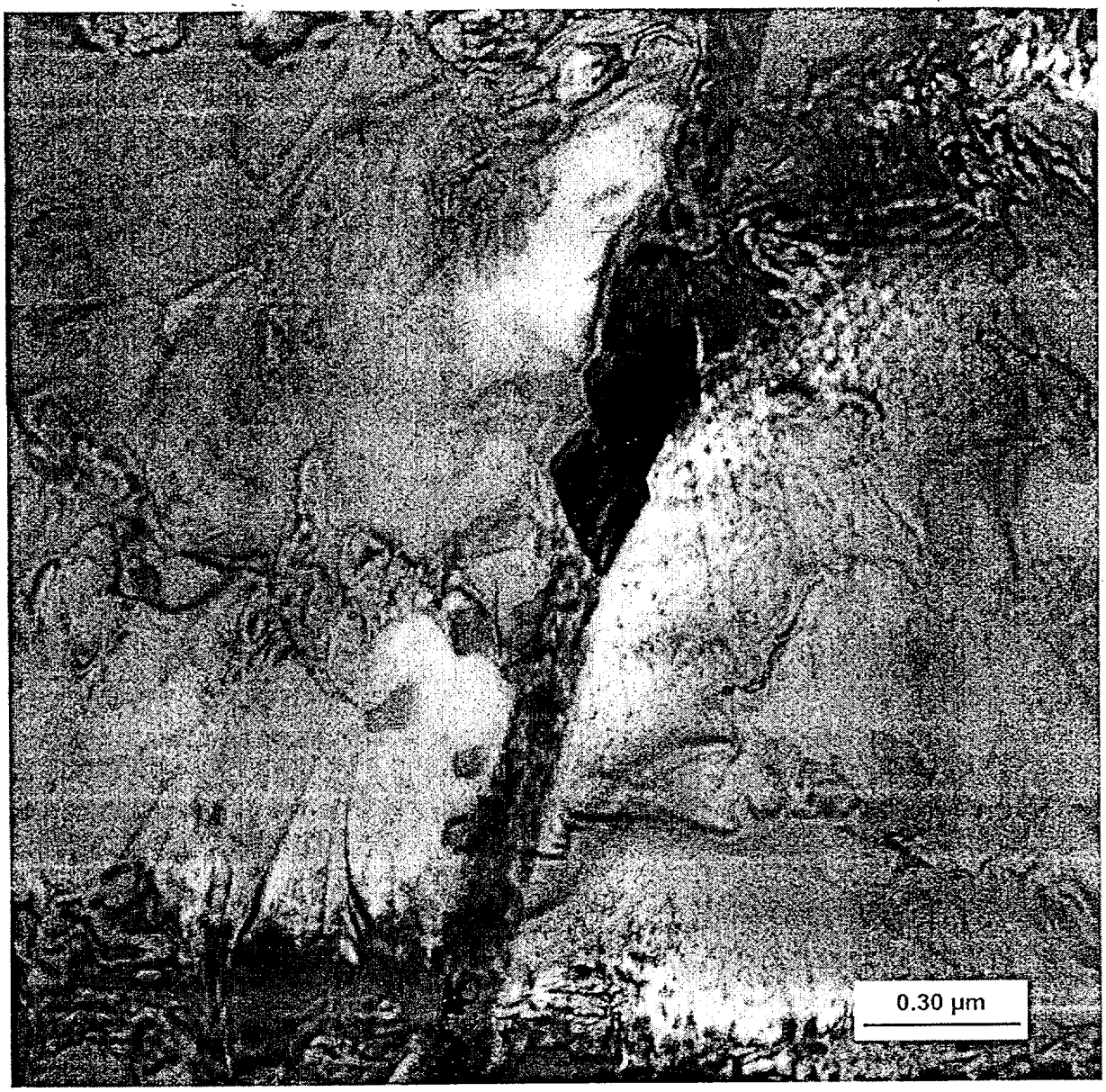


TS_AMR_fig4-01

NOTE: This phase was identified as P phase. (TS369-003a, Image S0125, 3/9/99, SN #434, p. 41)

Figure 4. Grain Boundary Precipitation in Alloy 22 Aged for 16,000 hr at 593°C [DTN # LL000115905924.113]

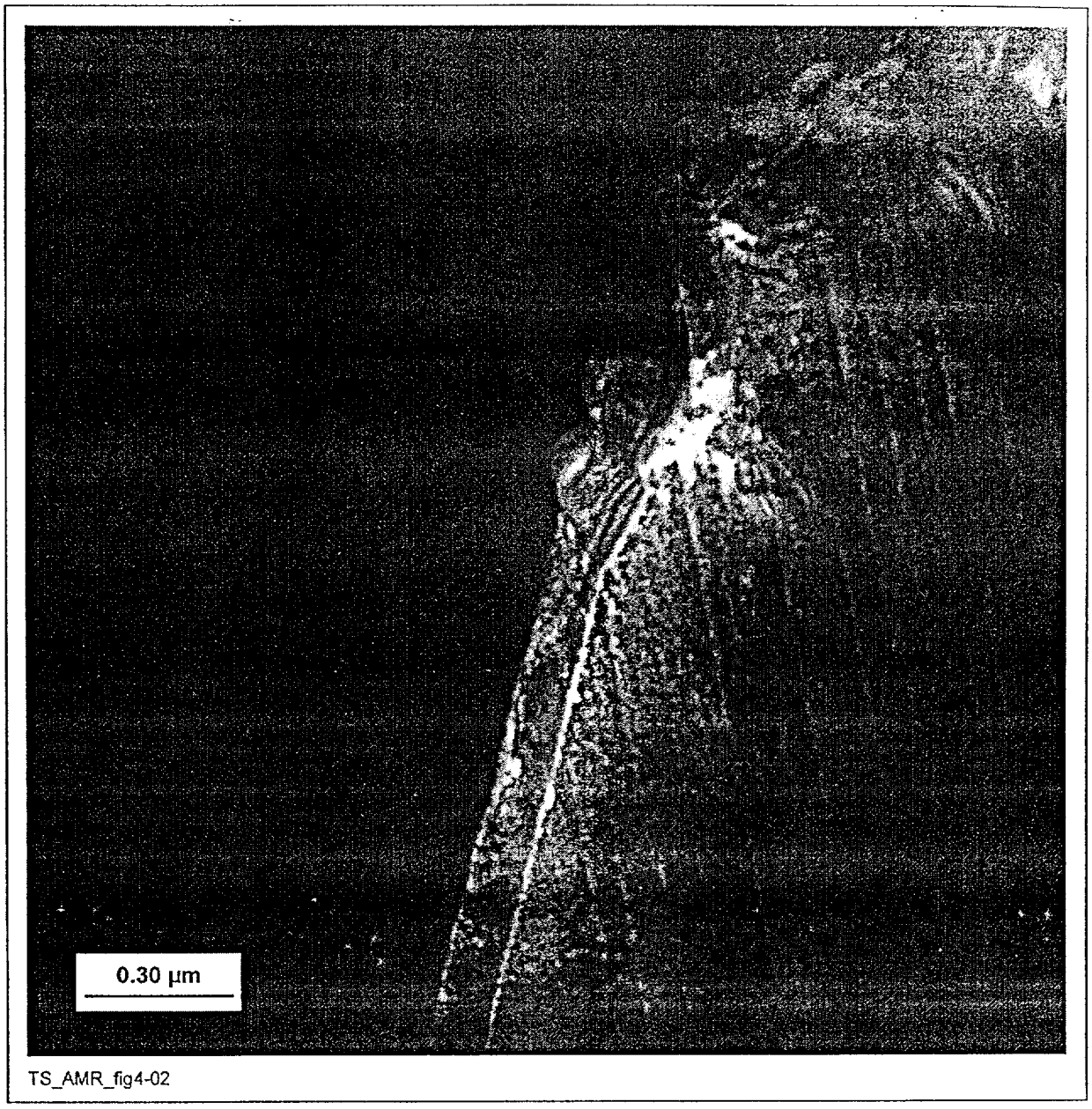


NOTE: The grain boundary precipitate identified as P appears light. (TS369-003a, Image S0126, 3/9/99, SN #434, p. 42)

Figure 5. Dark-Field Image Corresponding to Figure 4 [DTN # LL000115905924.113]

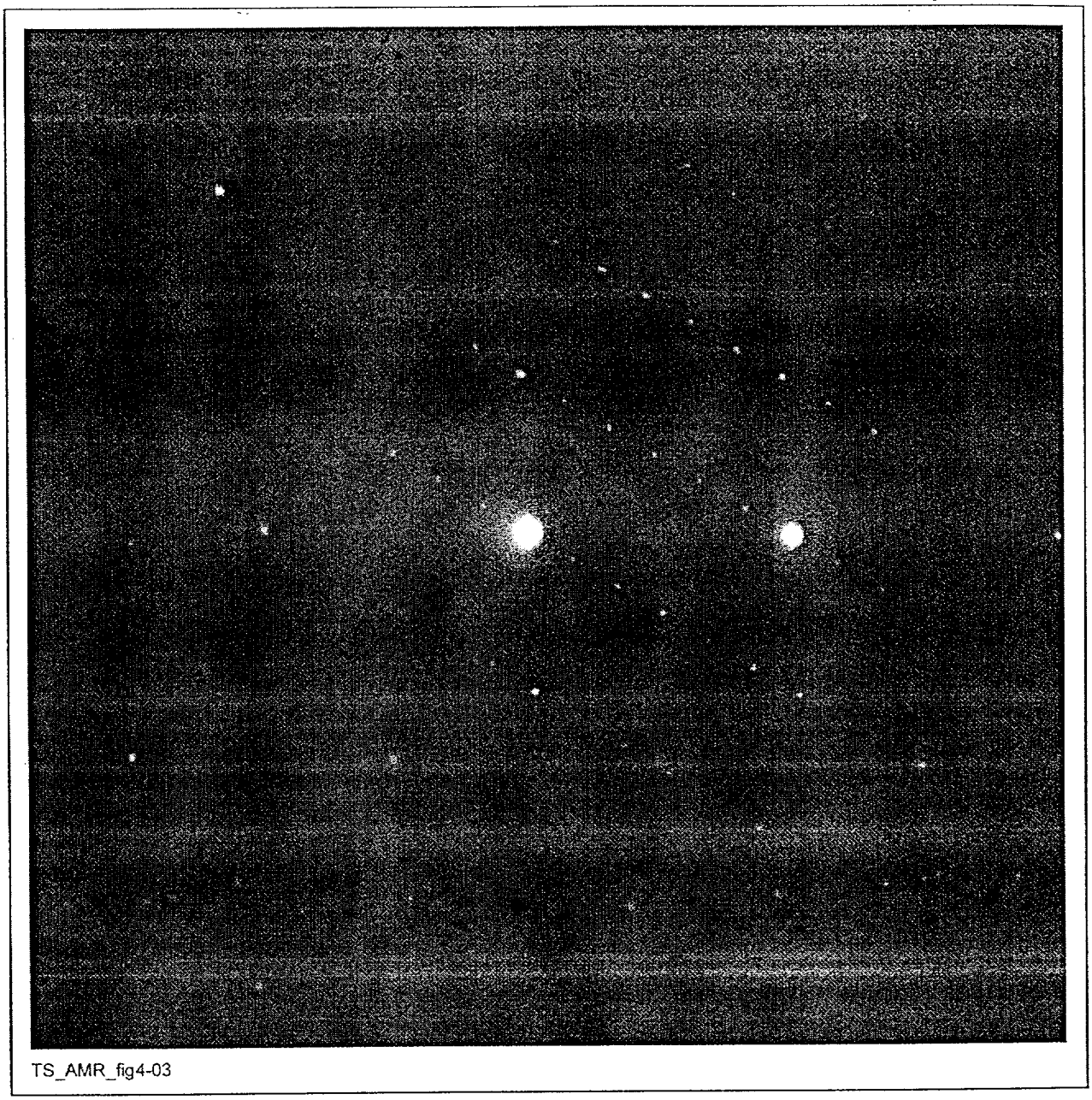

TS_AMR_fig4-03

NOTE: This pattern was indexed as P phase. (TS369-003a, Image S0124, 3/9/99, SN #434, p. 43)

Figure 6. SAD Pattern from the Grain Boundary Precipitate Shown in Figures 4 and 5 [DTN # LL000115905924.113]


NOTE: This phase was identified as carbide. (TS369-003a, Image 1490, 12/16/98, SN #393, p. 66)

Figure 7. Grain Boundary Precipitation in Alloy 22 Aged for 16,000 hr at 593°C [DTN # LL000115905924.113]

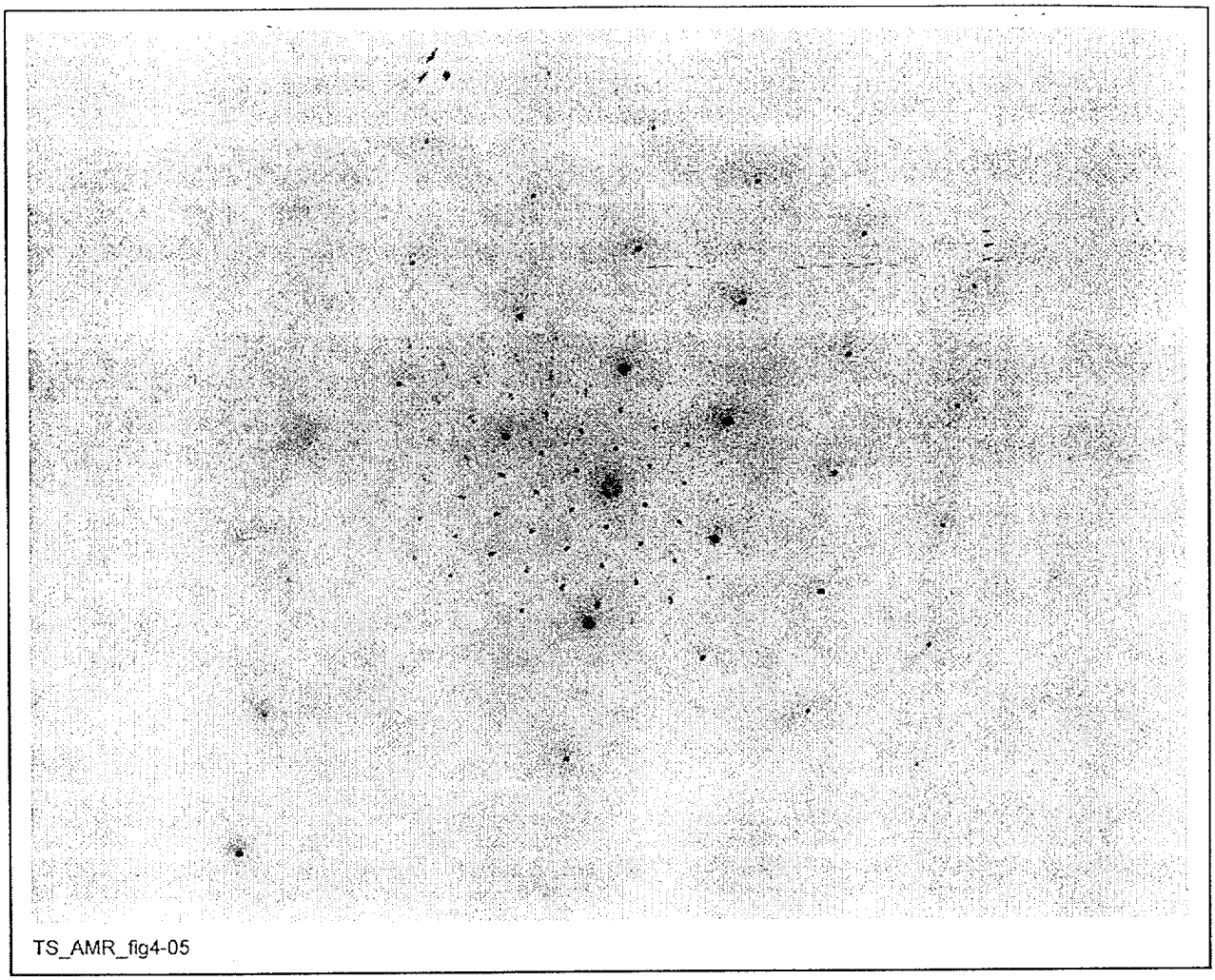


NOTE: This pattern was indexed as carbide. (TS369-003a, Image 1489, 12/16/98, SN #393, p. 66)

Figure 8. SAD Pattern from the Grain Boundary Precipitate Labeled Carbide in Figure 7 [DTN # LL000115905924.113]

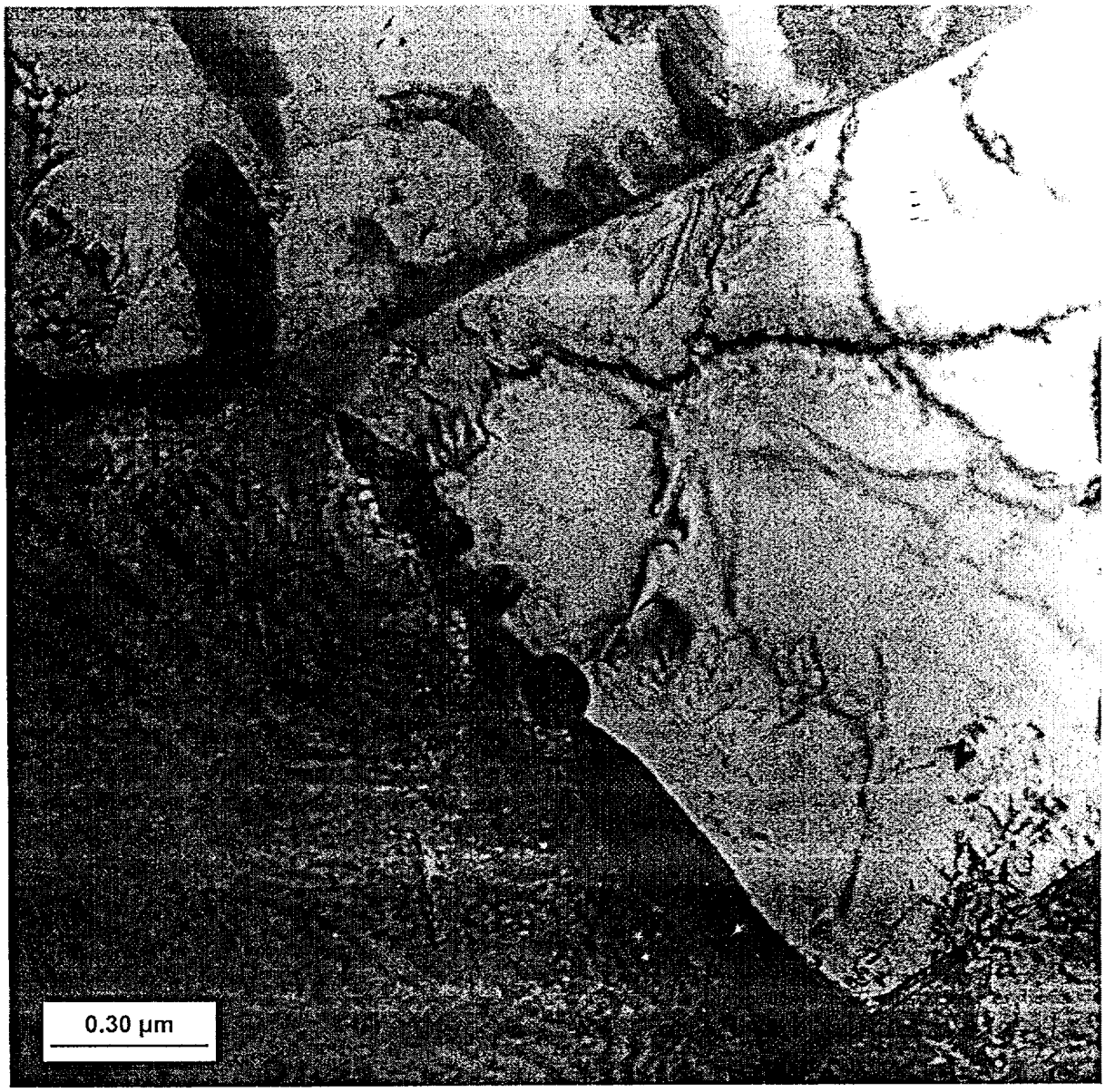


NOTE: This phase was identified as P phase. (TS369-008a, Image S0152, 3/17/99, SN #434, p. 46)

Figure 9. Grain Boundary Precipitation in Alloy 22 Aged for 16,000 hr at 649°C [DTN # LL000115905924.113]

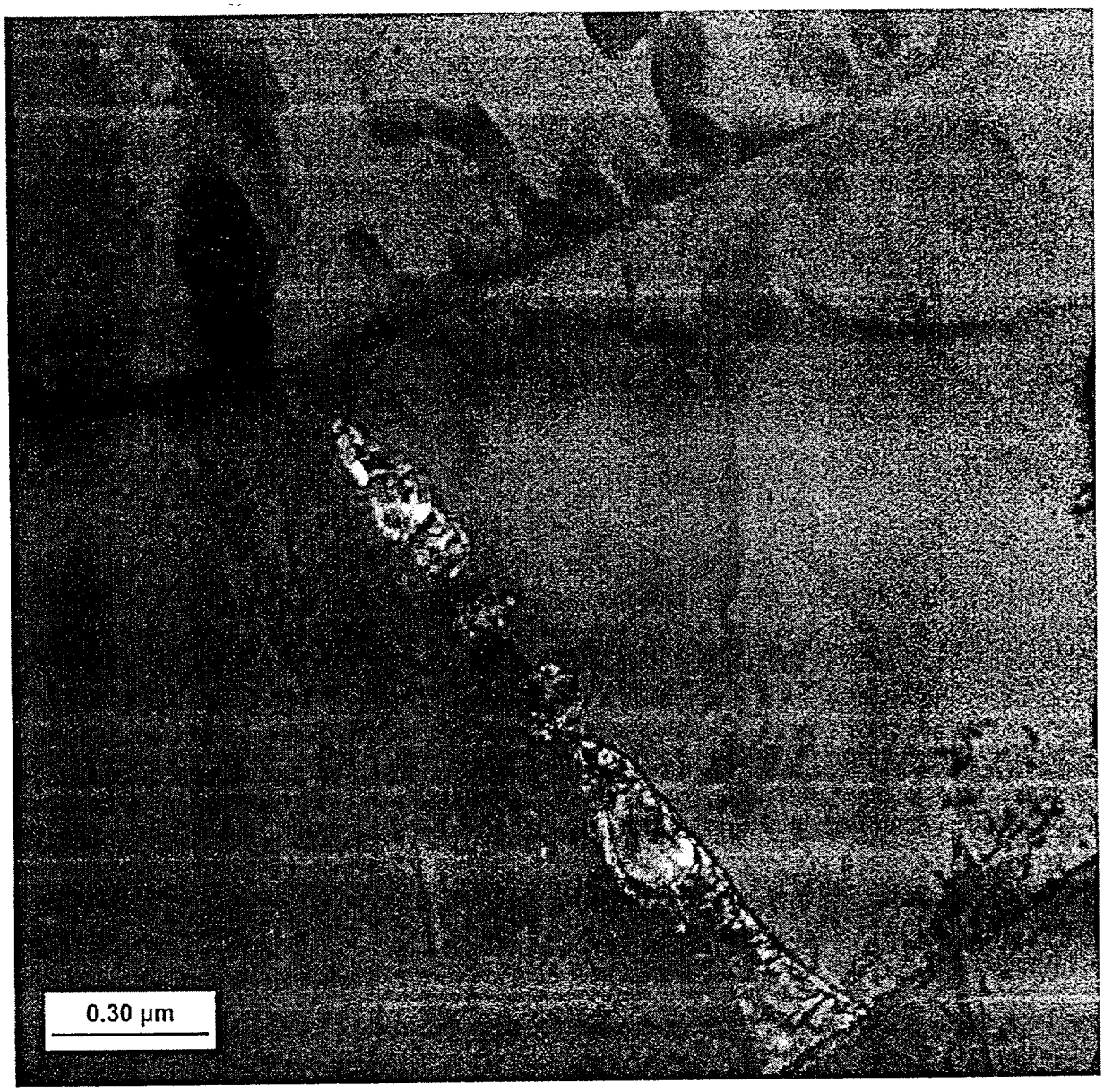


TS_AMR_fig4-07

NOTE: The grain boundary precipitate identified as P appears light. (TS369-008a, Image S0153, 3/17/99, SN #434, p. 46)

Figure 10. Dark-Field Image Corresponding to Figure 9 [DTN # LL000115905924.113]

TS_AMR_fig4-08

NOTE: (TS369-008a, Image S0151, 3/17/99, SN #434, p. 47)

Figure 11. SAD Pattern from the Grain Boundary Precipitate Shown in Figures 9 and 10 [DTN # LL000115905924.113]

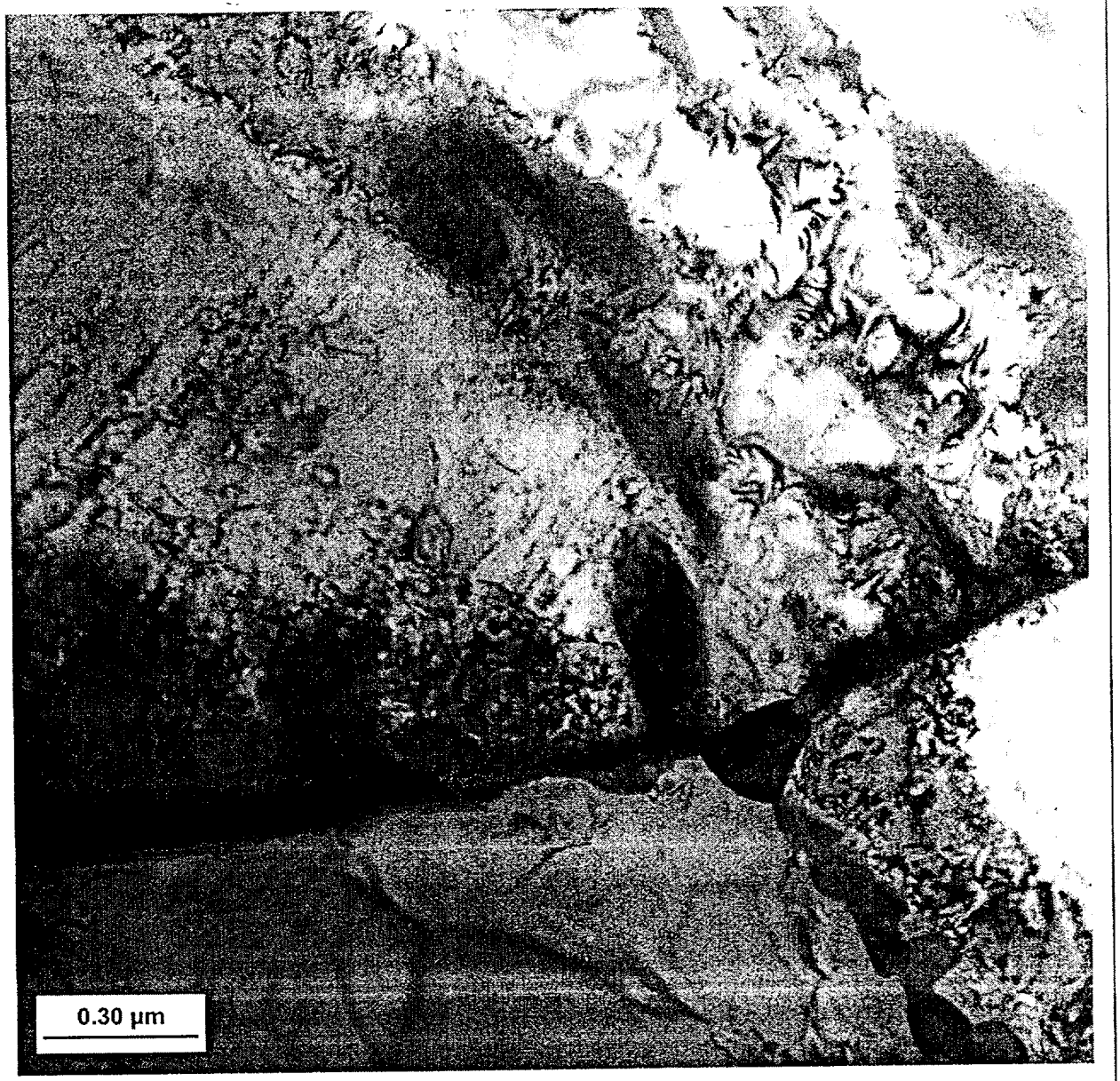


TS_AMR_fig4-09

NOTE: The phase at the grain boundary triple point appears to be $\mu$ phase. (TS369-008a, Image S0156, 3/17/99, SN #434, p. 49)

Figure 12. Grain Boundary Precipitation in Alloy 22 Aged for 16,000 hr at 649°C [DTN # LL000115905924.113]

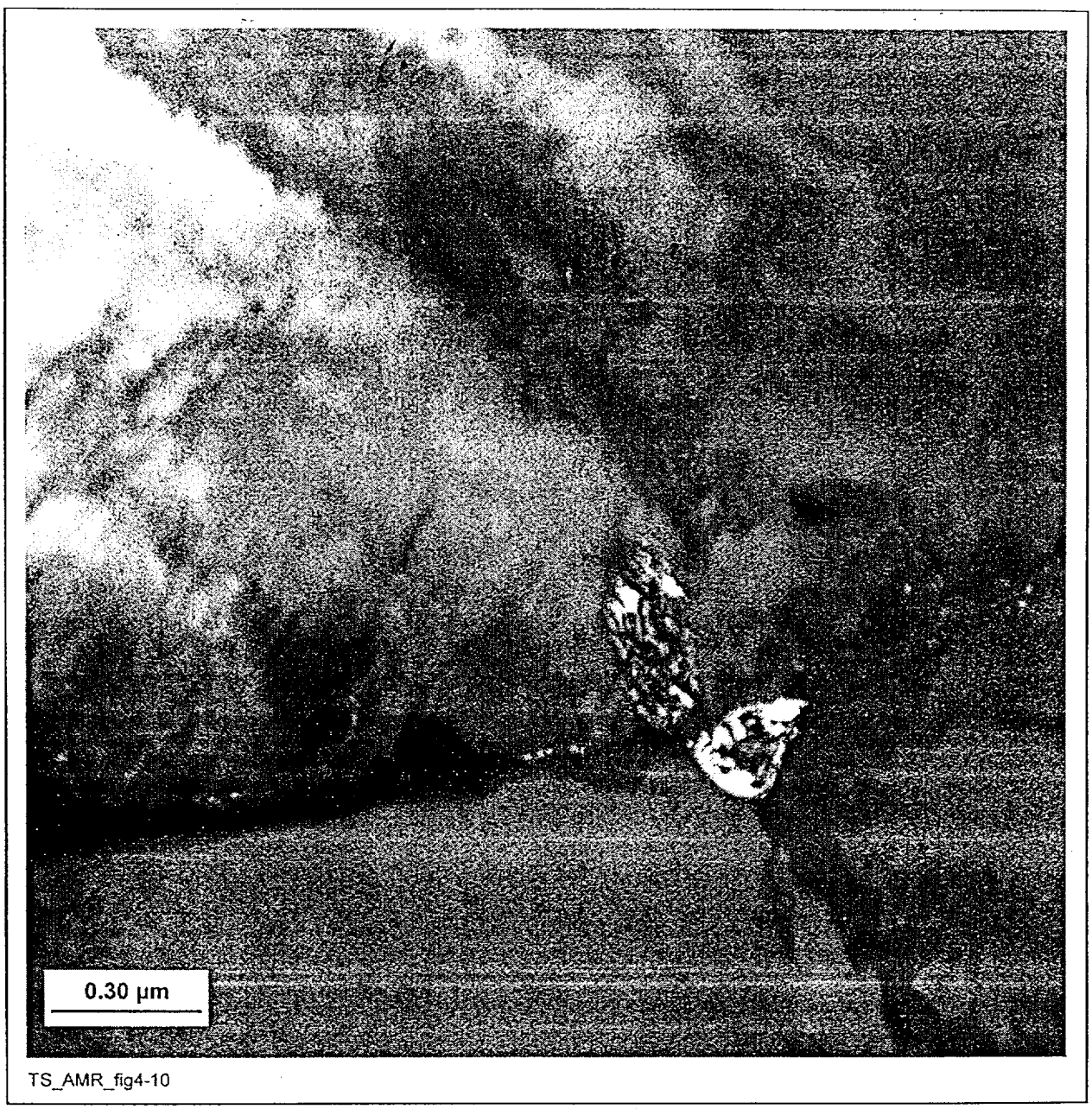


NOTE: The grain boundary precipitate tentatively identified as µ appears light. (TS369-008a, Image S0157, 3/17/99, SN #434, p. 49)

Figure 13. Dark-Field Image Corresponding to Figure 12 [DTN # LL000115905924.113]

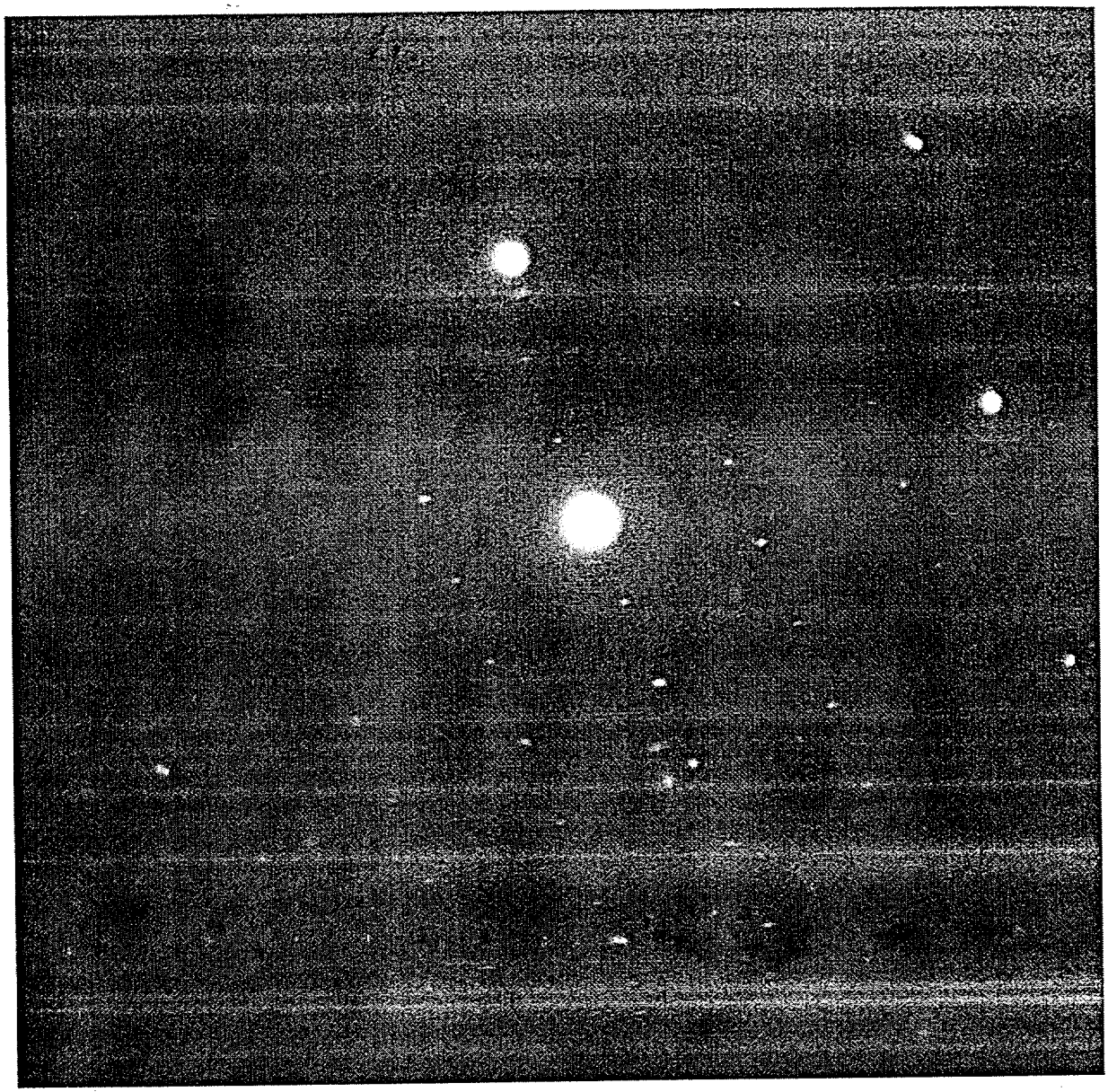

TS_AMR_fig4-11

NOTE: (TS369-008a, Image S0155, 3/17/99, SN #434, p. 50)

Figure 14. SAD Pattern from the Grain Boundary Precipitate Shown in Figures 12 and 13 [DTN # LL000115905924.113]

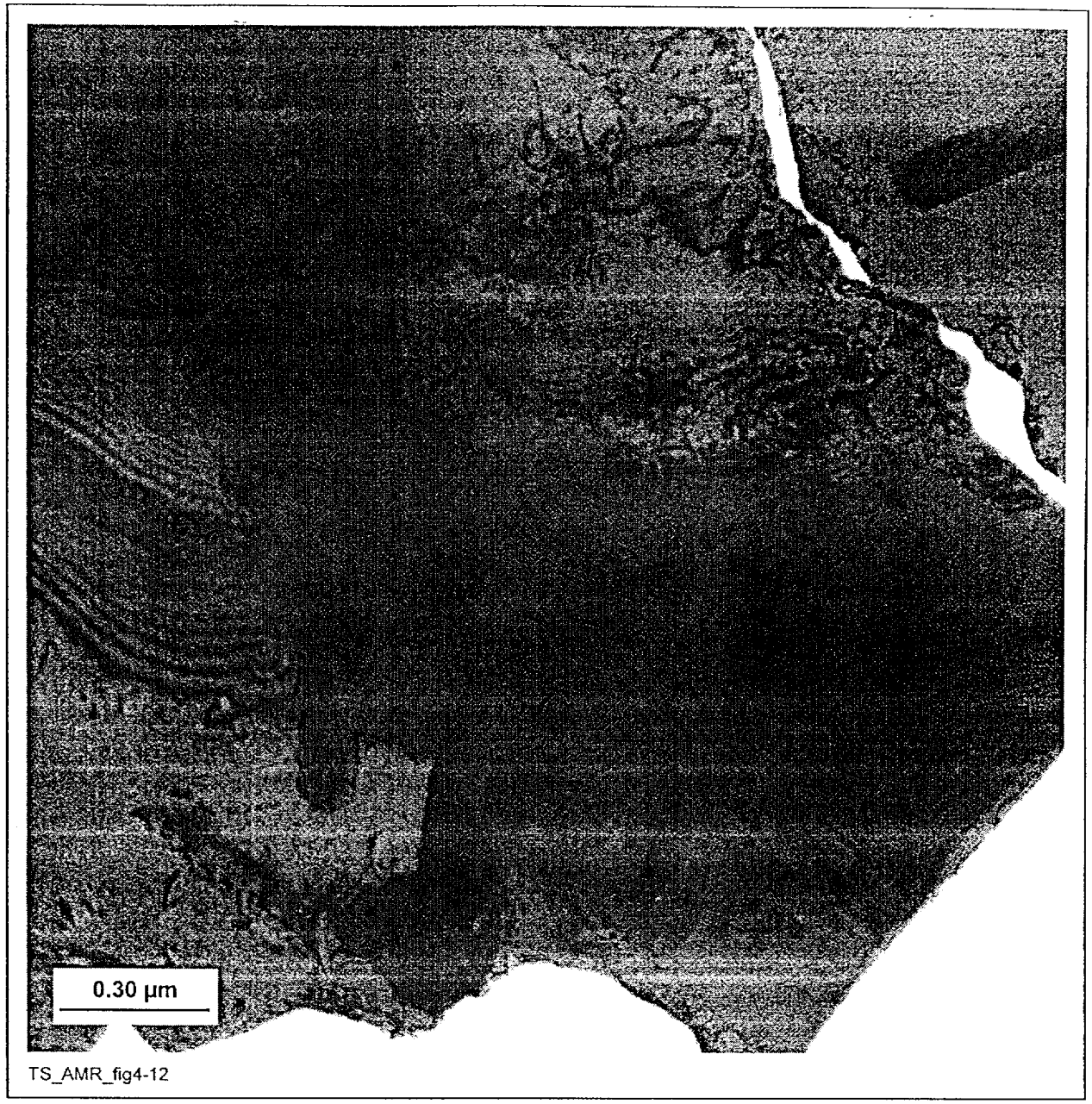


NOTE: This phase was identified as P phase. (TS369-009a, Image S0062, 2/19/99, SN #434, p. 60)

Figure 15. Precipitation in Alloy 22 Aged for 16,000 hr at 704°C [DTN # LL000115905924.113]


NOTE: The precipitate identified as P phase appears light. (TS369-009a, Image S0063, 2/19/99, SN #434, p. 60)

Figure 16. Dark-Field Image Corresponding to Figure 15 [DTN # LL000115905924.113]

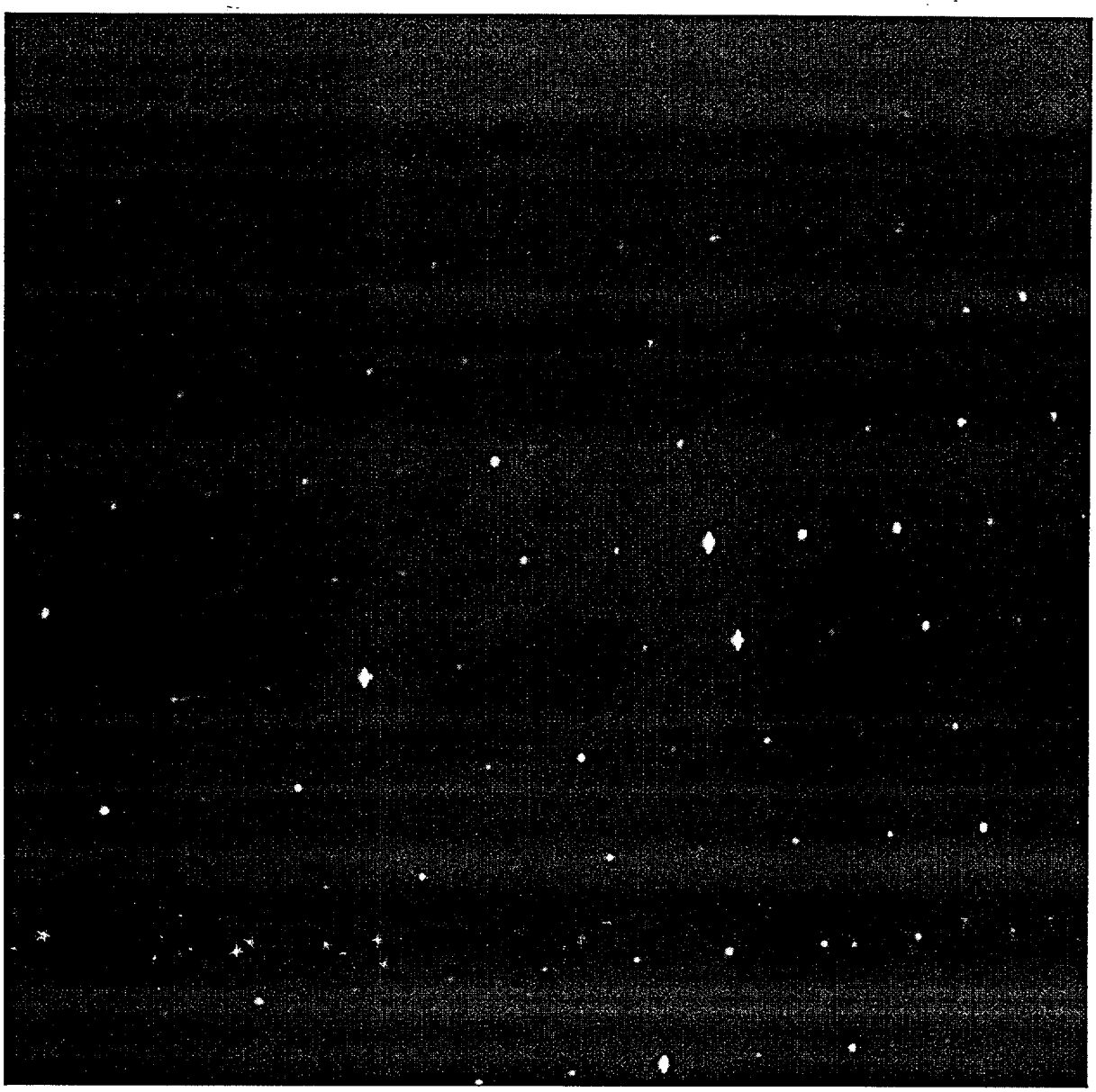

TS_AMR_fig4-14

NOTE: This pattern was indexed as P phase. (TS369-009a, Image S0061, 2/19/99, SN #434, p. 61)

Figure 17. SAD Pattern from the Precipitate Shown in Figures 15 and 16 [DTN # LL000115905924.113]

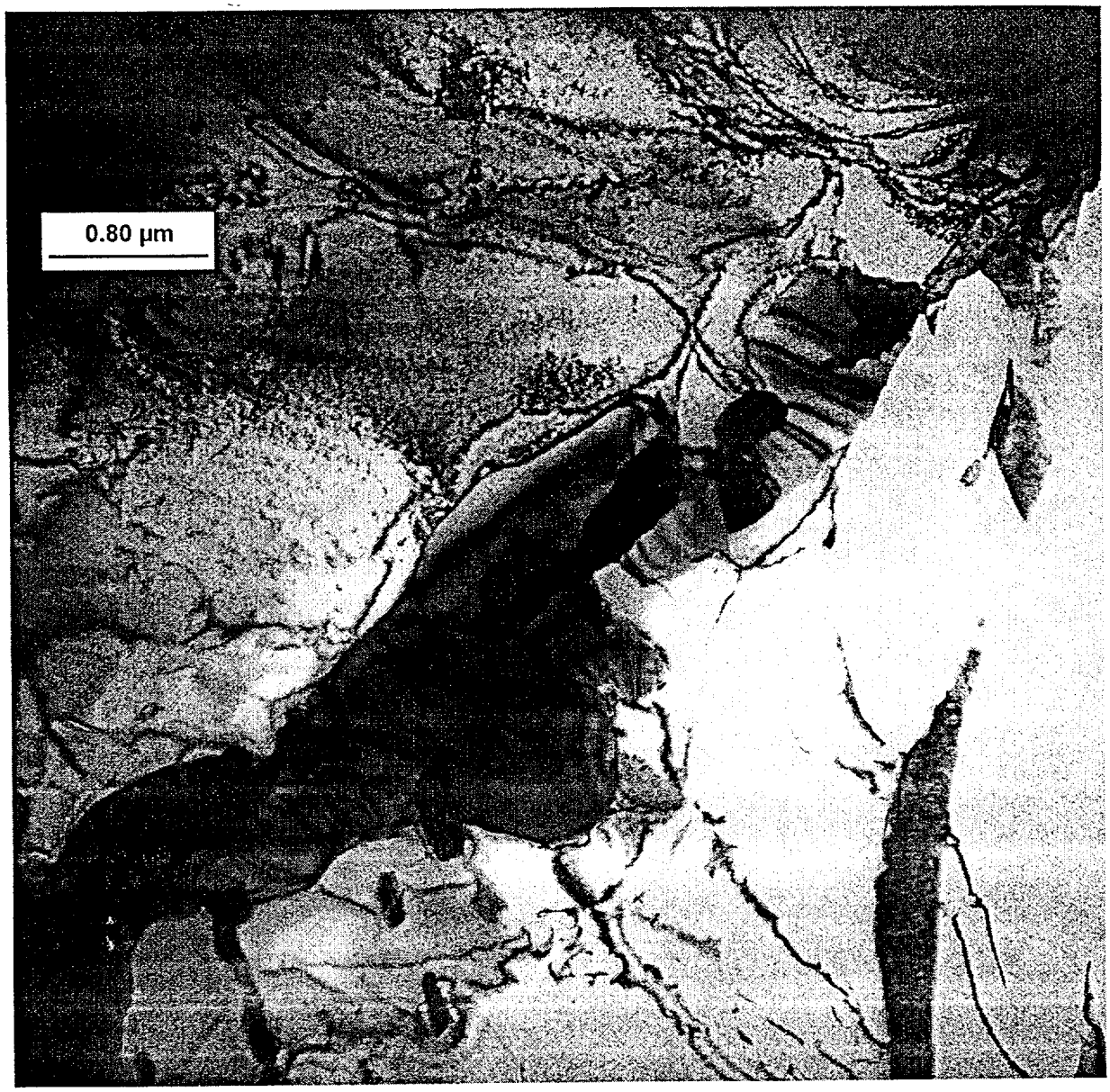


NOTE: Both carbide and µ phase were identified in this area of the sample. (TS369-009a, Image S0178, 3/17/99, SN #434, p. 54)

Figure 18. Grain Boundary Precipitation in Alloy 22 Aged for 16,000 hr at 704°C [DTN # LL000115905924.113]


TS_AMR_fig4-16

NOTE: The grain-boundary precipitate identified as carbide appears light. (TS369-009a, Image S0174, 3/17/99, SN #434, p. 54)

Figure 19. Dark-Field Image Corresponding to Figure 18 [DTN # LL000115905924.113]

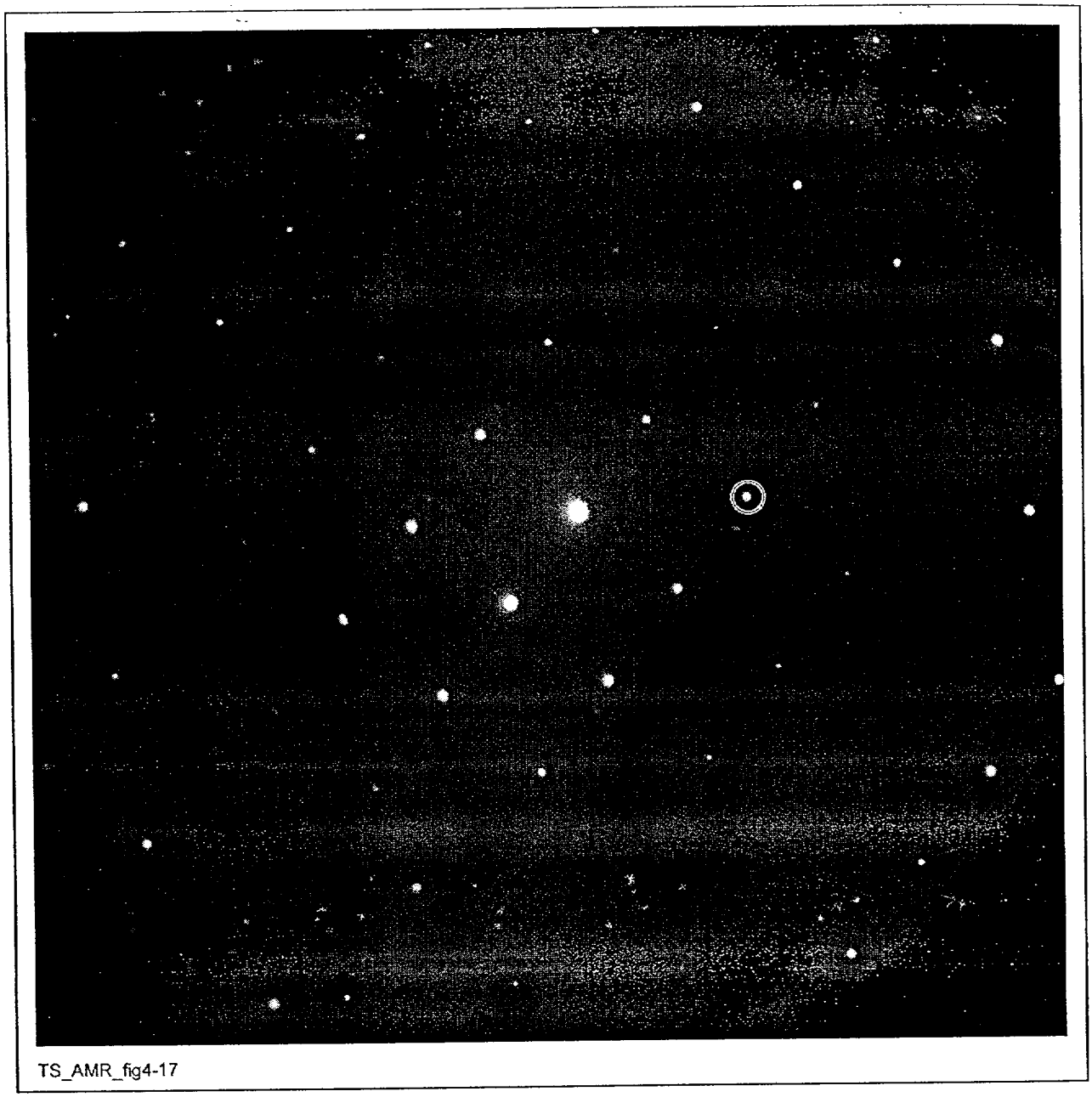


NOTE: (TS369-009a, Image S0175, 3/17/99, SN #434, p. 55)

Figure 20. SAD Pattern from the Grain Boundary Carbide Shown in Figures 18 and 19 [DTN # LL000115905924.113]

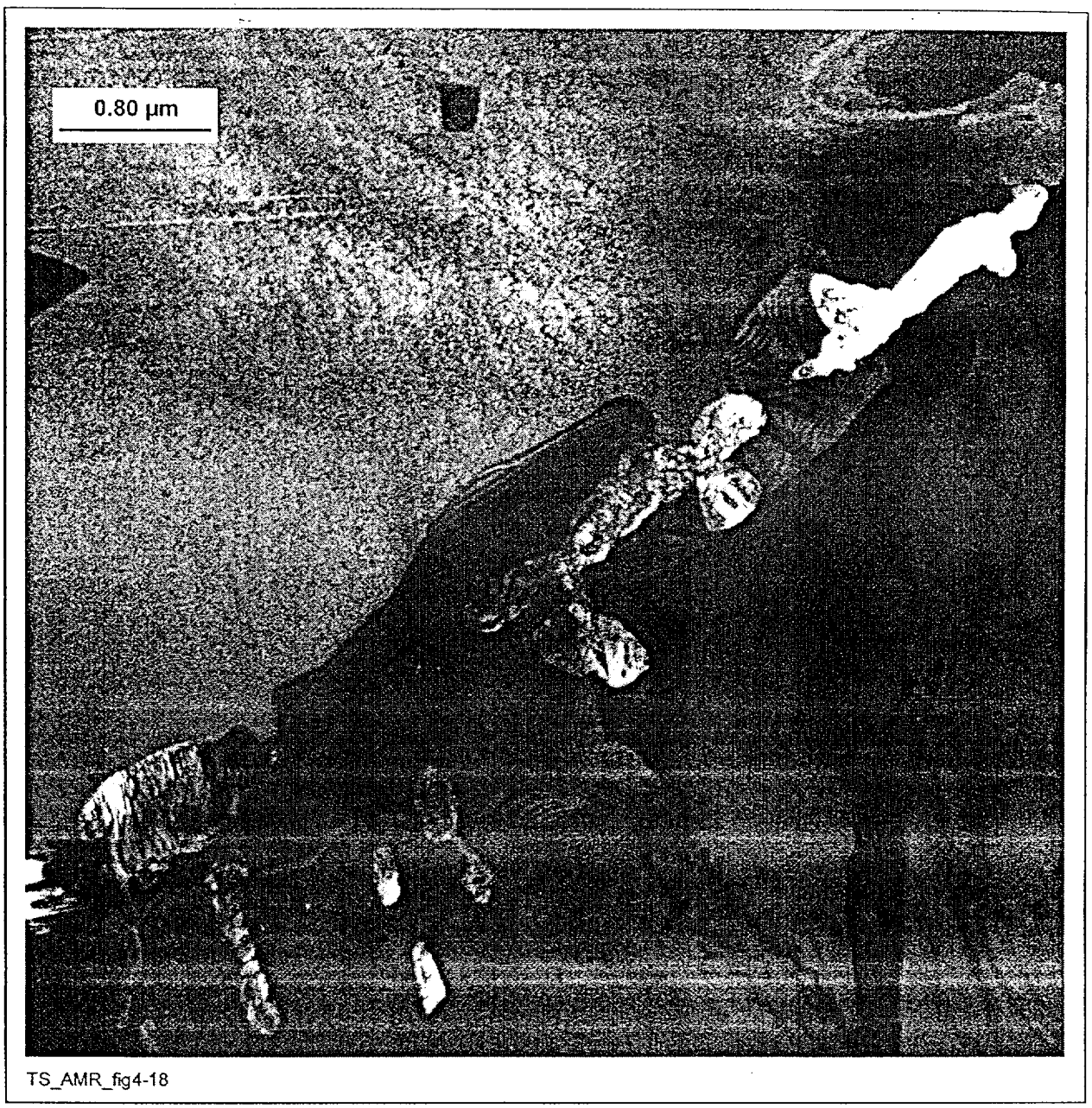


NOTE: The grain boundary precipitate identified as µ phase appears light. (TS369-009a, Image S0179, 3/17/99, SN #434, p. 57)

Figure 21. Dark-Field Image Corresponding to Figure 18 [DTN # LL000115905924.113]

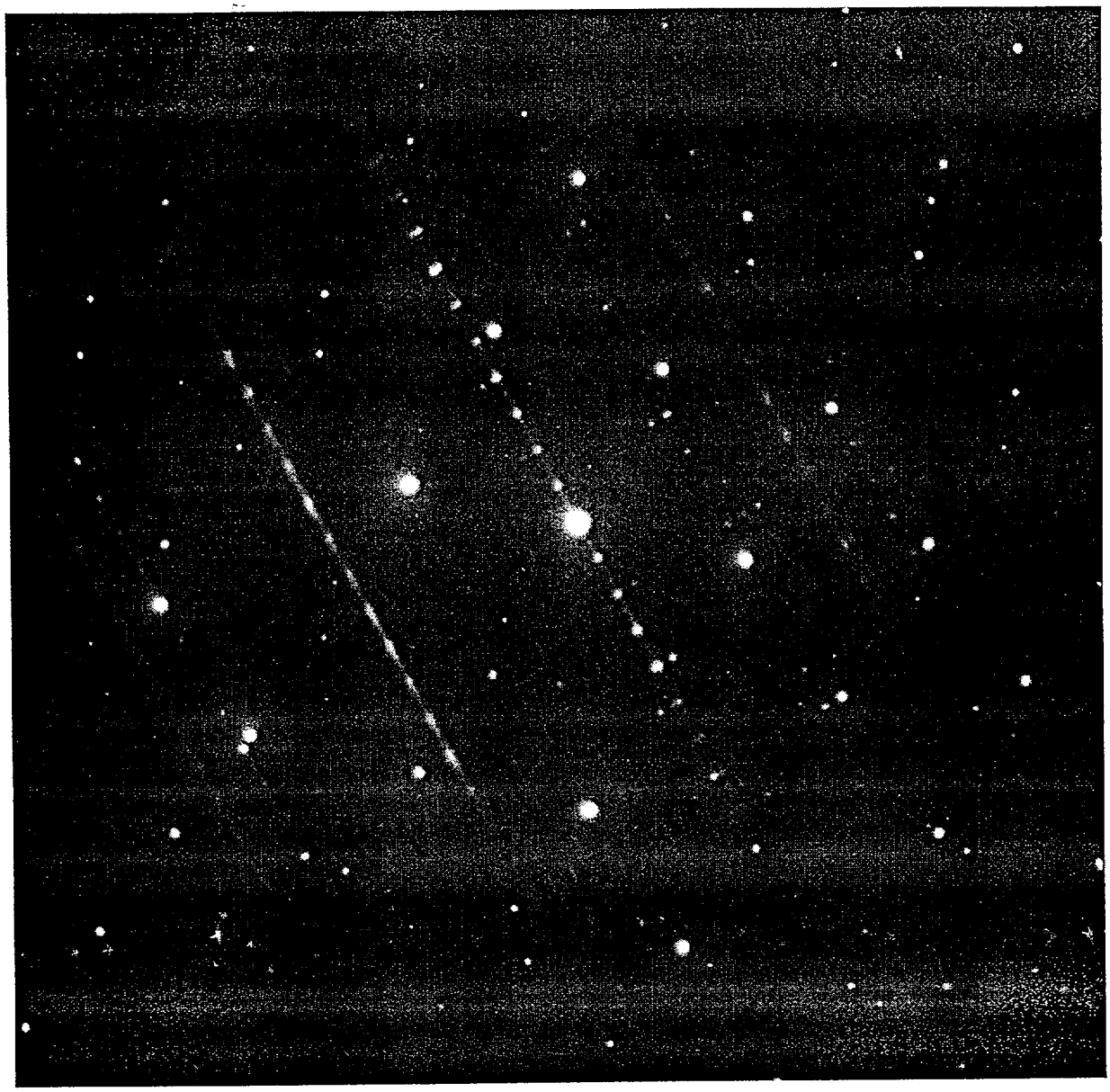

TS_AMR_fig4-19

NOTE: (TS369-009a, Image S0180, 3/17/99, SN #434, p. 58)

Figure 22. SAD Pattern from the Grain Boundary μ Phase Precipitates Shown in Figures 18 and 21 [DTN # LL000115905924.113]


TS_AMR_fig4-20

NOTE: This phase was identified as the carbide phase. (TS369-009a, Image 1883, 10/12/98, SN #393, p. 92)

Figure 23. Grain Boundary Precipitation in Alloy 22 Aged for 16,000 hr at 704°C [DTN # LL000115905924.113]


NOTE: This pattern was indexed as carbide. (TS369-009a, Image 1884, 10/12/98, SN #393, p. 93)

Figure 24. SAD Pattern from the Grain Boundary Precipitate Labeled Carbide in Figure 23 [DTN # LL000115905924.113]

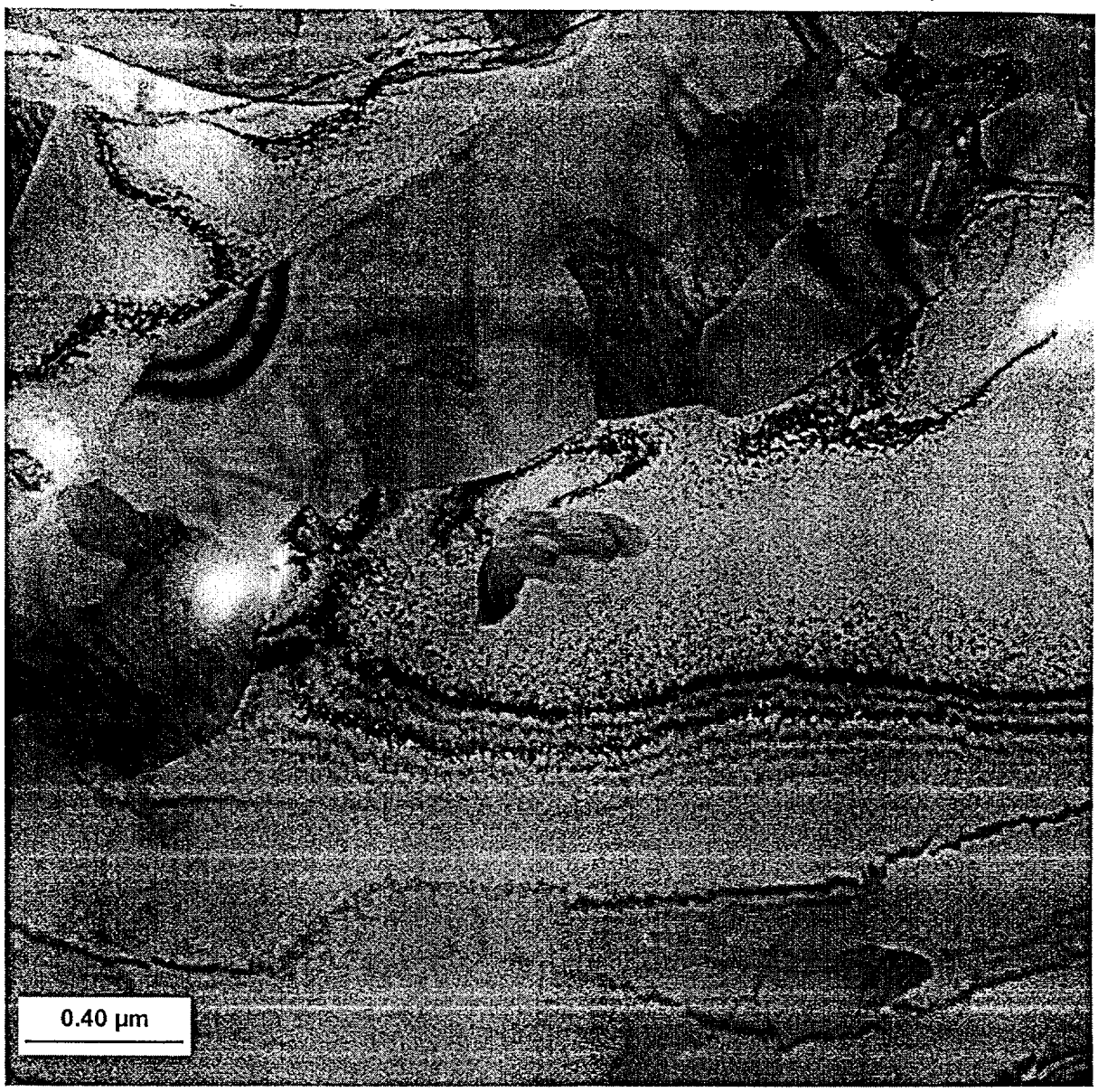


TS_AMR_fig4-22

NOTE: The larger, brighter phase was tentatively identified as σ phase. The smaller, darker particles appear to be µ phase. (TS369-009a, Image 1880, 10/12/98, SN #393, p. 86)

Figure 25. Grain Boundary Precipitation in Alloy 22 Aged for 16,000 hr at 704°C [DTN # LL000115905924.113]

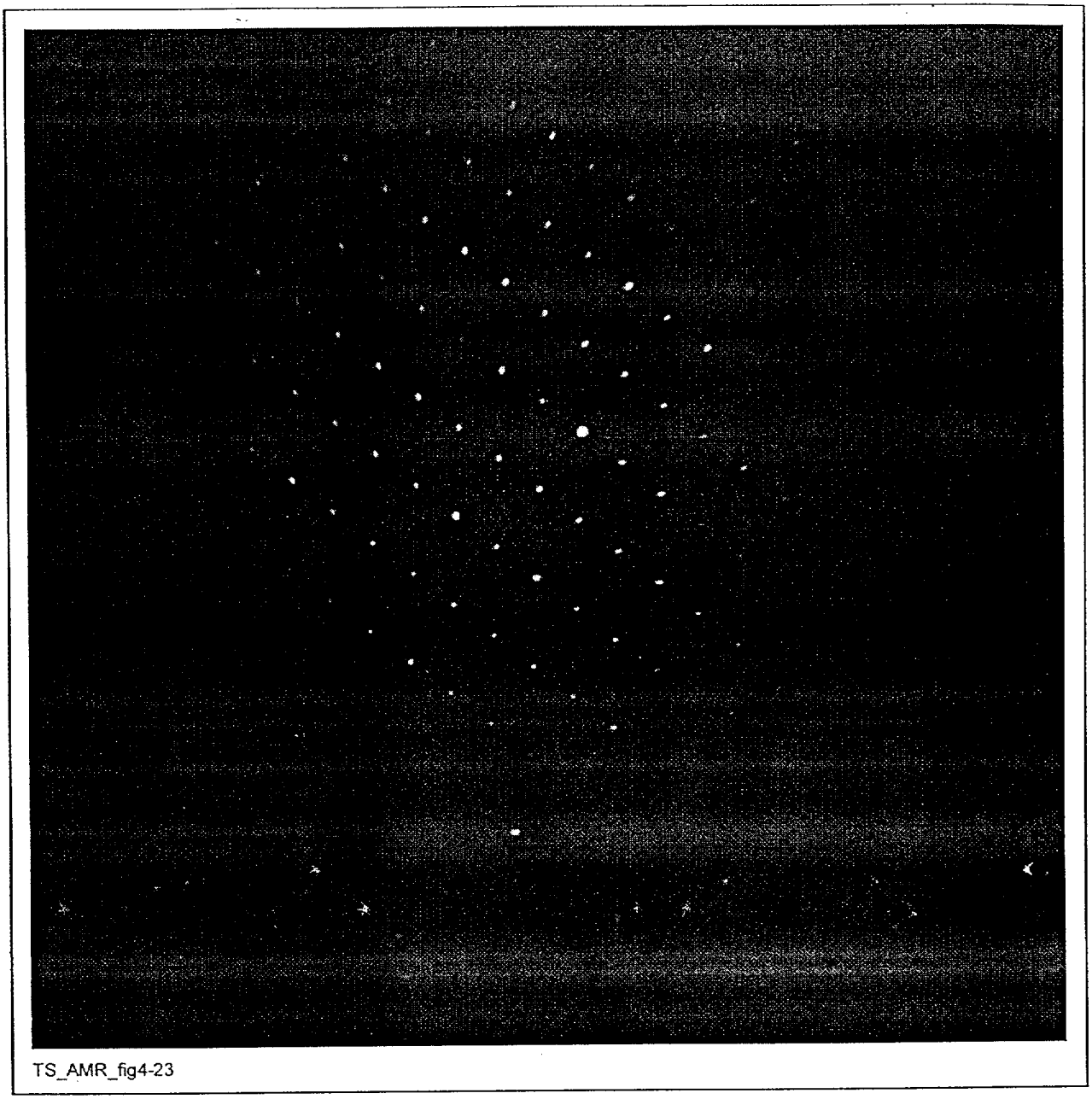

TS_AMR_fig4-23

NOTE: (TS369-009a, Image 1881, 10/12/98, SN #393, p. 87)

Figure 26. SAD Pattern from σ Phase in Figure 25 [DTN # LL000115905924.113]

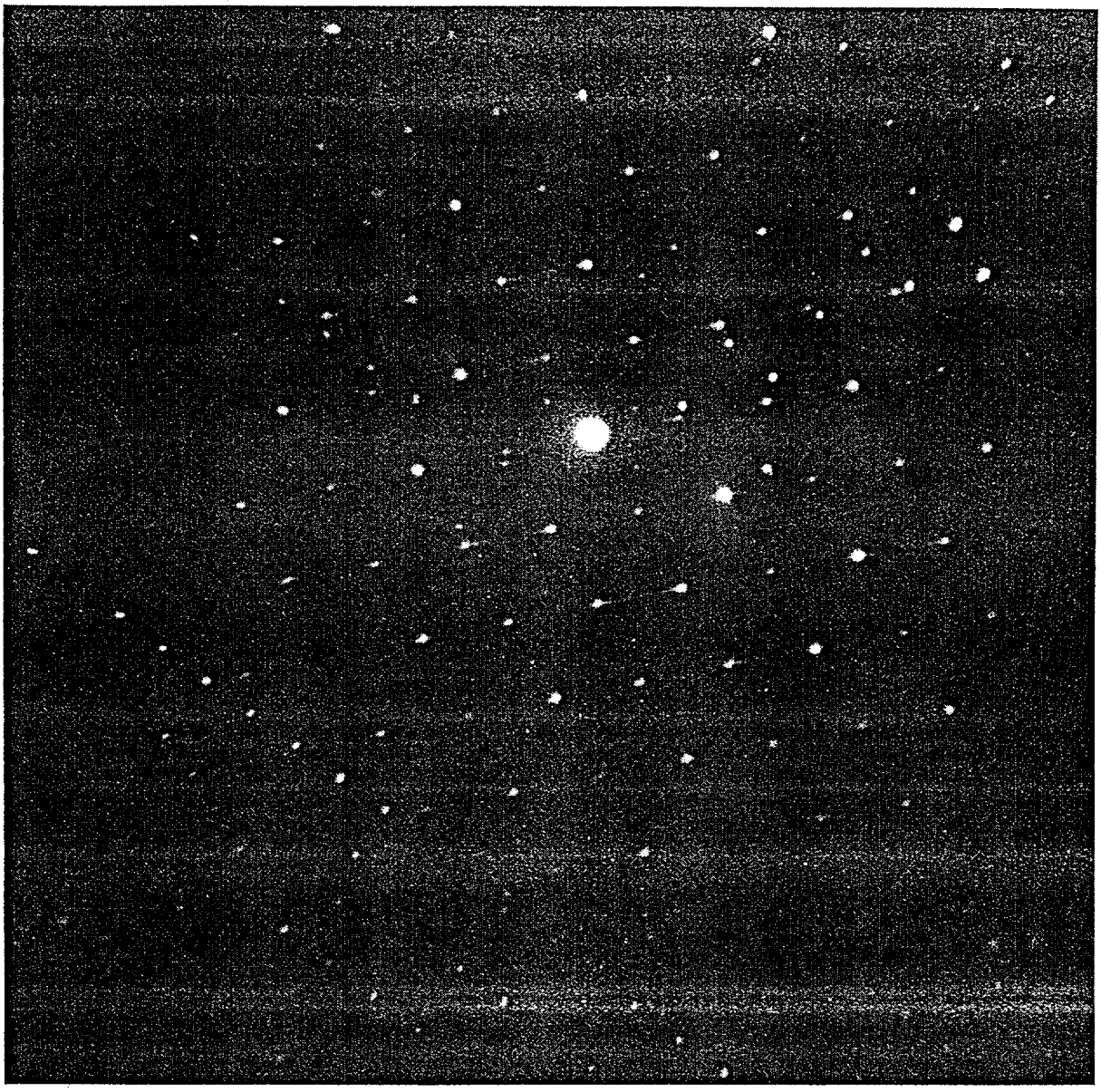

TS_AMR_fig4-24

NOTE: These precipitates were tentatively identified as μ phase. (TS369-009a, Image 1882, 10/12/98, SN #393, p. 89)

Figure 27. SAD Pattern from the Small, Dark Particles in Figure 25 [DTN # LL000115905924.113]

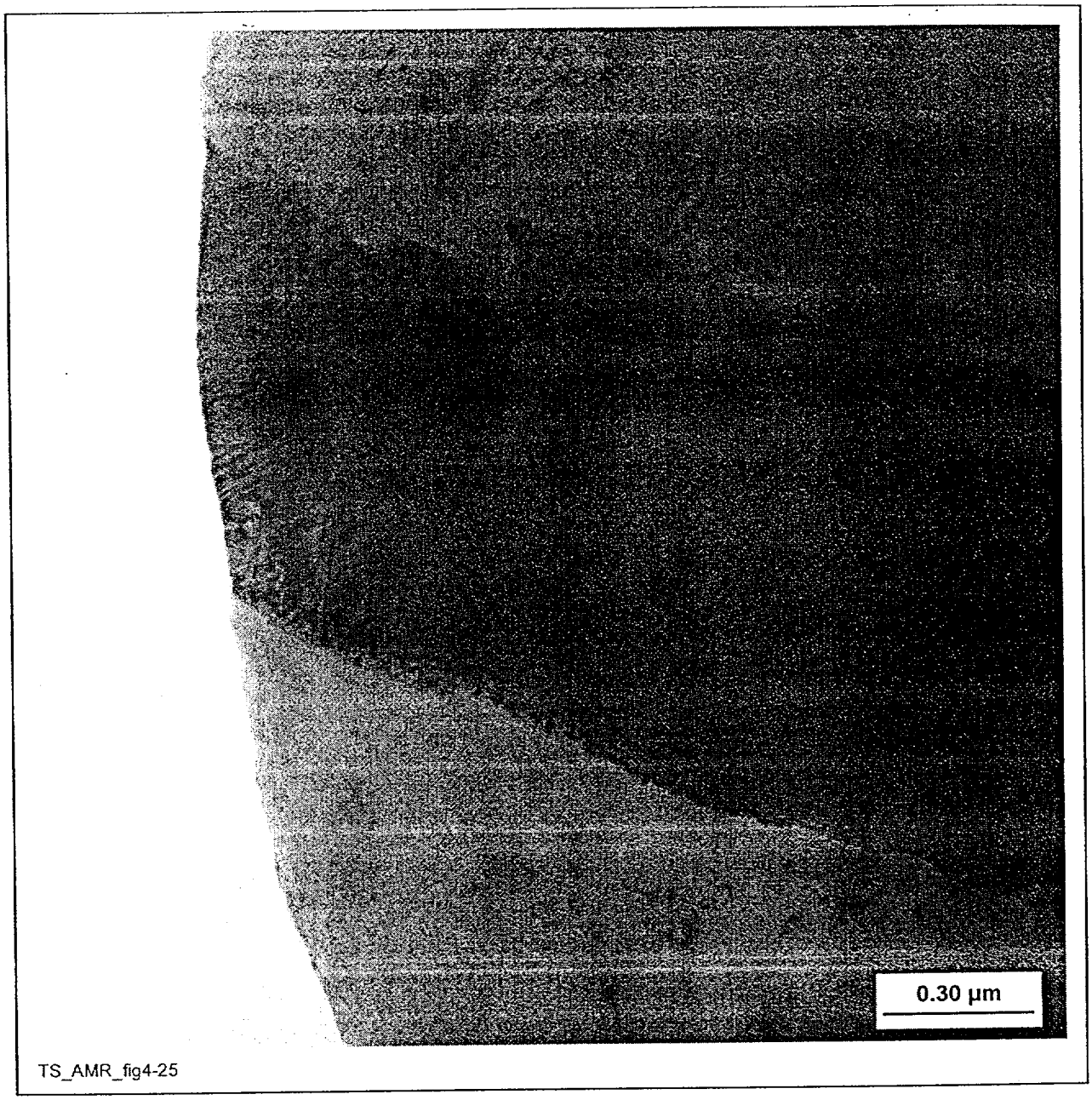


NOTE: This phase was identified as P'phase. (TS369-004a, Image S0037, 2/16/99, SN #434, p. 63)

Figure 28. Precipitate in Alloy 22 Aged for 16,000 hr at 760°C [DTN # LL000115905924.113]

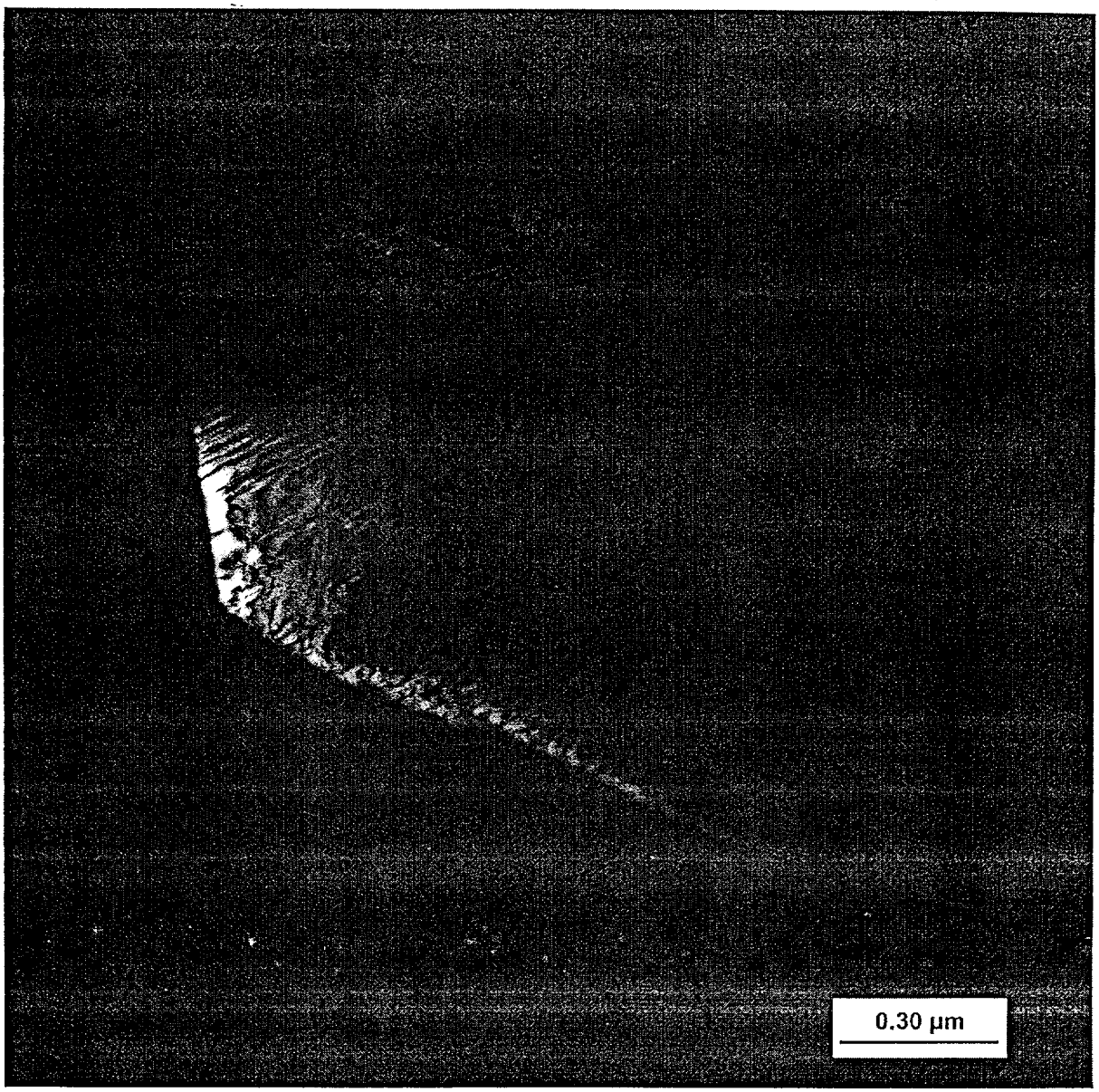


NOTE: The precipitate identified as P phase appears light. (TS369-004a, Image S0038, 2/16/99, SN #434, p. 63)

Figure 29. Dark-Field Image Corresponding to Figure 28 [DTN # LL000115905924.113]

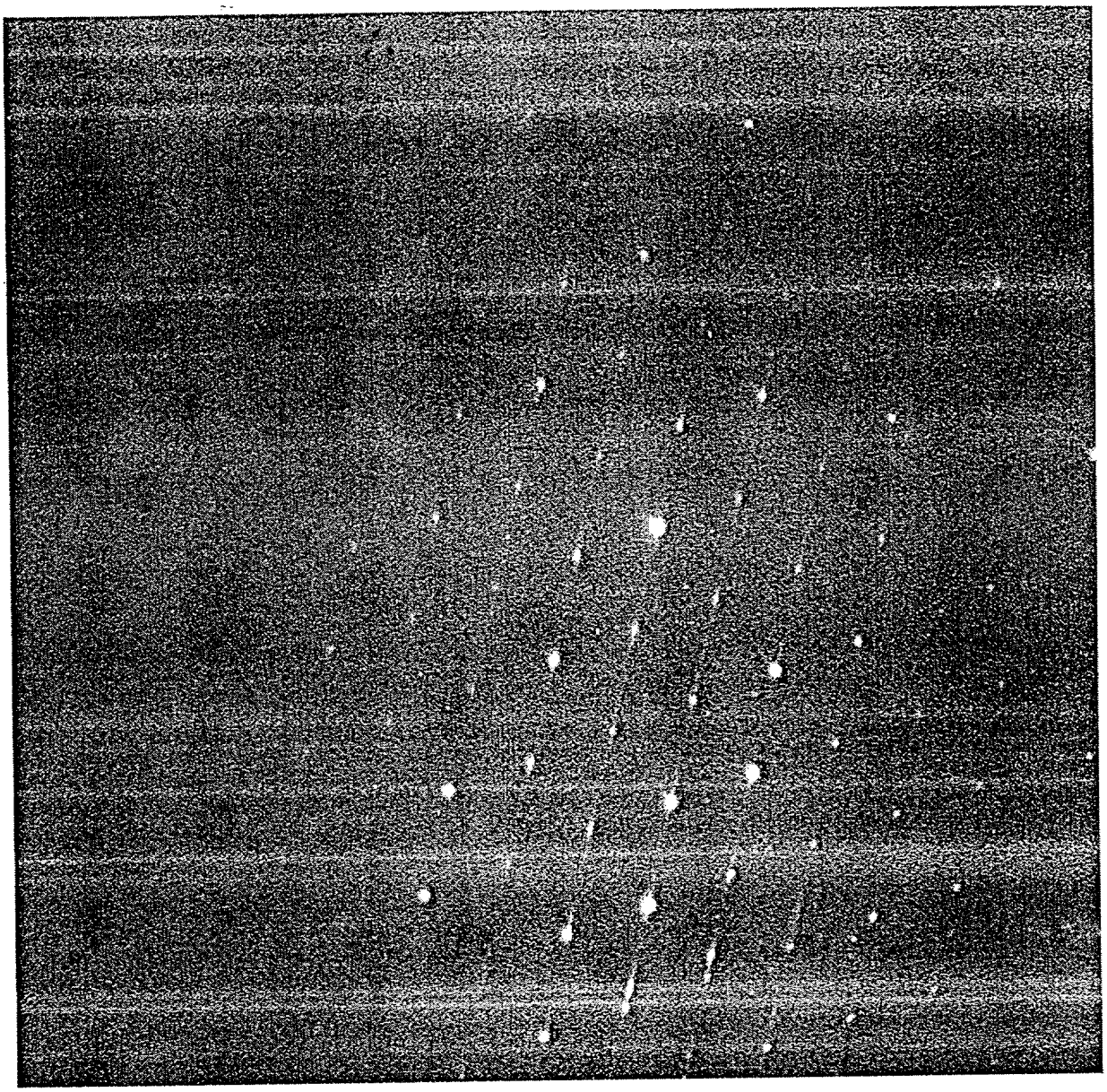

TS_AMR_fig4-27

NOTE: (TS369-004a, Image S0036, 2/16/99, SN #434, p. 64)

Figure 30. SAD Pattern from the P Phase Precipitate Shown in Figures 28 and 29 [DTN # LL000115905924.113]


NOTE: The larger, brighter phase was identified as σ. The smaller precipitates are either µ or P phase. (TS369-004a, Image 1300, 3/14/98, SN #369, p. 66)

Figure 31. Grain Boundary Precipitation in Alloy 22 Aged for 16,000 hr at 760°C [DTN # LL000115905924.113]


NOTE: [TS369-004a, Image 1306, tilted (–11,–9) from image 1300, 3/14/98, SN #369, p. 98]

Figure 32. SAD Pattern from the σ Phase Precipitate Shown in Figure 31 [DTN # LL000115905924.113]

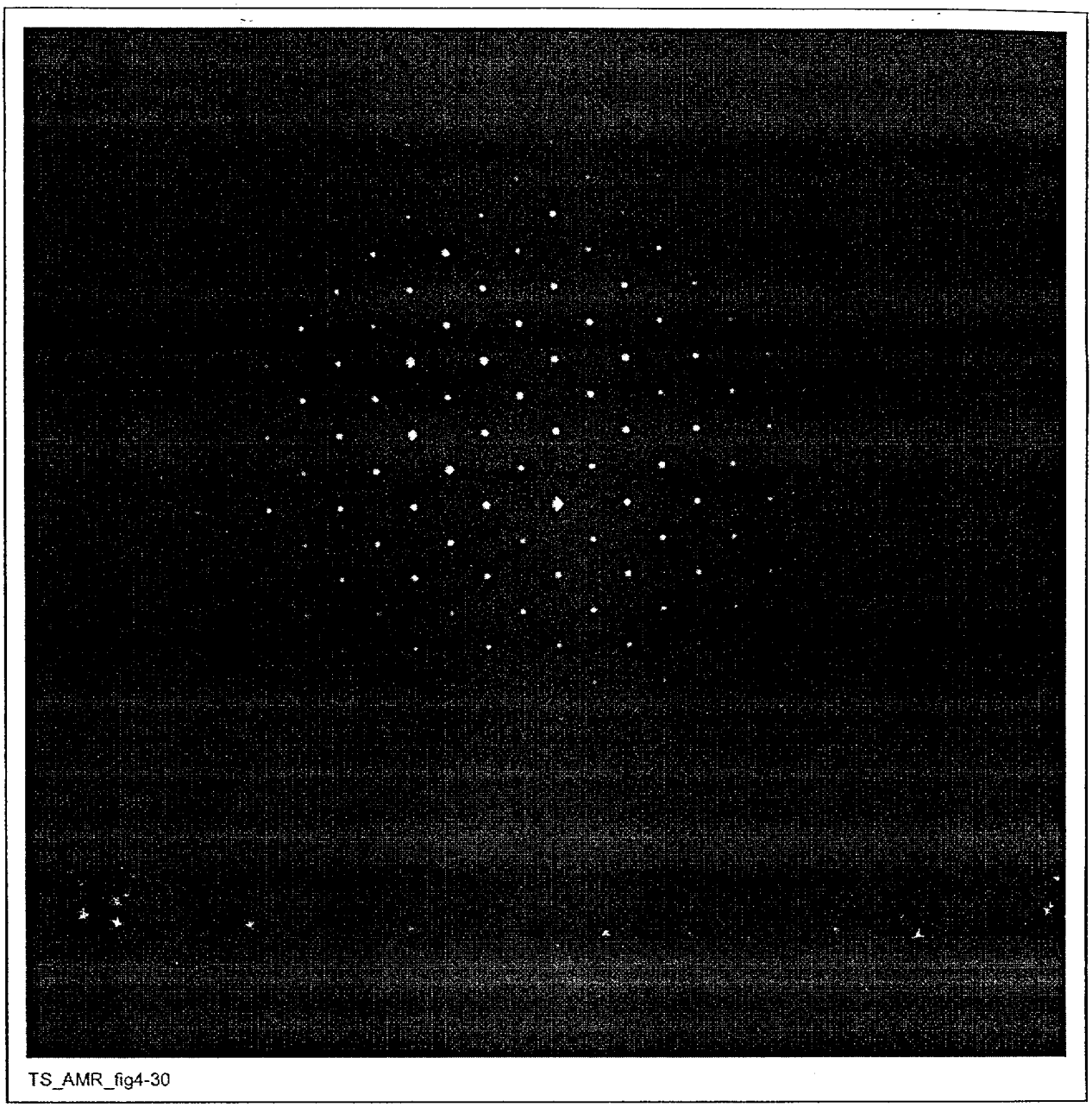


NOTE: [TS369-004a, Image 1307, tilted (–10,+18) from image 1300, 3/14/98, SN #369, p. 106]

Figure 33. SAD Pattern from the σ Phase Precipitate Shown in Figure 31 [DTN # LL000115905924.113]

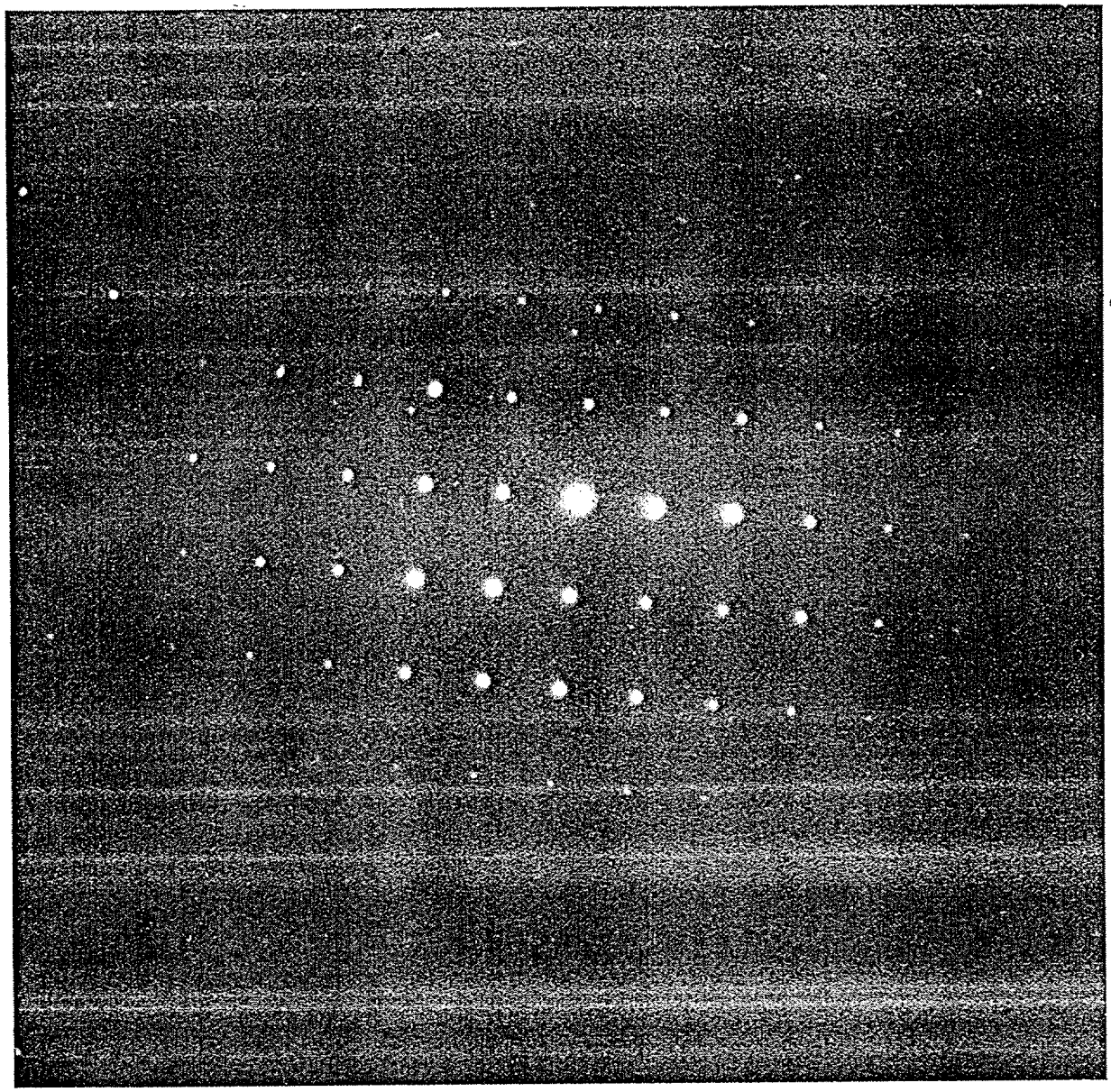

TS_AMR_fig4-31

NOTE: [TS369-004a, Image 1308, tilted (–35,–2) from image 1300, 3/14/98, SN #369, p. 113]

Figure 34. SAD Pattern from the σ Phase Precipitate Shown in Figure 31 [DTN # LL000115905924.113]

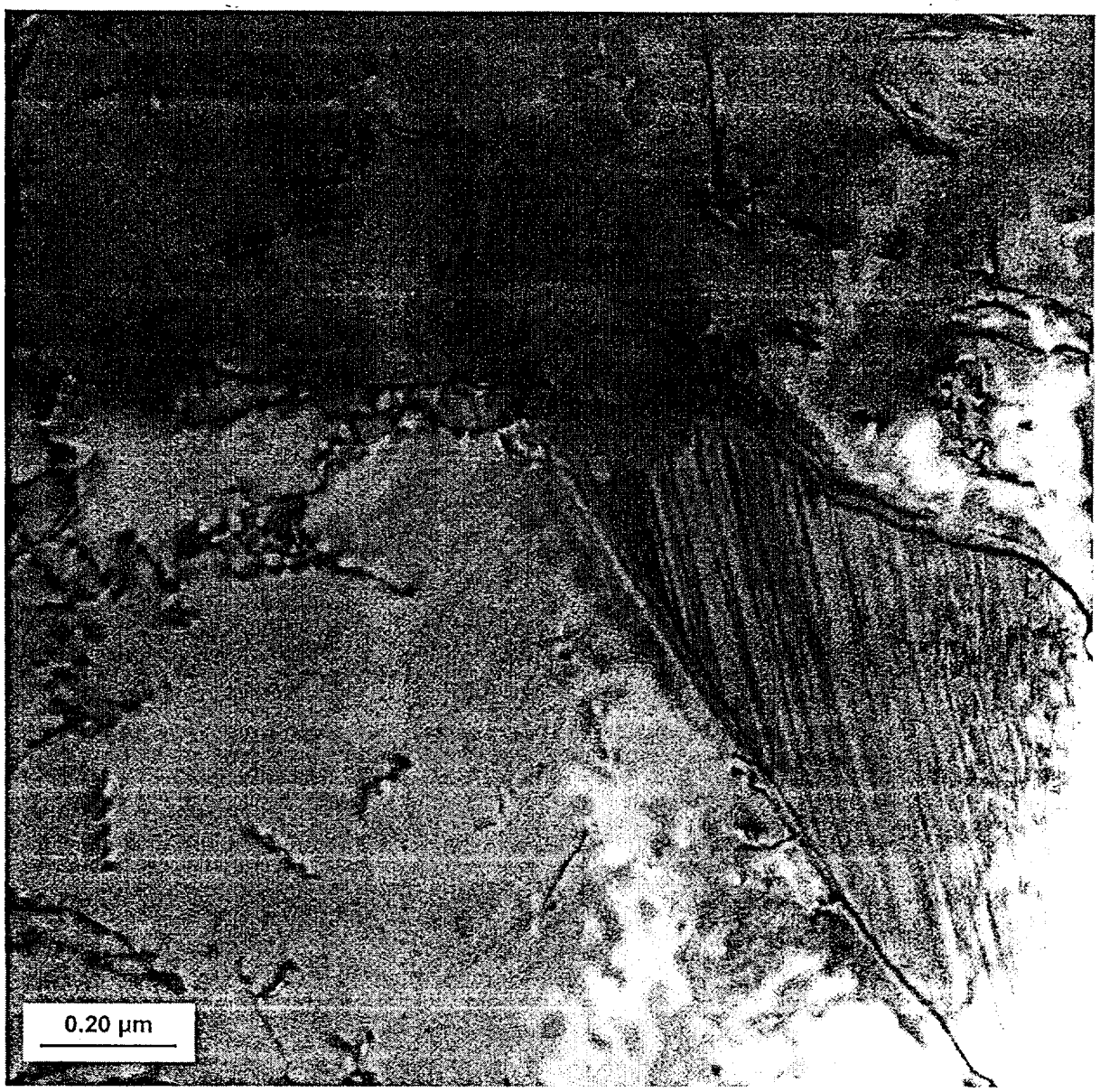


NOTE: This phase was tentatively identified as µ phase. (TS369-004a, Image 1312, 3/14/98, SN #393, p. 11)

Figure 35. Precipitation in Alloy 22 Aged for 16,000 hr at 760°C [DTN # LL000115905924.113]

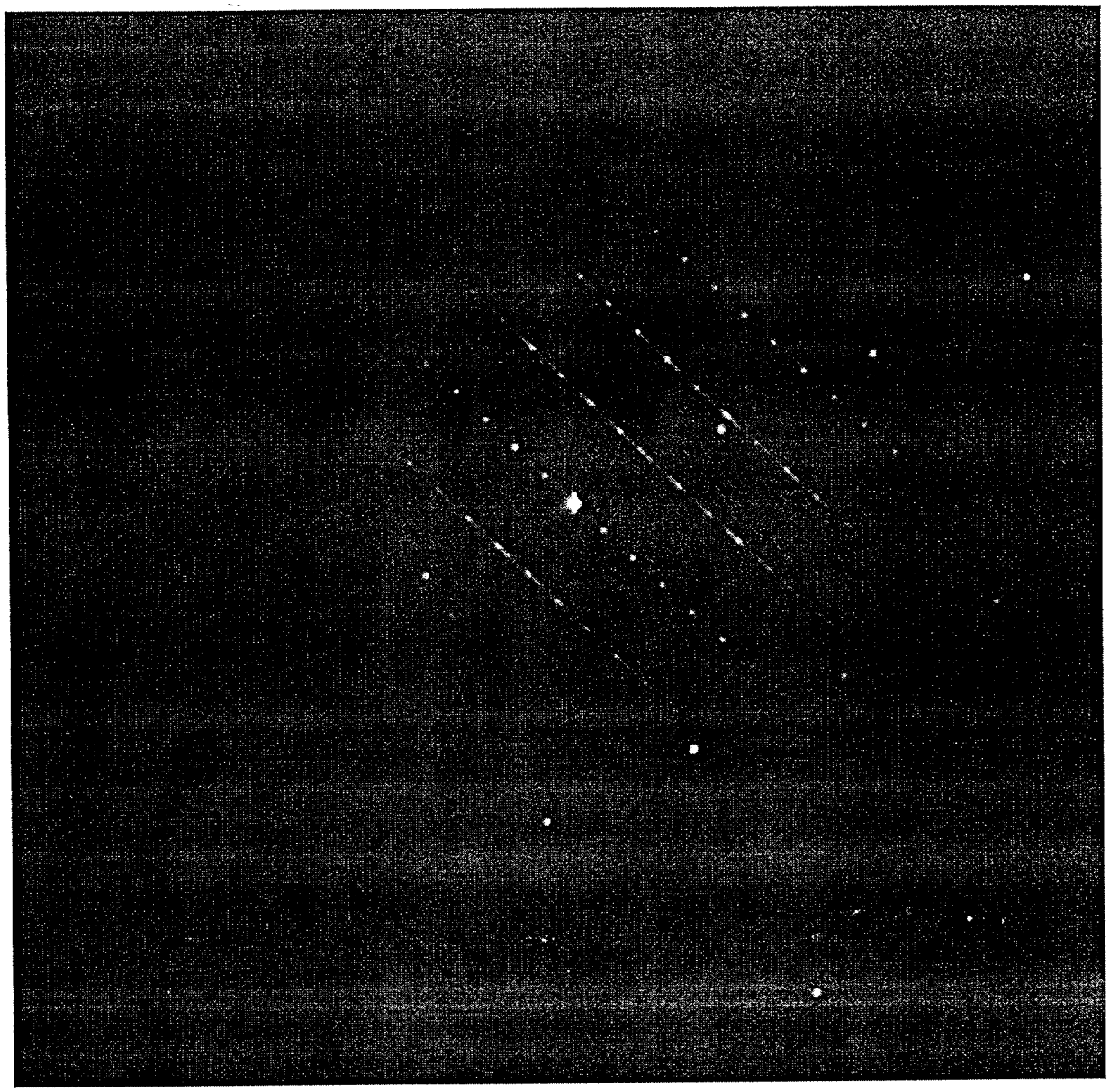

TS_AMR_fig4-33

NOTE: (TS369-004a, Image 1314, 3/14/98, SN #393, p. 13)

Figure 36. SAD Pattern from the μ Phase Precipitate Shown in Figure 35 [DTN # LL000115905924.113]

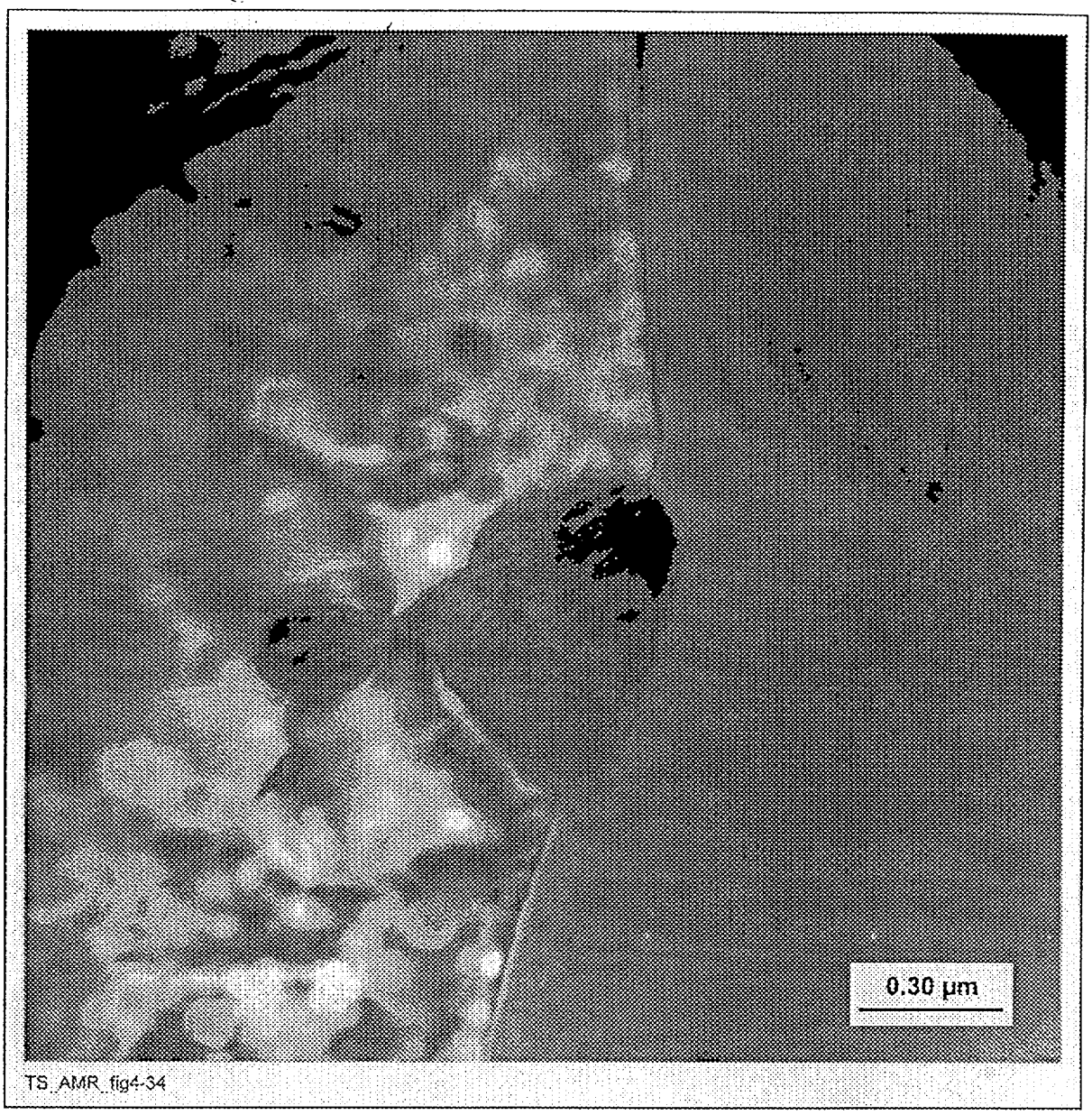


NOTE: This phase was identified as µ phase. (TS369-004a, Image 1309, 3/14/98, SN #369, p. 135)

Figure 37. Grain Boundary Precipitation in Alloy 22 Aged for 16,000 hr at 760°C [DTN # LL000115905924.113]

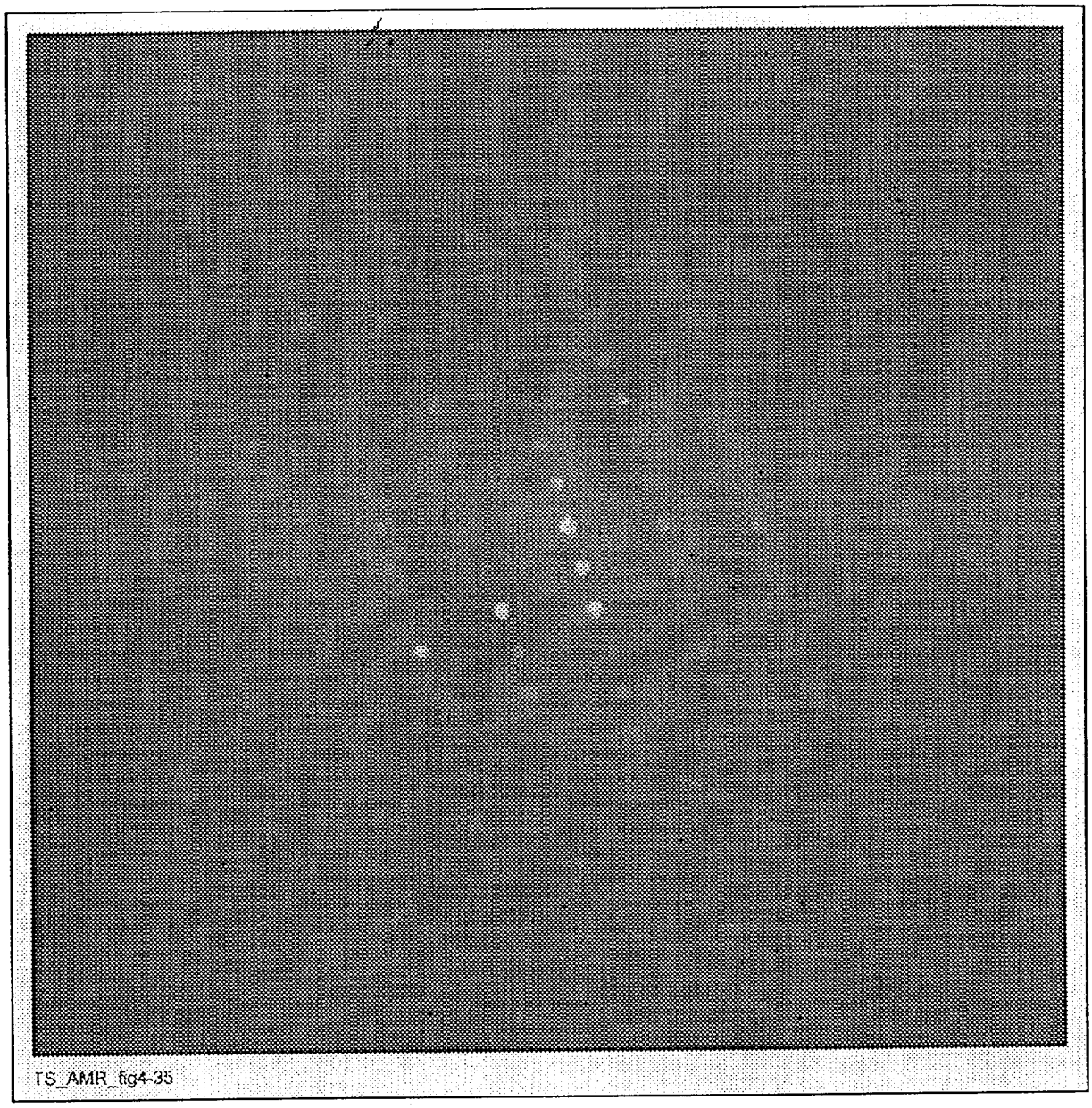


NOTE: (TS369-004a, Image 1310, 3/14/98, SN #369, p. 150)

Figure 38. SAD Pattern from the μ Phase Precipitate Shown in Figure 37 [DTN # LL000115905924.113]

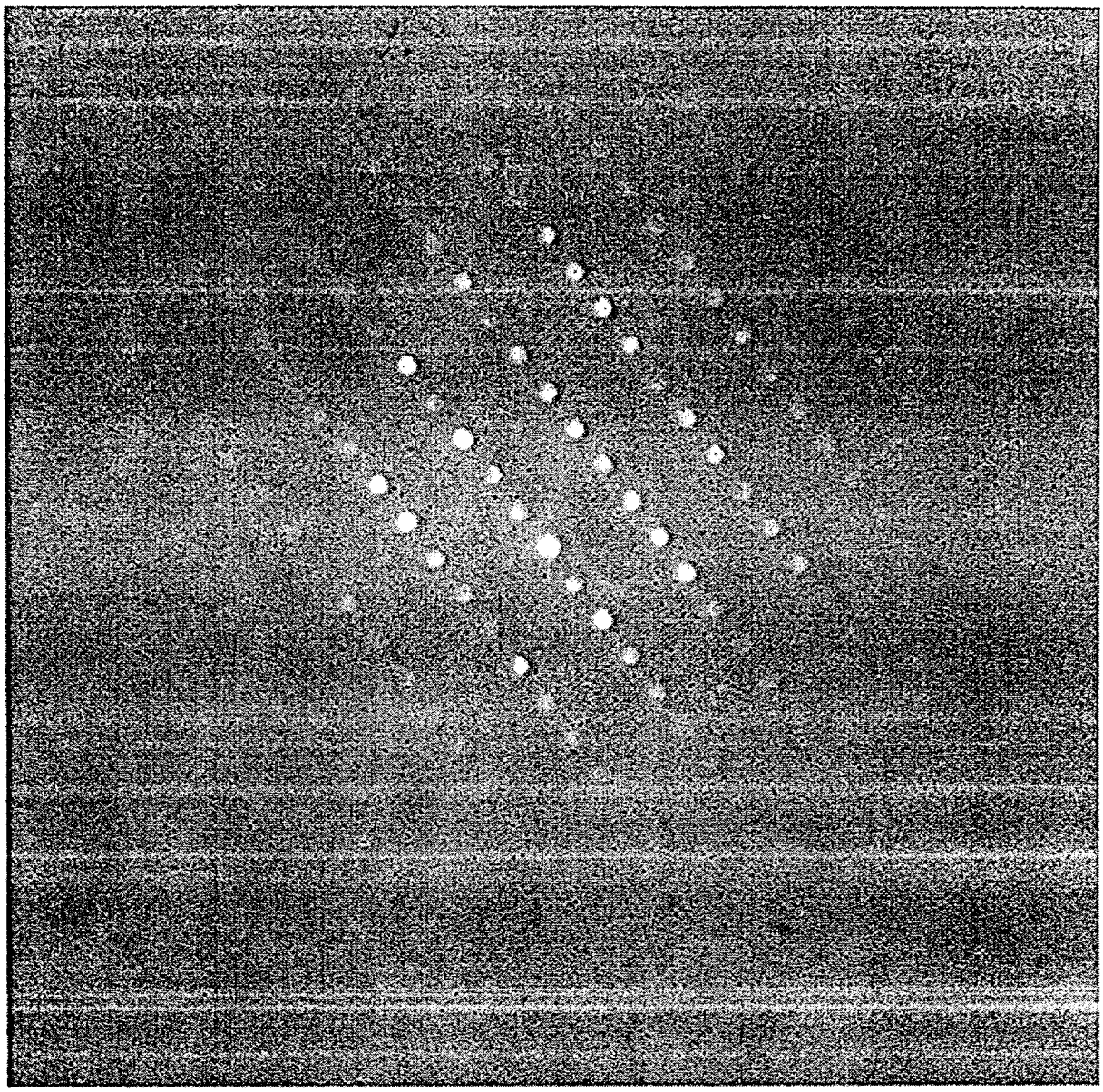

TS_AMR_fig4-36

NOTE: (TS369-004a, Image 1311, 3/14/98, SN #369, p. 153)

Figure 39. SAD Pattern from the μ Phase Precipitate in Figure 37 [DTN # LL000115905924.113]

### 4.1.2 Micrographs Showing Precipitation in Alloy 22 Beginning on and Covering Grain Boundaries, Beginning on Twin Boundaries, and Beginning within the Grains

This section contains optical and scanning electron microscopy (SEM) images (Figures 40 through 63) used to determine the time at which the various stages of intermetallic and carbide precipitation occur in Alloy 22 base metal after aging in the temperature range of 600 to 800°C. No distinction has been made between the various intermetallics and the carbides that form in Alloy 22. The intermetallic phases $\mu$, P, and $\sigma$ are virtually indistinguishable in the SEM, and there is relatively little carbide precipitation.

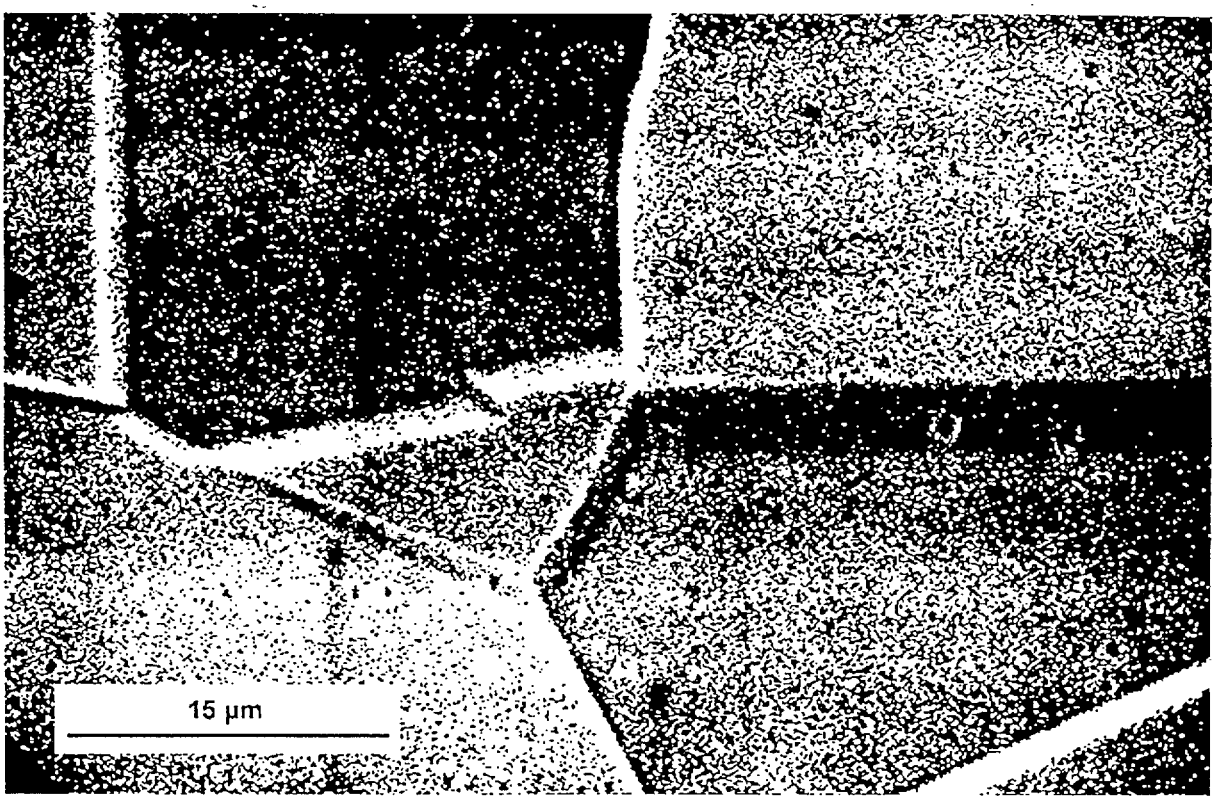


NOTE: (TS393-028a, 2/15/99, SN #434, p. 7)

Figure 40. SEM Micrograph Showing Precipitation Just Beginning on Grain Boundaries After Aging Alloy 22 for 10 hr at 593°C [DTN # LL000115905924.113]

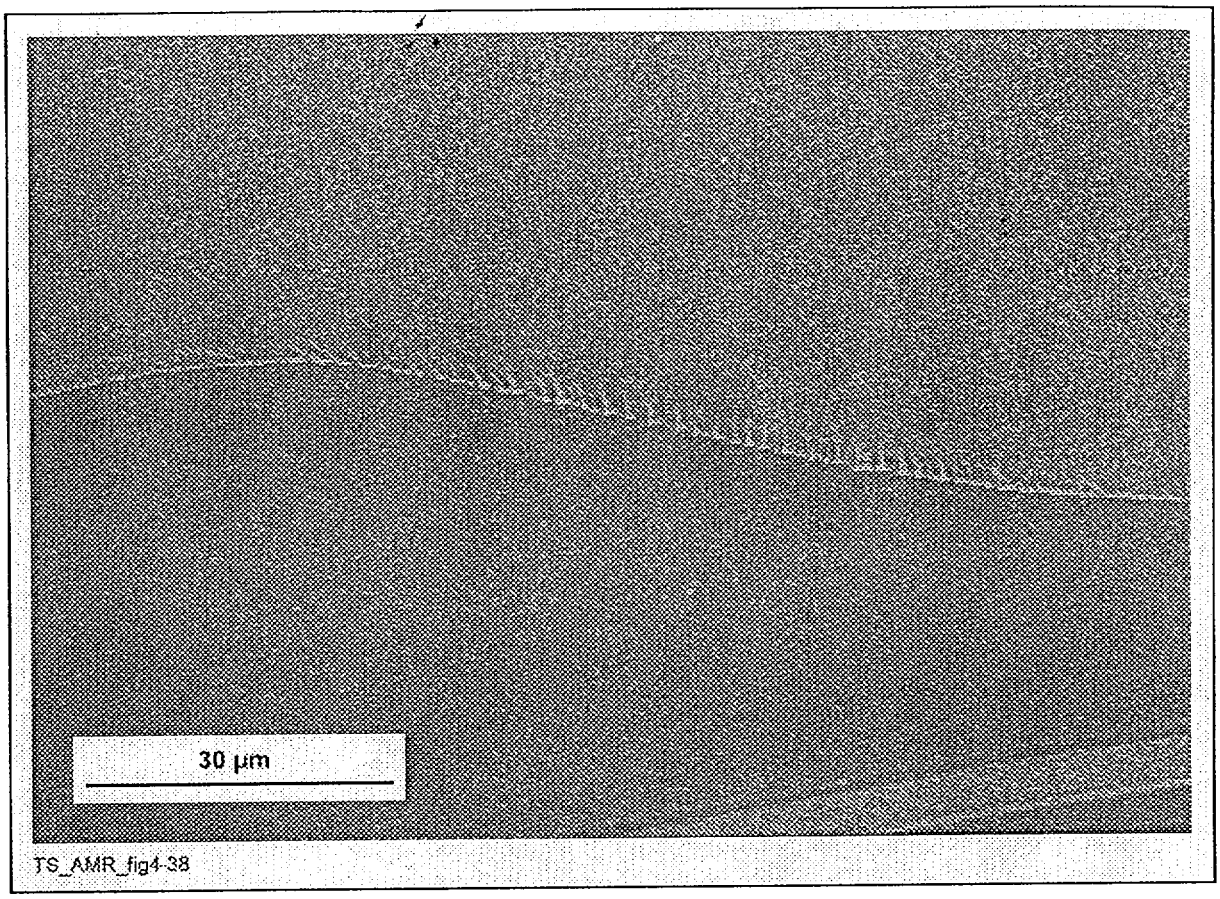


NOTE: (TS393-029a, 2/15/99, SN #434, p. 8)

Figure 41. SEM Micrograph Showing Precipitation on Grain Boundaries After Aging Alloy 22 for 100 hr at 593°C [DTN # LL000115905924.113]

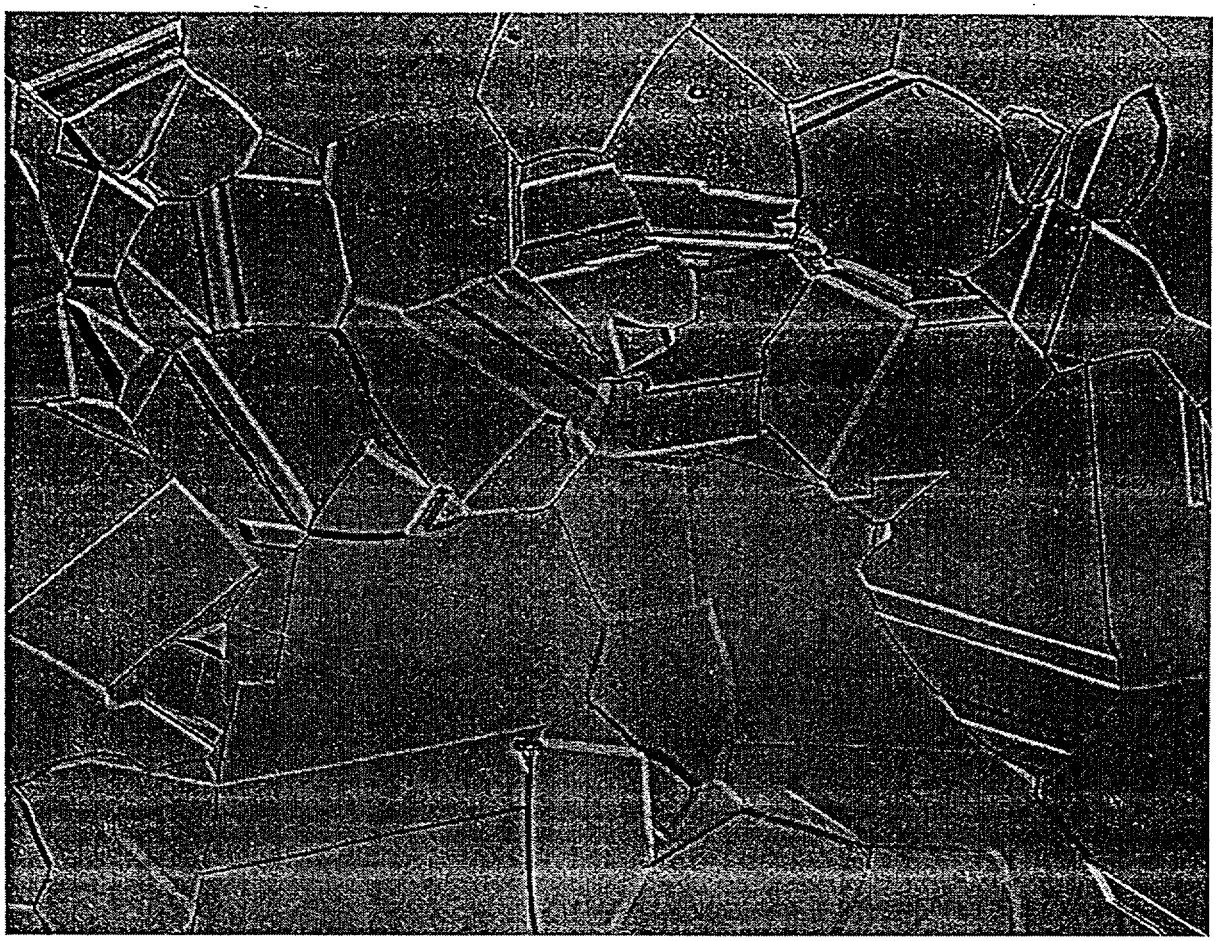

TS_AMR_fig4-39

NOTE: (TS393-008a, 12/7/98, SN#434, p. 10)

Figure 42. Optical Micrograph Showing No Precipitation on Grain Boundaries After Aging Alloy 22 for 1 hr at 649°C [DTN # LL000115905924.113]

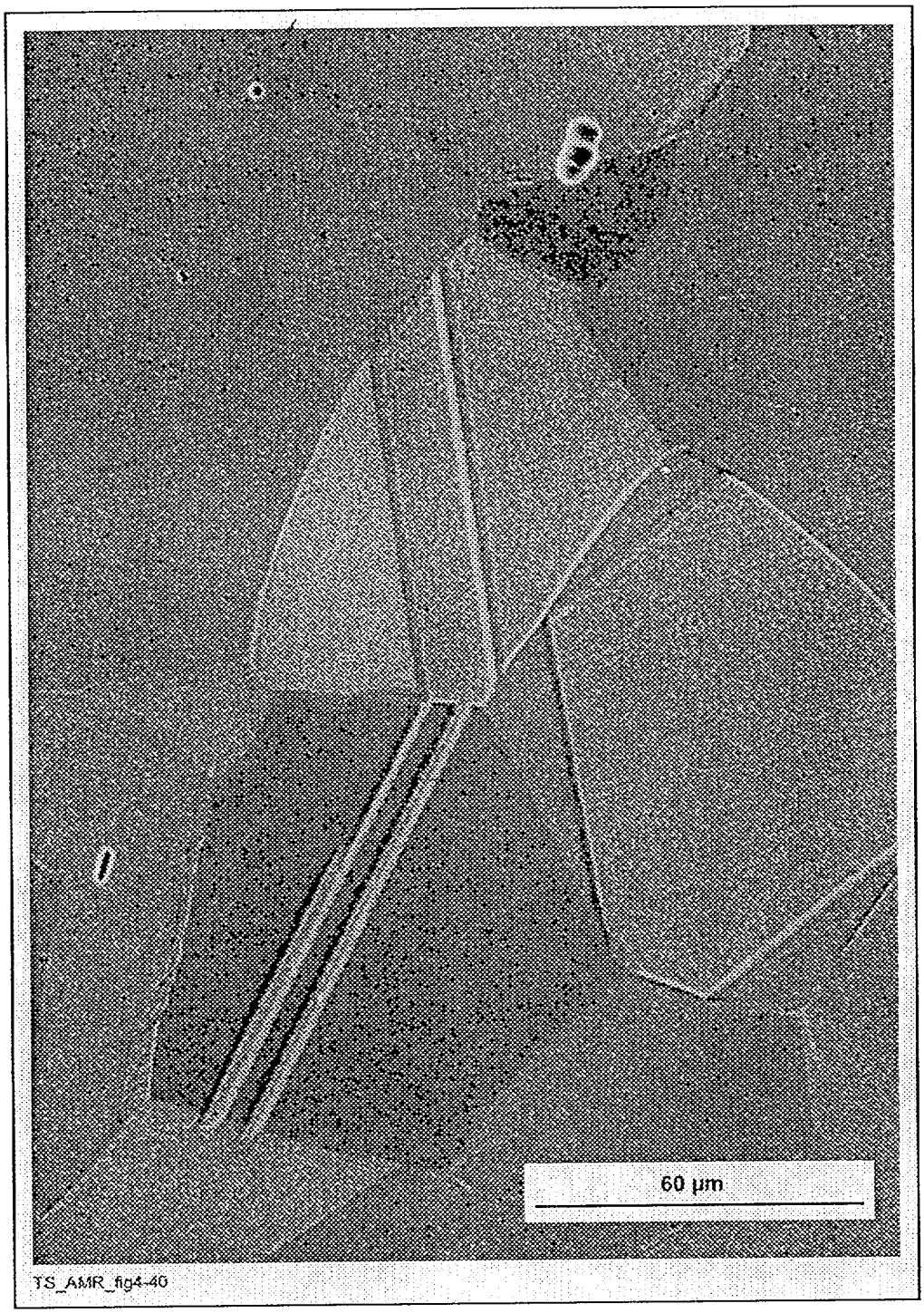


NOTE: (TS393-008a, 12/7/98, SN #434, p. 10)

Figure 43. SEM Micrograph Showing Little or no Precipitation on Grain Boundaries After Aging Alloy 22 for 1 hr at 649°C [DTN # LL000115905924.113]

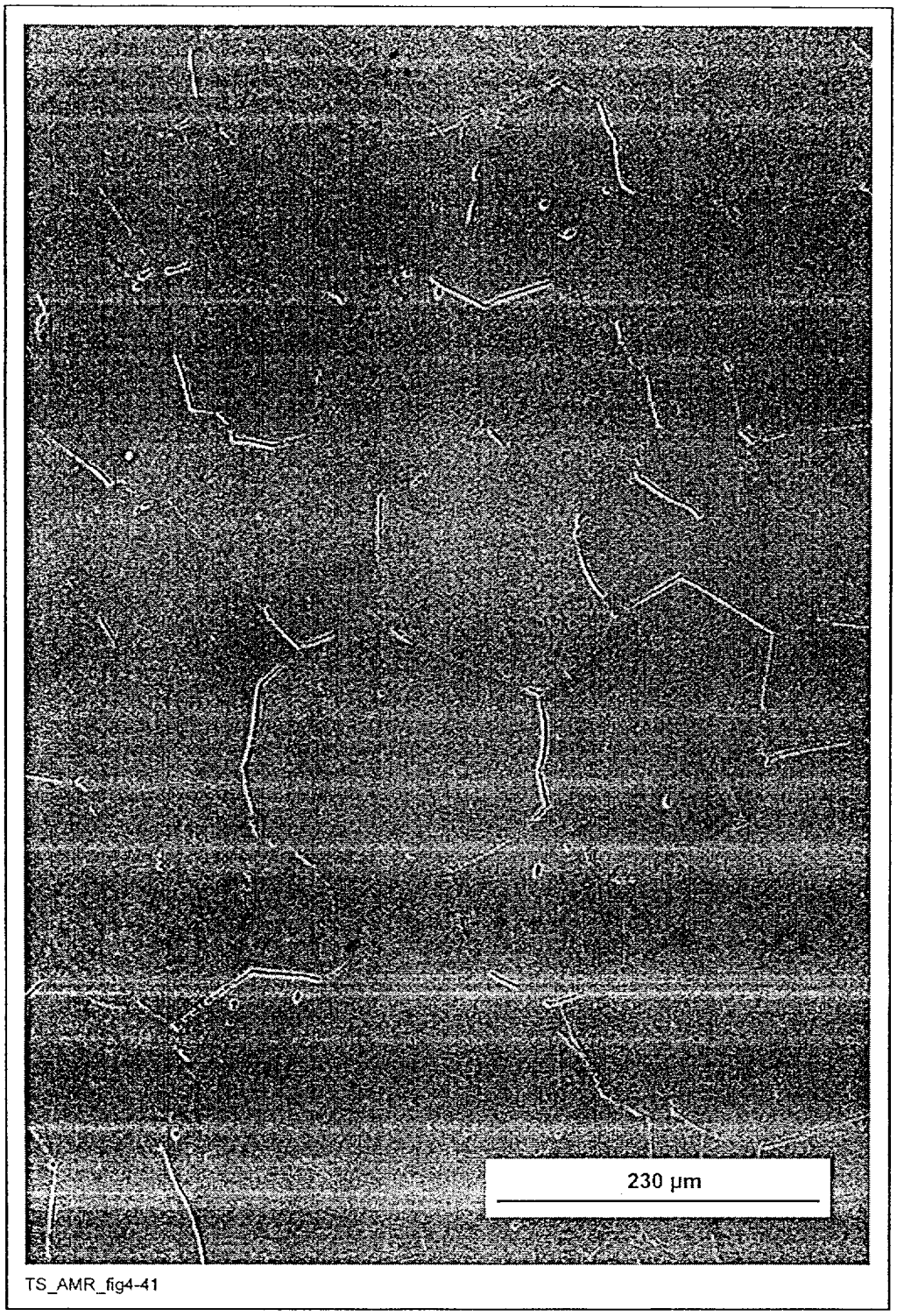


NOTE: (TS393-009a, 12/7/98, SN #434, p. 11)

Figure 44. SEM Micrograph Showing Precipitation on Grain Boundaries After Aging Alloy 22 for 10 hr at 649°C [DTN # LL000115905924.113]


NOTE: (TS393-010a, 12/7/98, SN #434, p. 12)

Figure 45. SEM Micrograph Showing Precipitation on Grain Boundaries After Aging Alloy 22 for 100 hr at 649°C [DTN # LL000115905924.113]

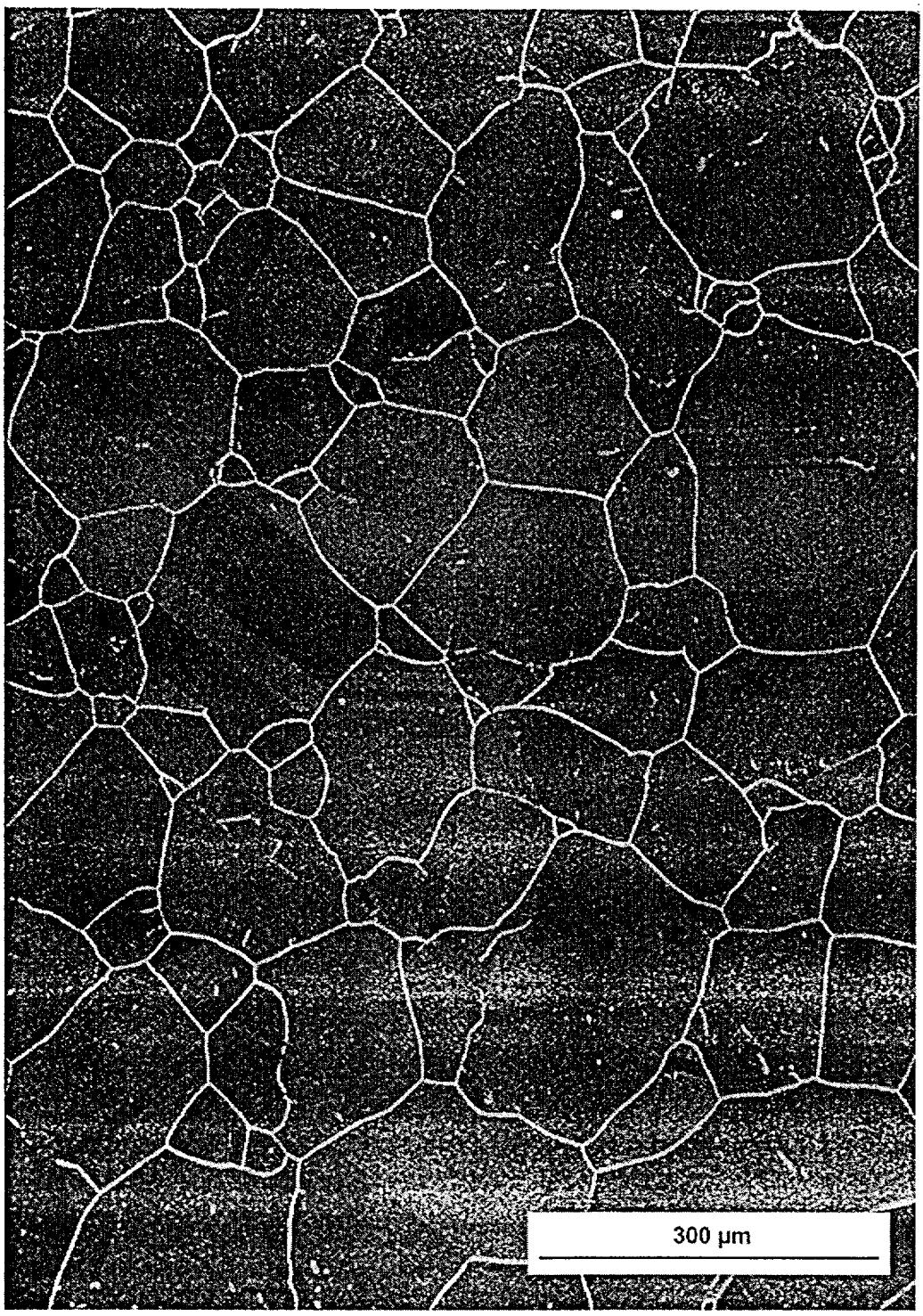


TS_AMR_fig4-43

NOTE: (TS393-011a, 12/7/98, SN #434, p. 12)

Figure 46. SEM Micrograph Showing Precipitation on Grain Boundaries After Aging Alloy 22 for 1000 hr at 649°C [DTN # LL000115905924.113]

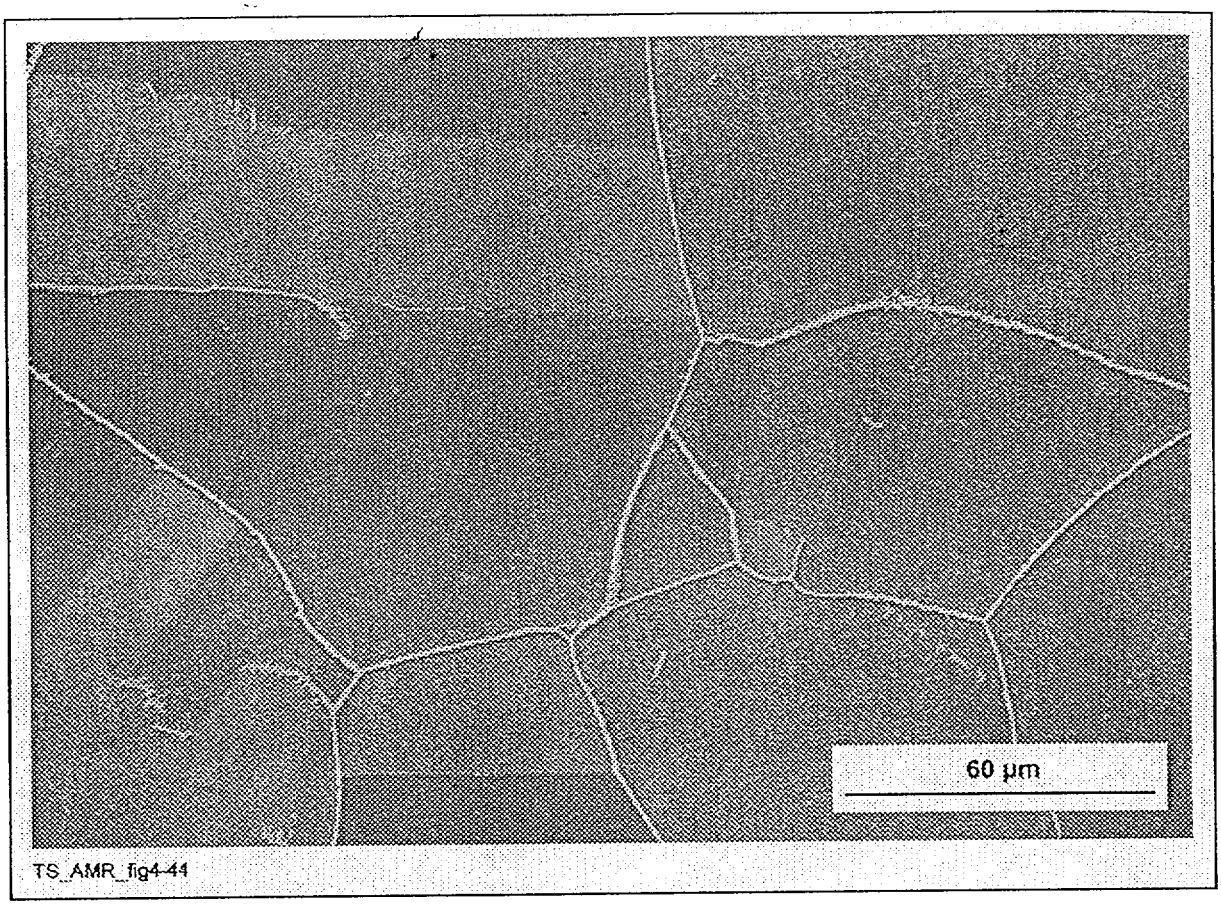


NOTE: (TS393-011a, 12/7/98, SN #434, p. 13)

Figure 47. SEM Micrograph Showing Precipitation on Grain and on Twin Boundaries After Aging Alloy 22 for 1000 hr at 649°C [DTN # LL000115905924.113]

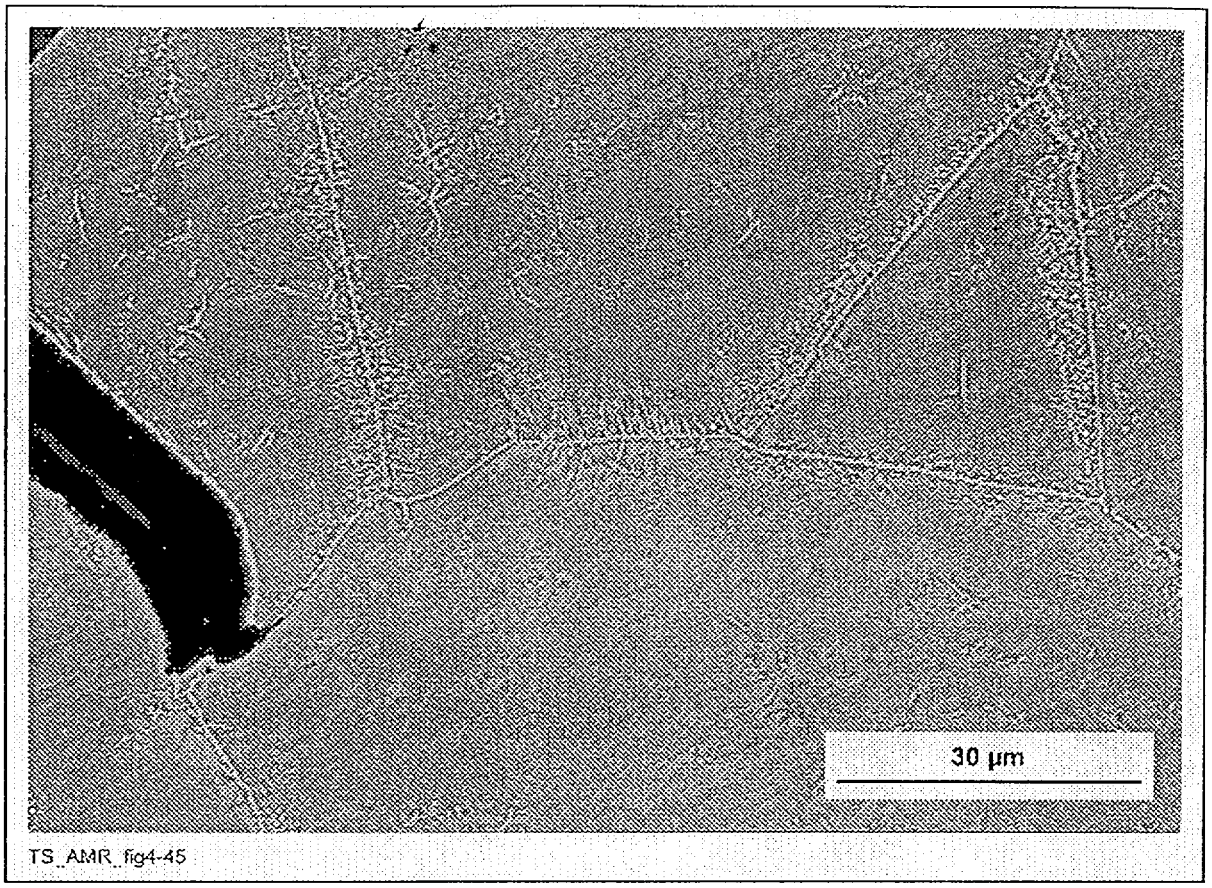


NOTE: (TS369-008b, 8/28/98, SN #434, p. 14)

Figure 48. SEM Micrograph Showing Precipitation on Grain Boundaries and Within the Grains After Aging Alloy 22 for 16,000 hr at 649°C [DTN # LL000115905924.113]

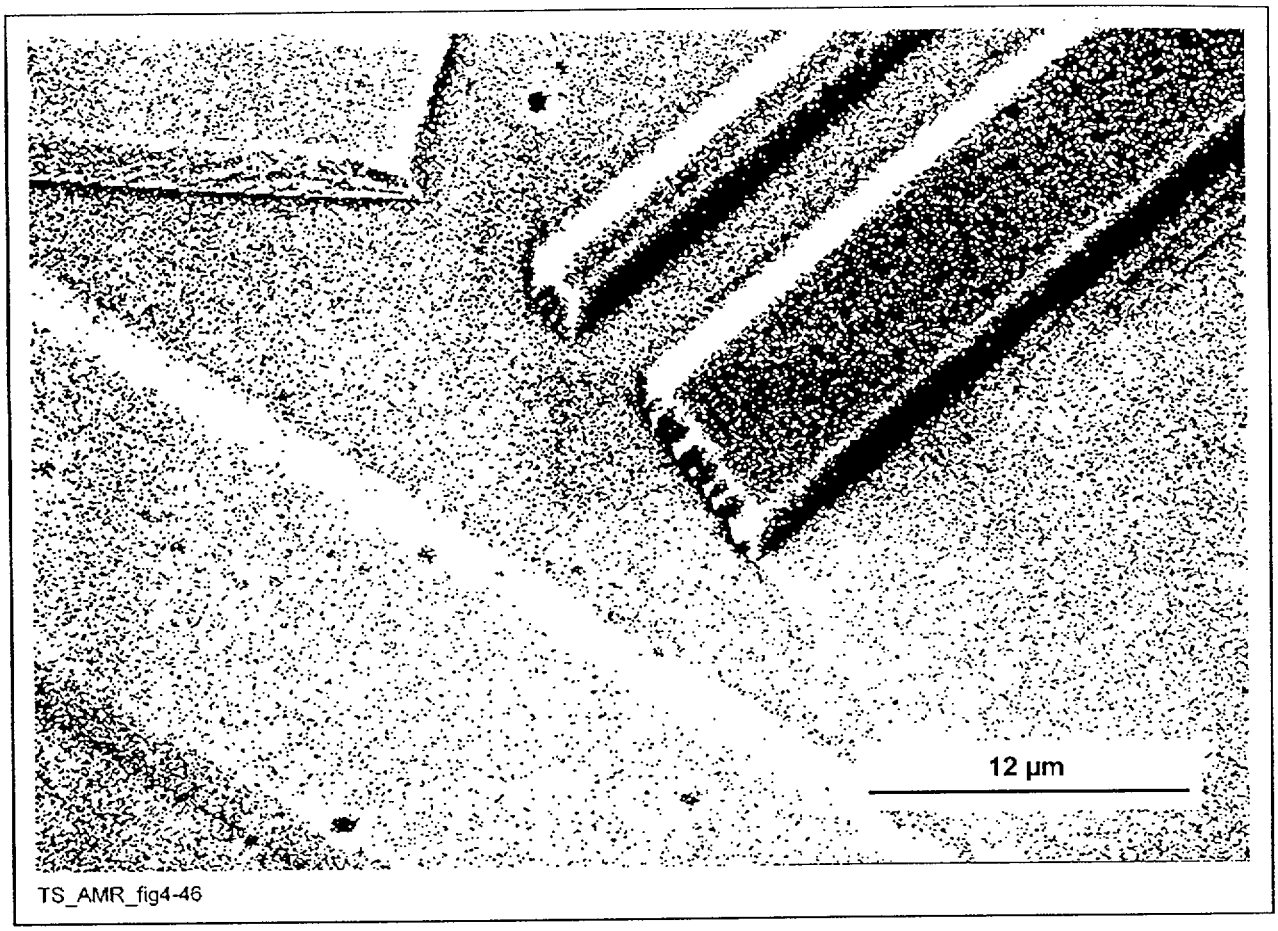


NOTE: (TS393-012a, 12/7/98, SN #434, p. 15)

Figure 49. SEM Micrograph Showing Precipitation That Occurs at a Limited Number of Sites on Grain Boundaries in Alloy 22 After Aging for 1 hr at 704°C [DTN # LL000115905924.113]

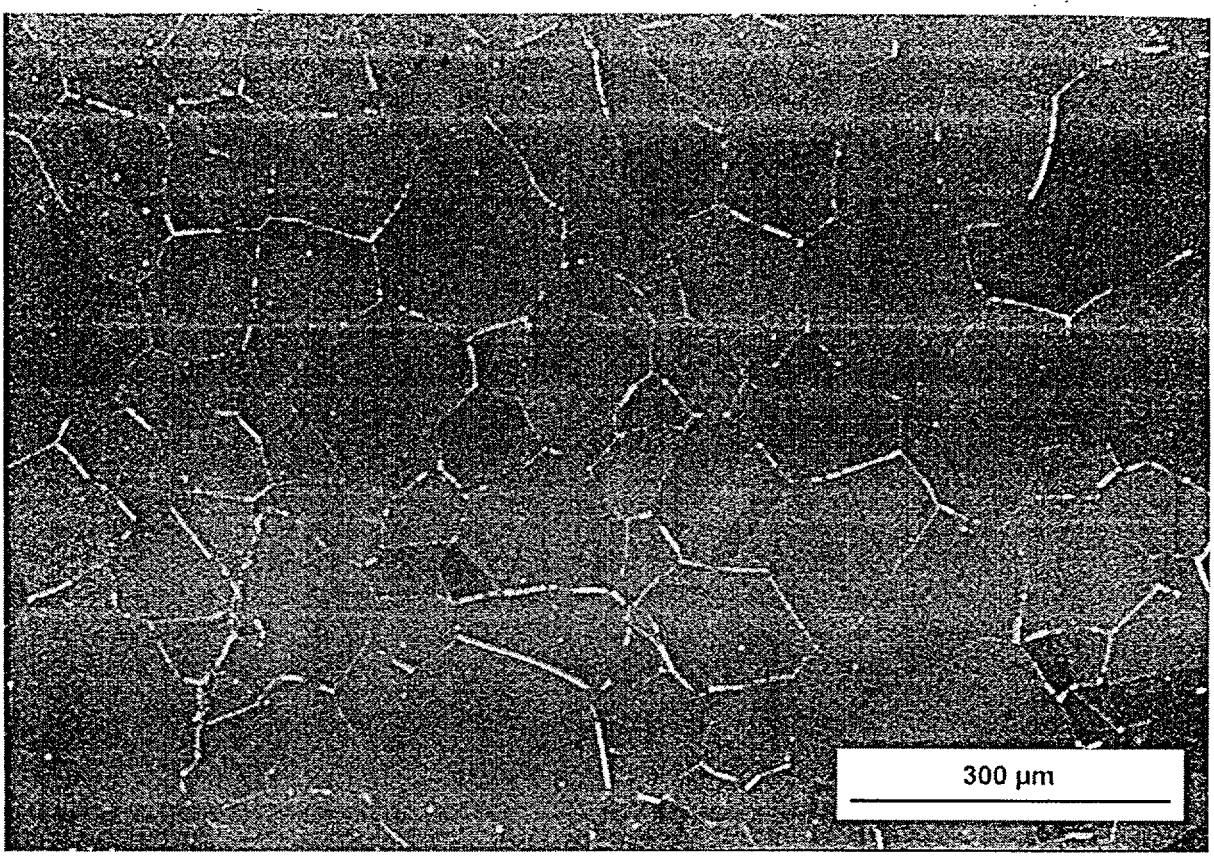


TS_AMR_fig4-47

NOTE: (TS393-013a, 12/7/98, SN #434, p. 15)

Figure 50. SEM Micrograph Showing Precipitation on Grain Boundaries After Aging Alloy 22 for 10 hr at 704°C [DTN # LL000115905924.113]

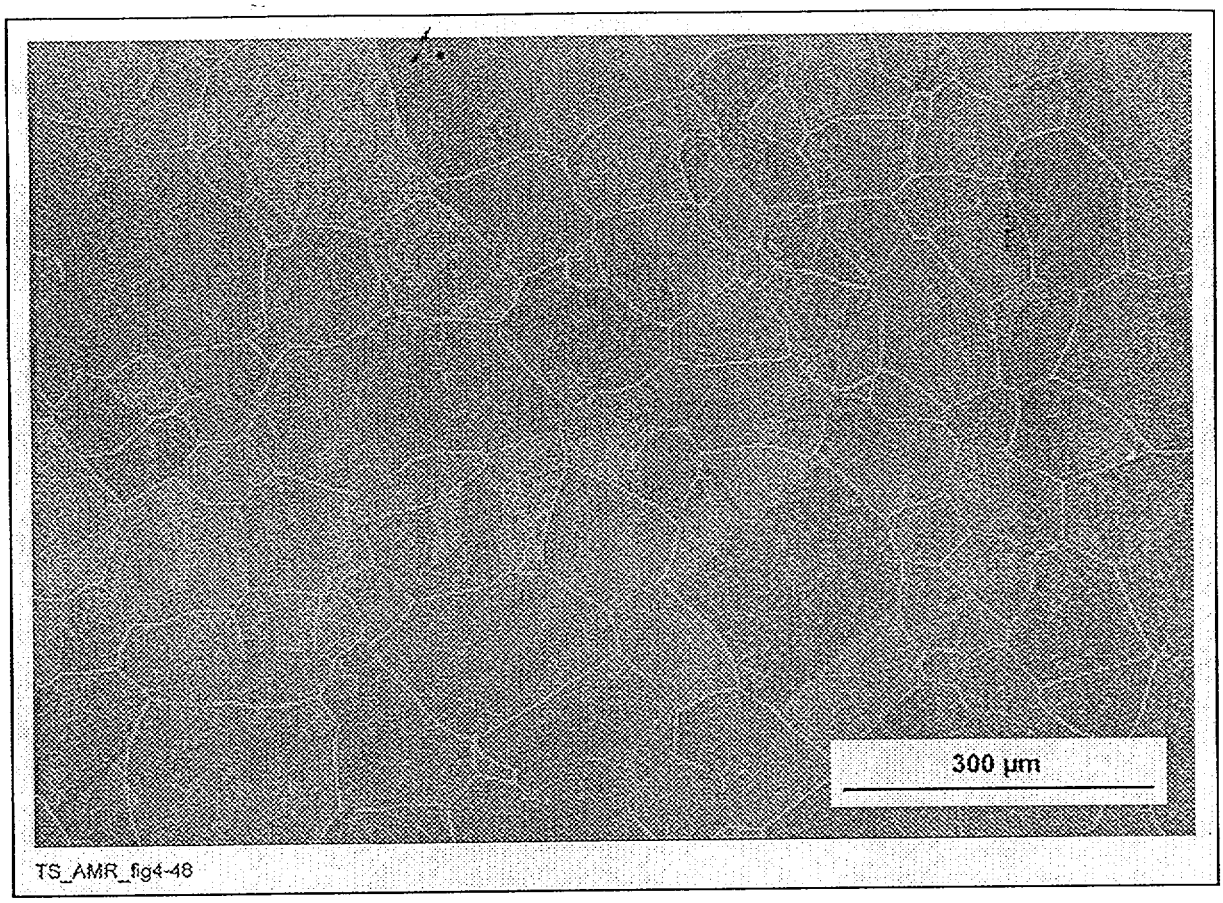


NOTE: (TS393-014a, 12/7/98, SN #434, p. 16)

Figure 51. SEM Micrograph Showing Significant Grain Boundary Precipitation After Aging Alloy 22 for 100 hr at 704°C [DTN # LL000115905924.113]

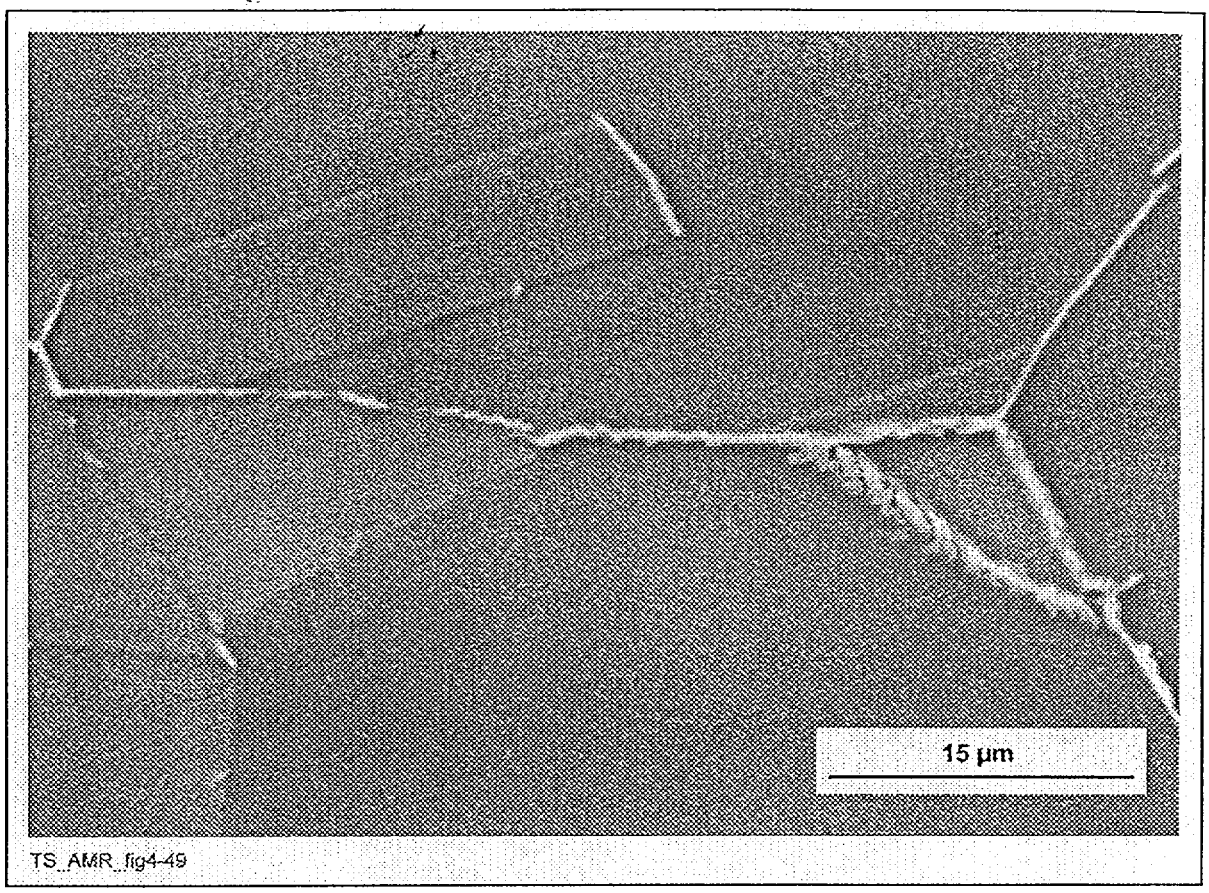


NOTE: (TS393-014a, 12/7/98, SN #434, p. 17)

Figure 52. SEM Micrograph Showing Precipitation Just Beginning on Twin Boundaries After Aging Alloy 22 for 100 hr at 704°C [DTN # LL000115905924.113]

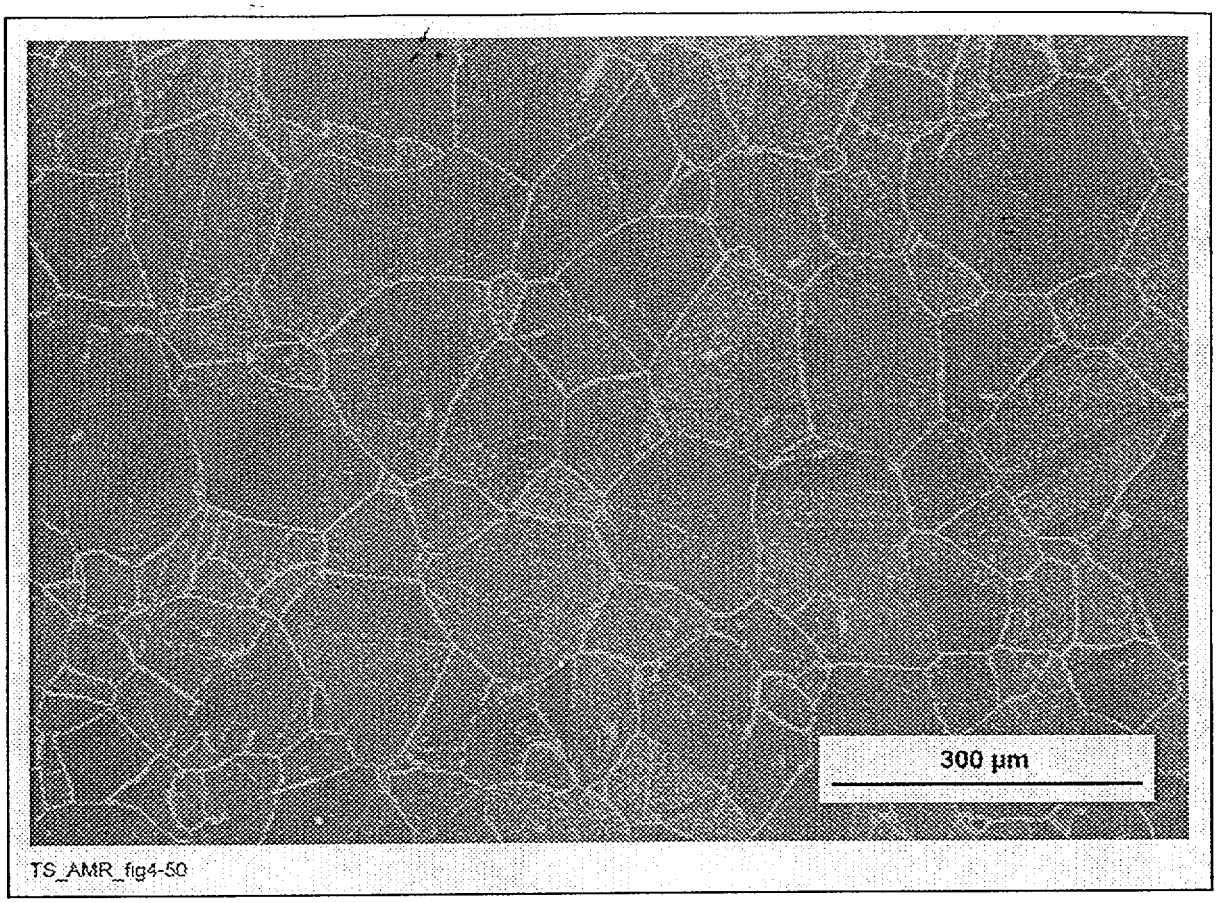


NOTE: (TS393-015a, 12/7/98, SN #434, p. 17)

Figure 53. SEM Micrograph Showing Complete Grain Boundary Coverage by and Precipitation on Twin Boundaries After Aging Alloy 22 for 1000 hr at 704°C [DTN # LL000115905924.113]

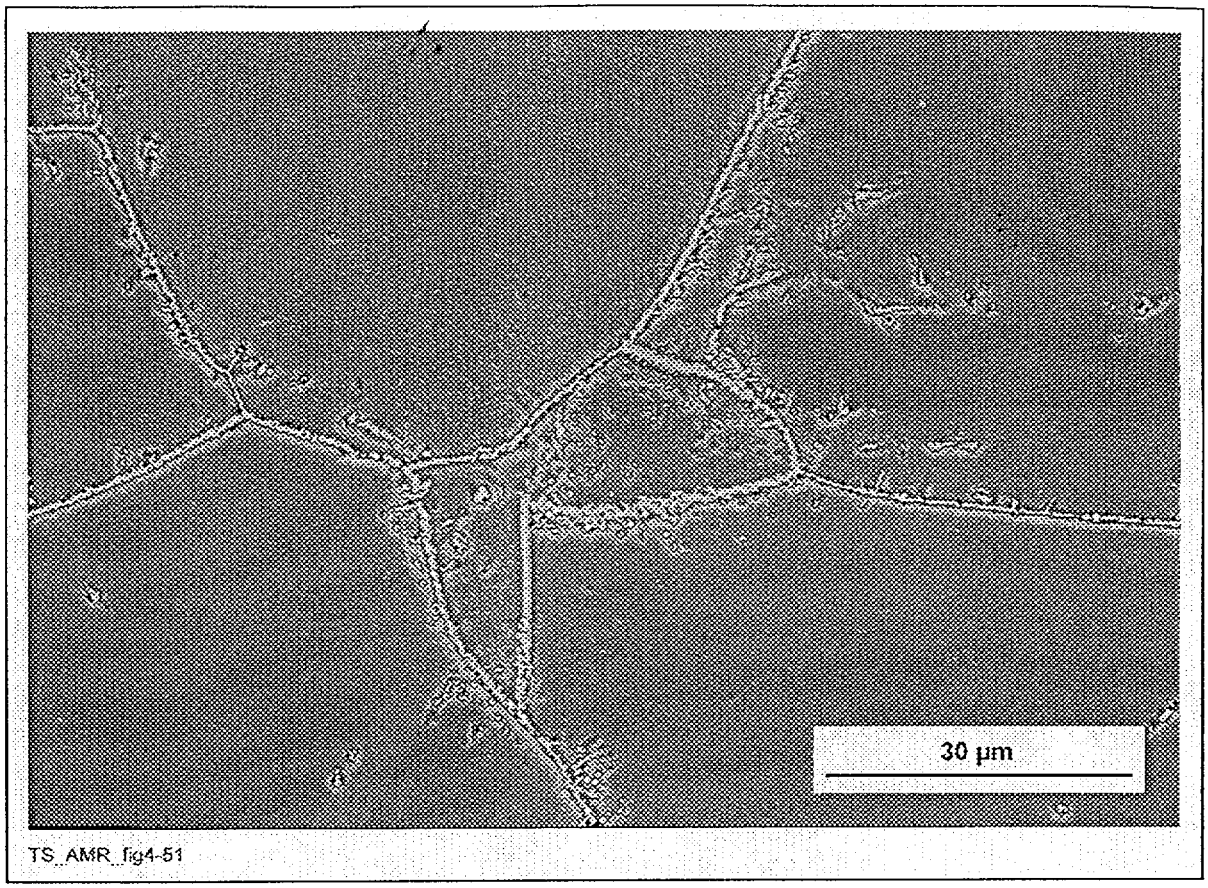


NOTE: (TS393-015a, 12/7/98, SN #434, p. 18)

Figure 54. SEM Micrograph Showing Precipitation Beginning Within the Grains Boundaries After Aging Alloy 22 for 1000 hr at 704°C [DTN # LL000115905924.113]

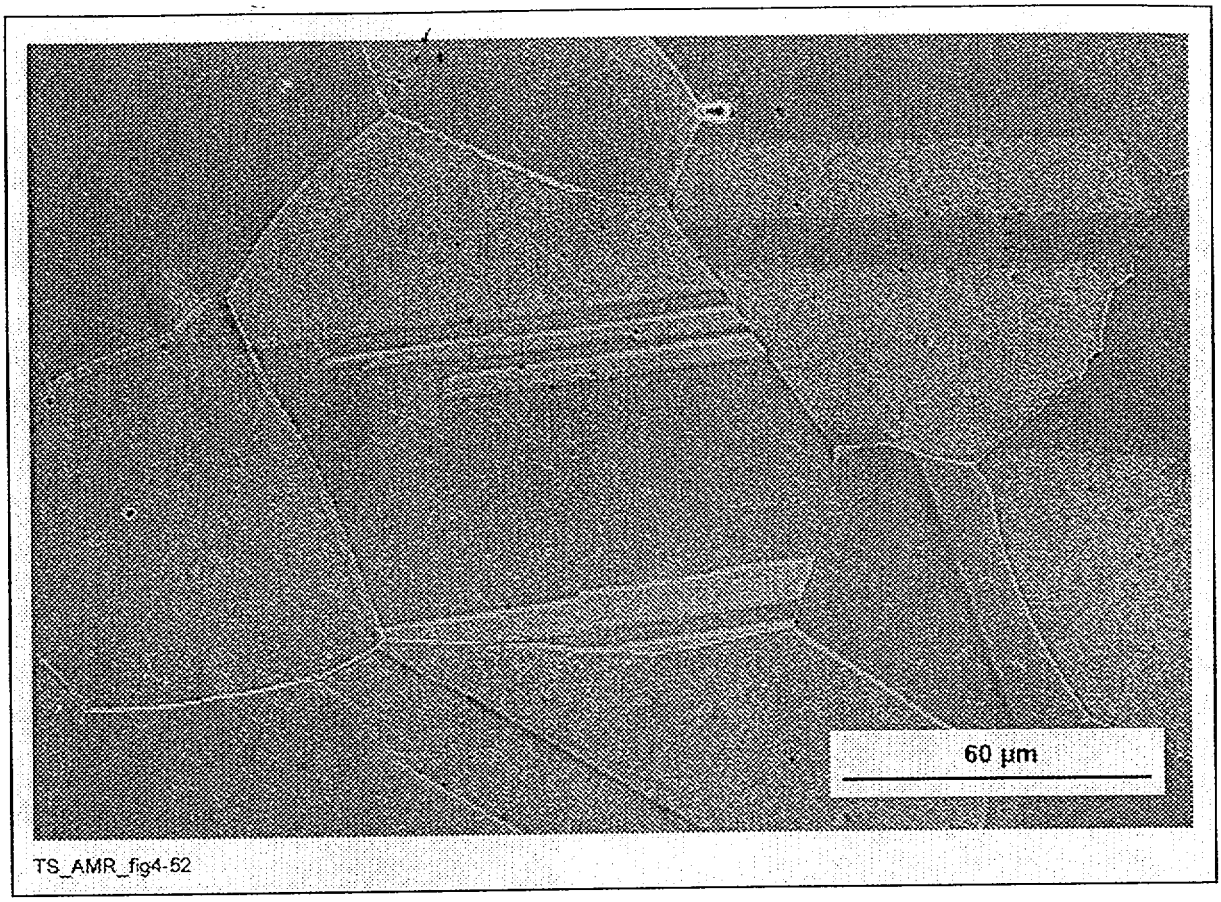


NOTE: (TS369-014, 11/30/98, SN #434, p. 19)

Figure 55. SEM Micrograph Showing That Grain Boundary Precipitation Has Begun After Aging Alloy 22 for 1 hr at 760°C [DTN # LL000115905924.113]

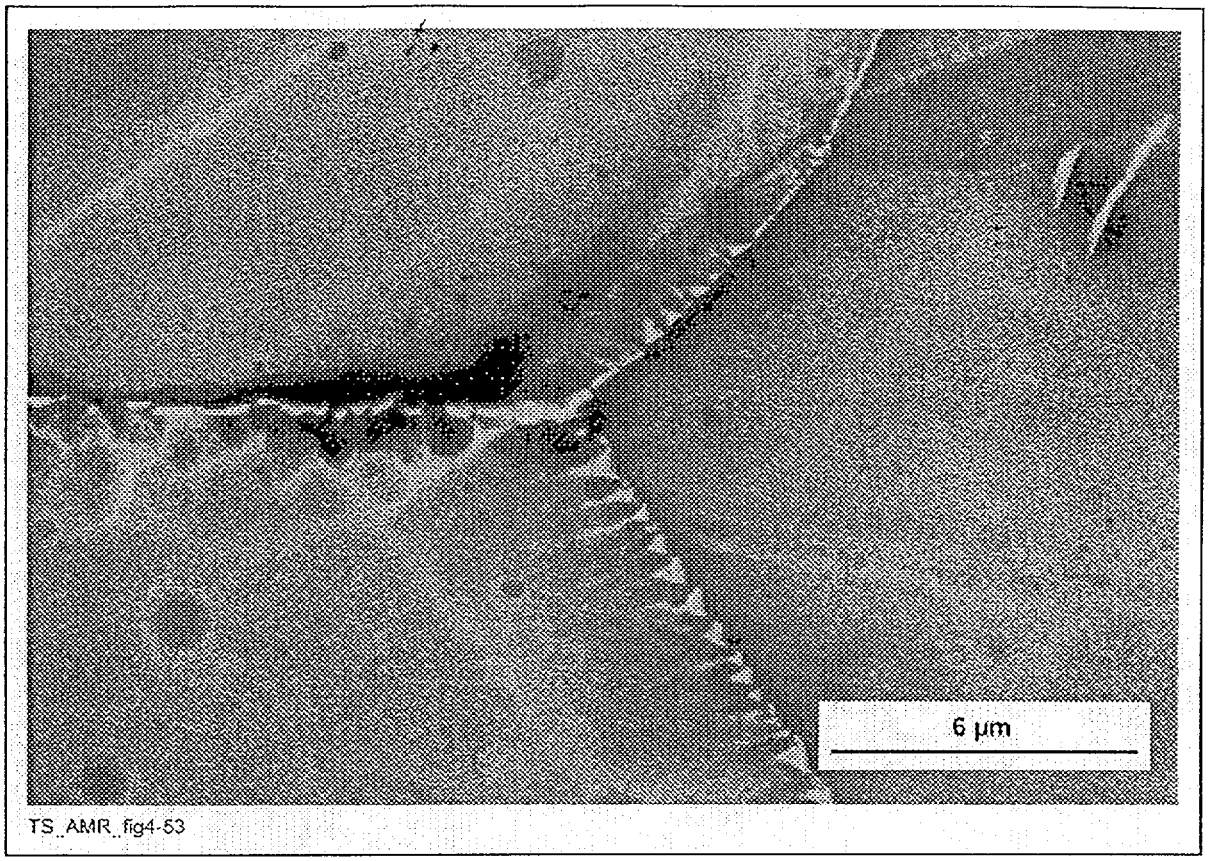


NOTE: (TS369-014, 11/30/98, SN #434, p. 20)

Figure 56. SEM Micrograph Showing That Grain Boundary Precipitation Has Begun After Aging Alloy 22 for 1 hr at 760°C [DTN # LL000115905924.113]

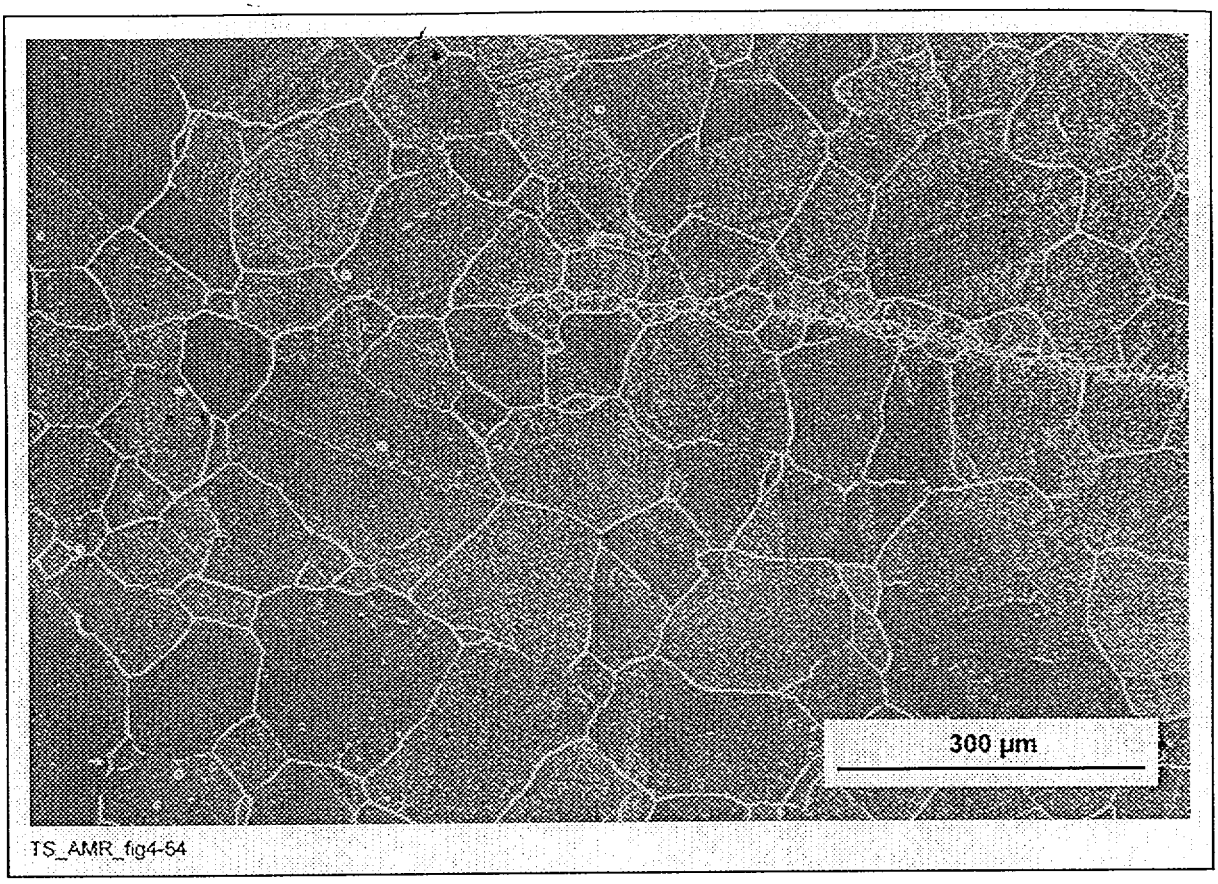


NOTE: (TS369-015, 11/30/98, SN #434, p. 21)

Figure 57. SEM Micrograph Showing Significant Grain Boundary Precipitation After Aging Alloy 22 for 10 hr at 760°C [DTN # LL000115905924.113]

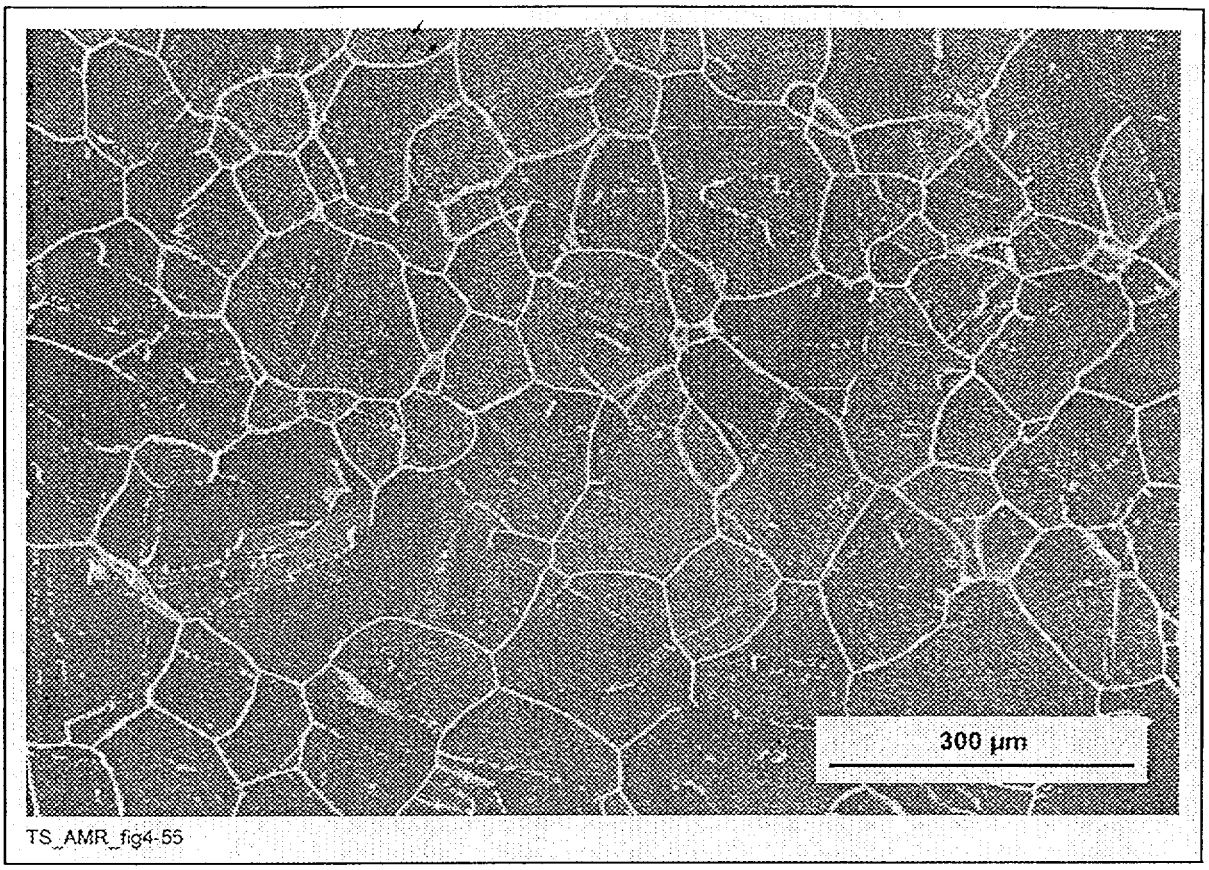


NOTE: (TS369-016, 11/30/98, SN #434, p. 22)

Figure 58. SEM Micrograph Showing Significant Grain Boundary Precipitation and Precipitation on Twin Boundaries After Aging Alloy 22 for 119 hr at 760°C [DTN # LL000115905924.113]

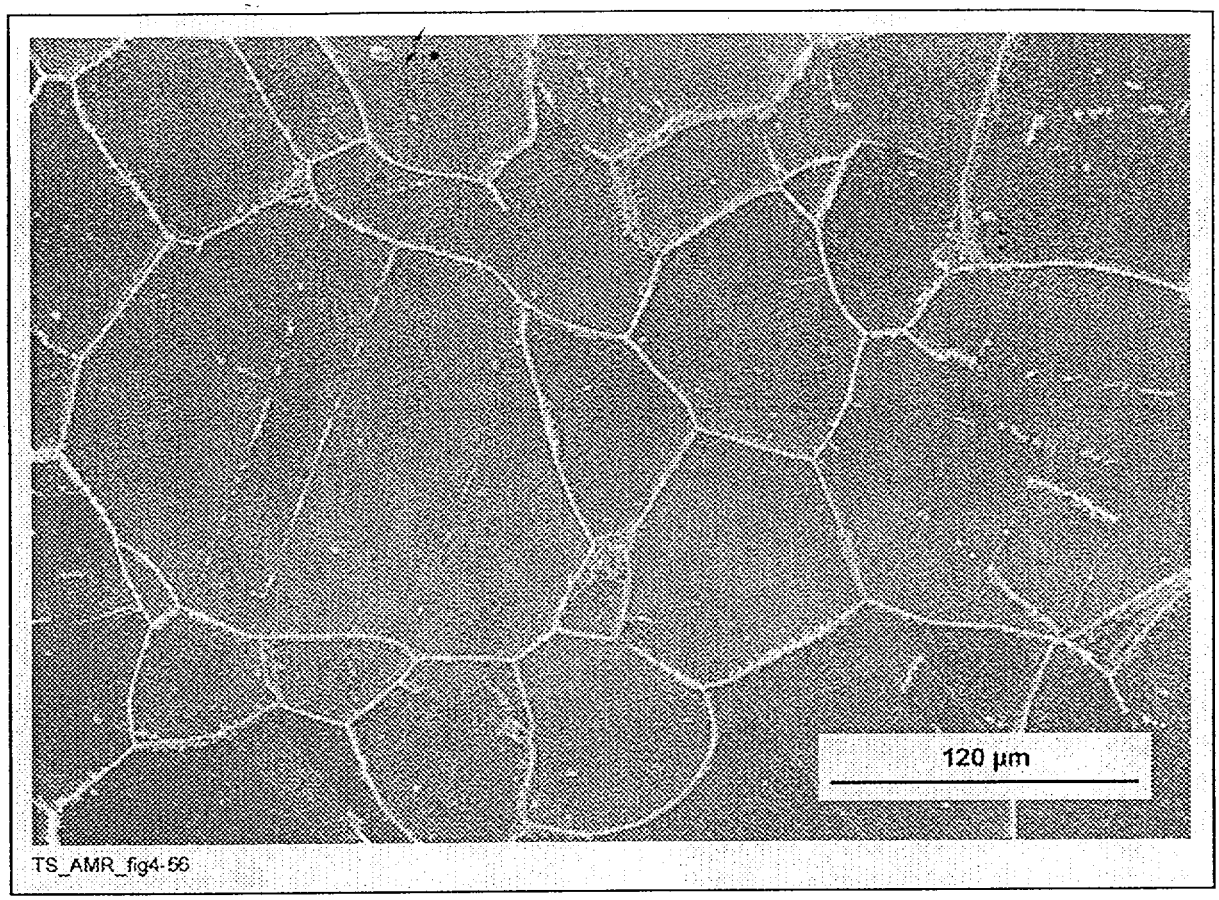


NOTE: (TS369-016, 11/30/98, SN #434, p. 24)

Figure 59. SEM Micrograph Showing Precipitation on Grain Boundaries, on Twin Boundaries, and Within the Grains After Aging Alloy 22 for 119 hr at 760°C [DTN # LL000115905924.113]

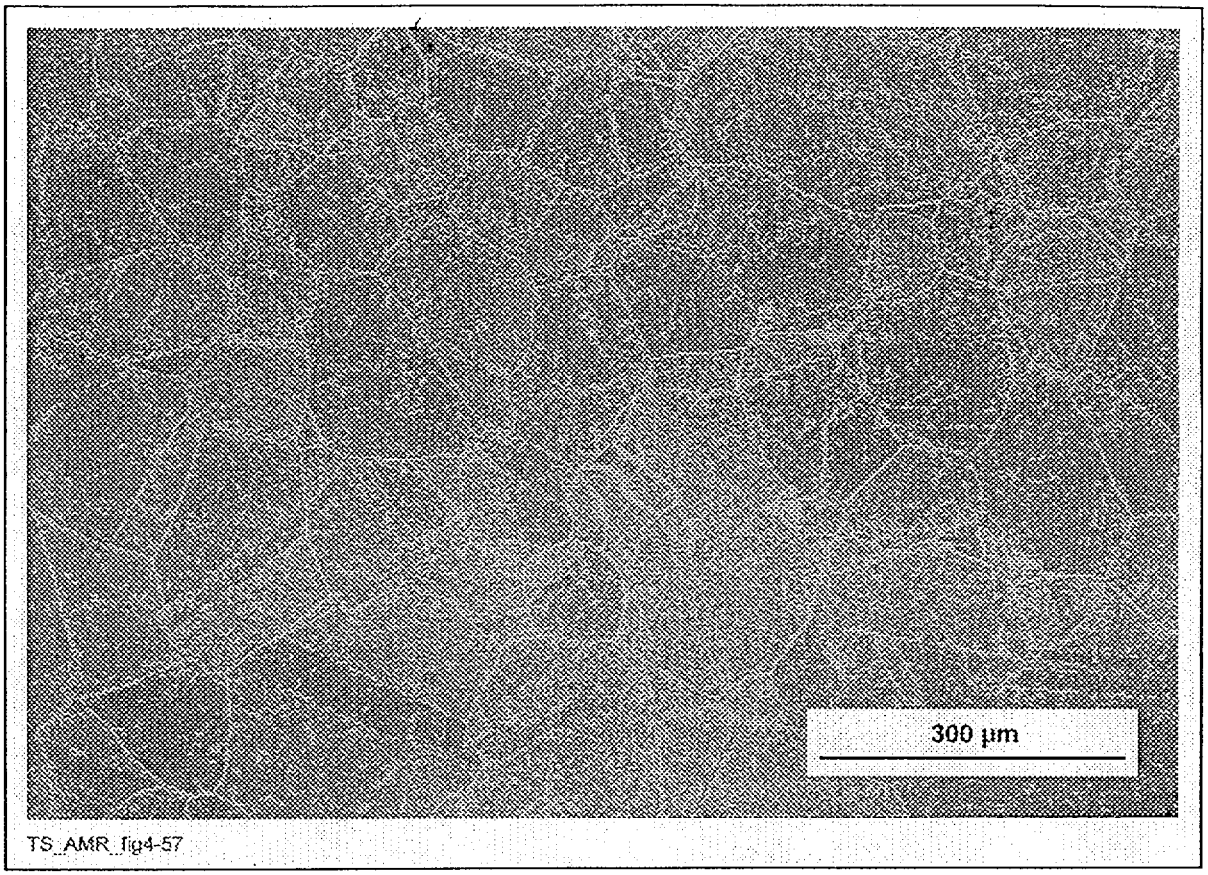


NOTE: (TS393-007a, 12/7/98, SN #434, p. 22)

Figure 60. SEM Micrograph Showing Significant Precipitation Within the Grains of Alloy 22 After Aging for 1000 hr at 760°C [DTN # LL000115905924.113]

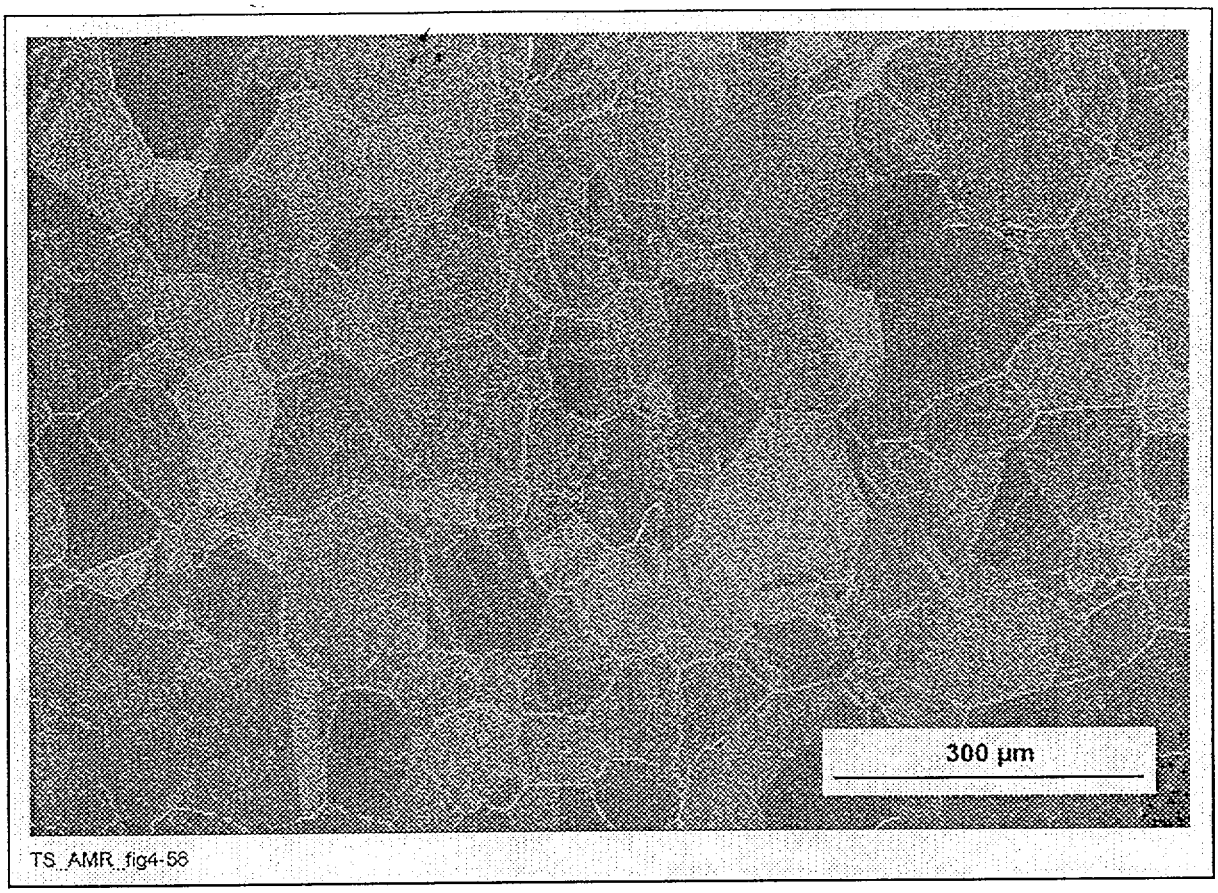


NOTE: (TS393-020a, 2/15/99, SN #434, p. 25)

Figure 61. SEM Micrograph Showing Grain Boundary Precipitation in Alloy 22 After Aging for 1 hr at 800°C [DTN # LL000115905924.113]

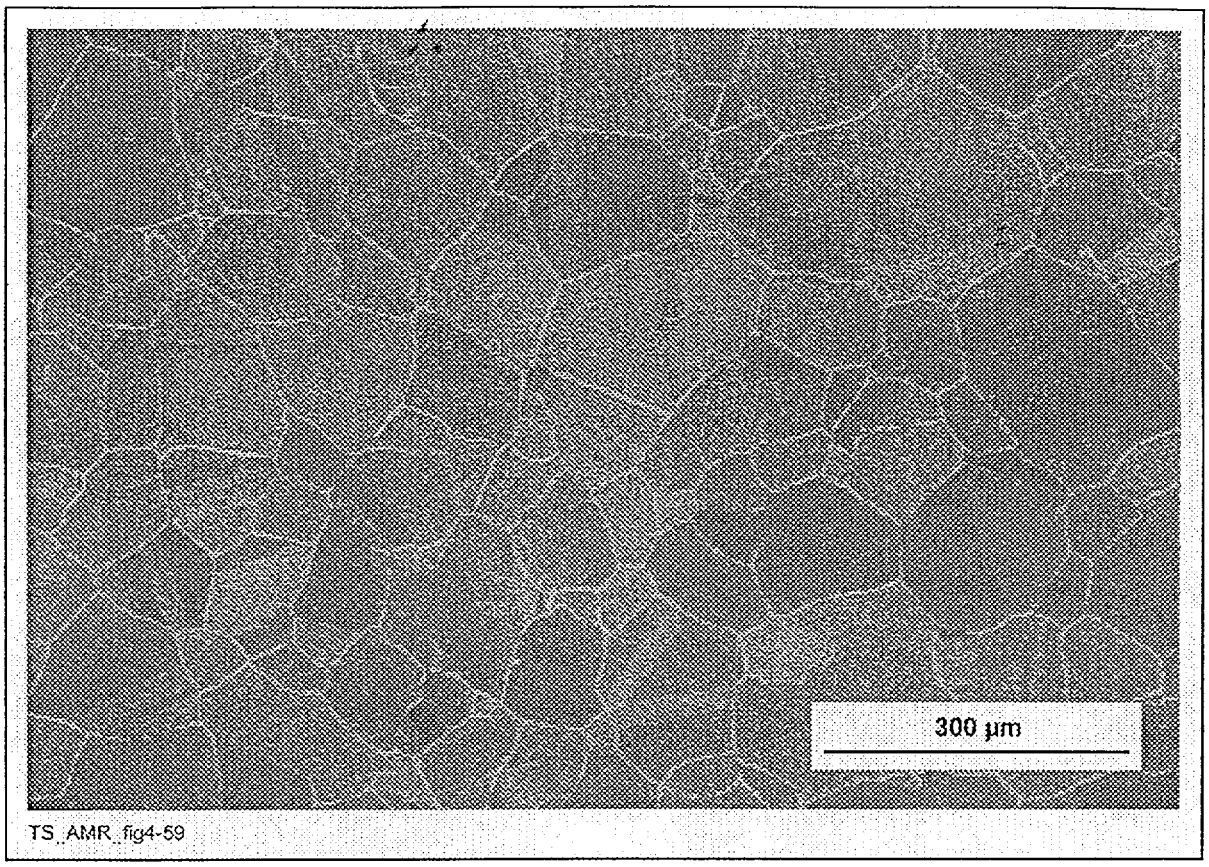


NOTE: (TS393-021a, 2/15/99, SN #434, p. 26)

Figure 62. SEM Micrograph Showing Significant Grain Boundary Precipitation in Alloy 22 After Aging for 10 hr at 800°C [DTN # LL000115905924.113]

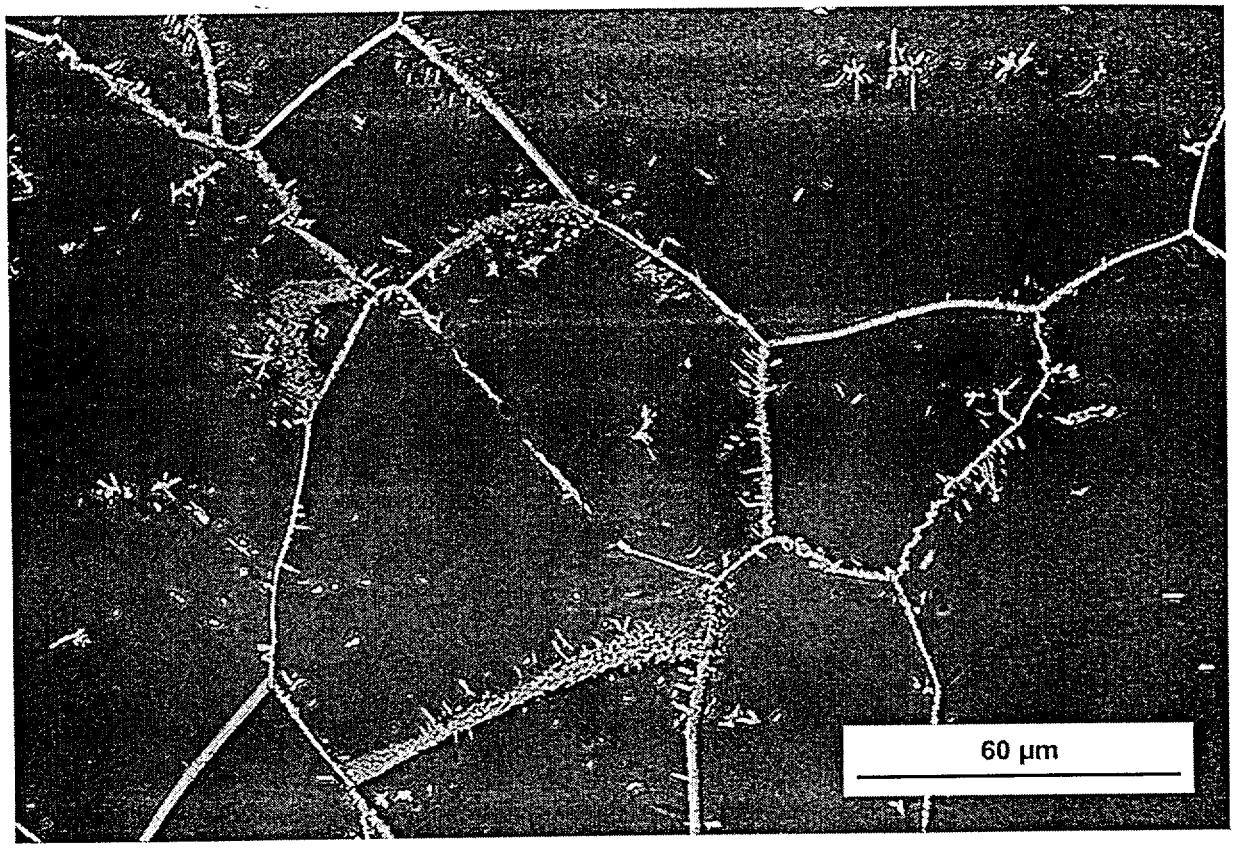


TS_AMR_fig4-60

NOTE: (TS393-022a, 2/15/99, SN #434, p. 27)

Figure 63. SEM Micrograph Showing Precipitation on Grain Boundaries, on Twin Boundaries, and Within the Grains After Aging Alloy 22 for 100 hr at 800°C [DTN # LL000115905924.113]

### 4.1.3 Micrographs Showing Intermetallic Particles in Alloy 22 Welds

The intermetallic phases μ, P, and σ are known to form in Alloy 22 welds (Cieslak et al. 1986, p. 2041, ¶ 2). This section contains optical, SEM, and TEM images (Figures 64 to 74) in the preliminary characterization of Alloy 22 welds. Two samples have been examined: one was examined in the as-welded condition; the other was aged for 40,000 hr at 427°C. Although the two welds were produced in the same way, the aged sample did not come from the same weld as did the unaged sample. Therefore, some variation is expected between the samples, and direct comparisons on the small scale of differences seen between these samples should not be made.

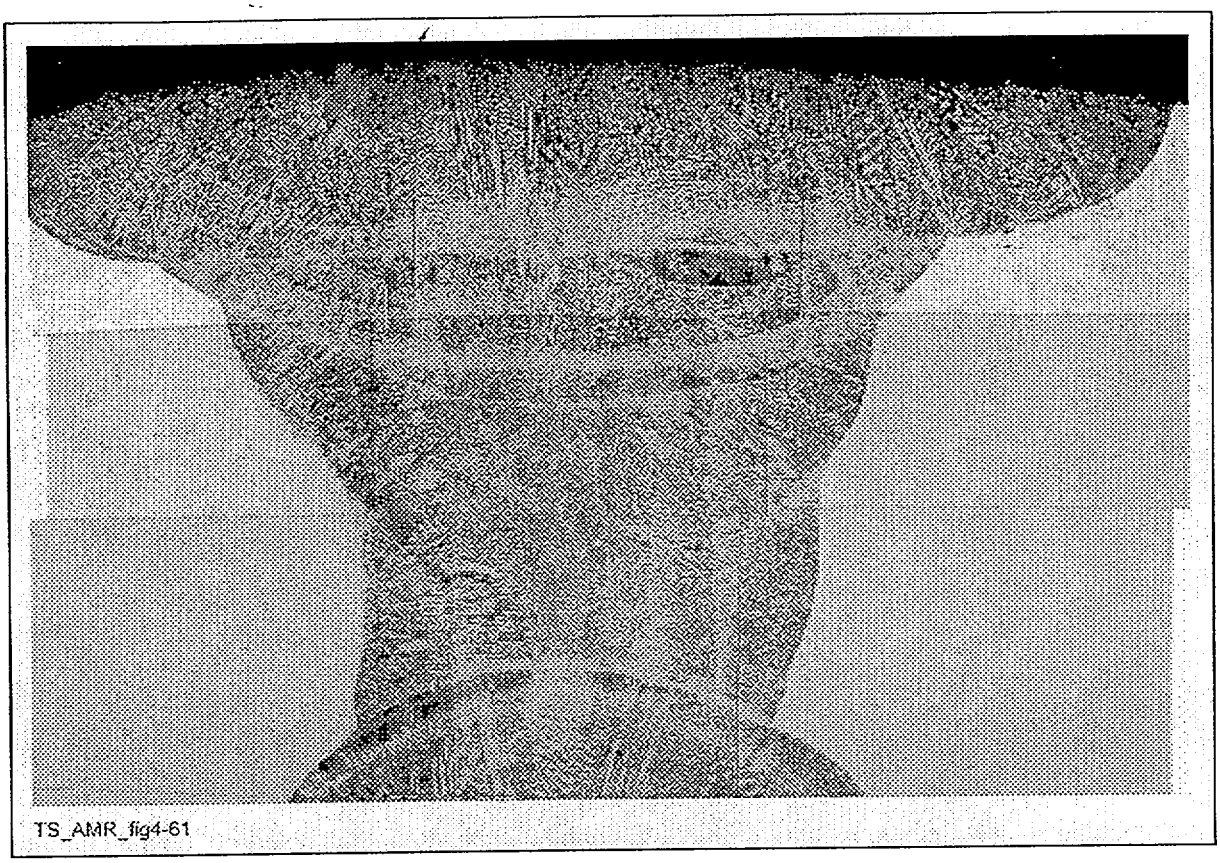


NOTE: Only approximately three-quarters of the half-inch plate is shown. (TS393-019, 8/28/98, SN #393, pp. 9 - 10)

Figure 64. Low-Magnification Optical Micrograph of an Alloy 22 Multipass, Double-V Gas-Tungsten-Arc-Welding (GTAW) Weld with Matching Filler Metal [DTN # LL000115905924.113]

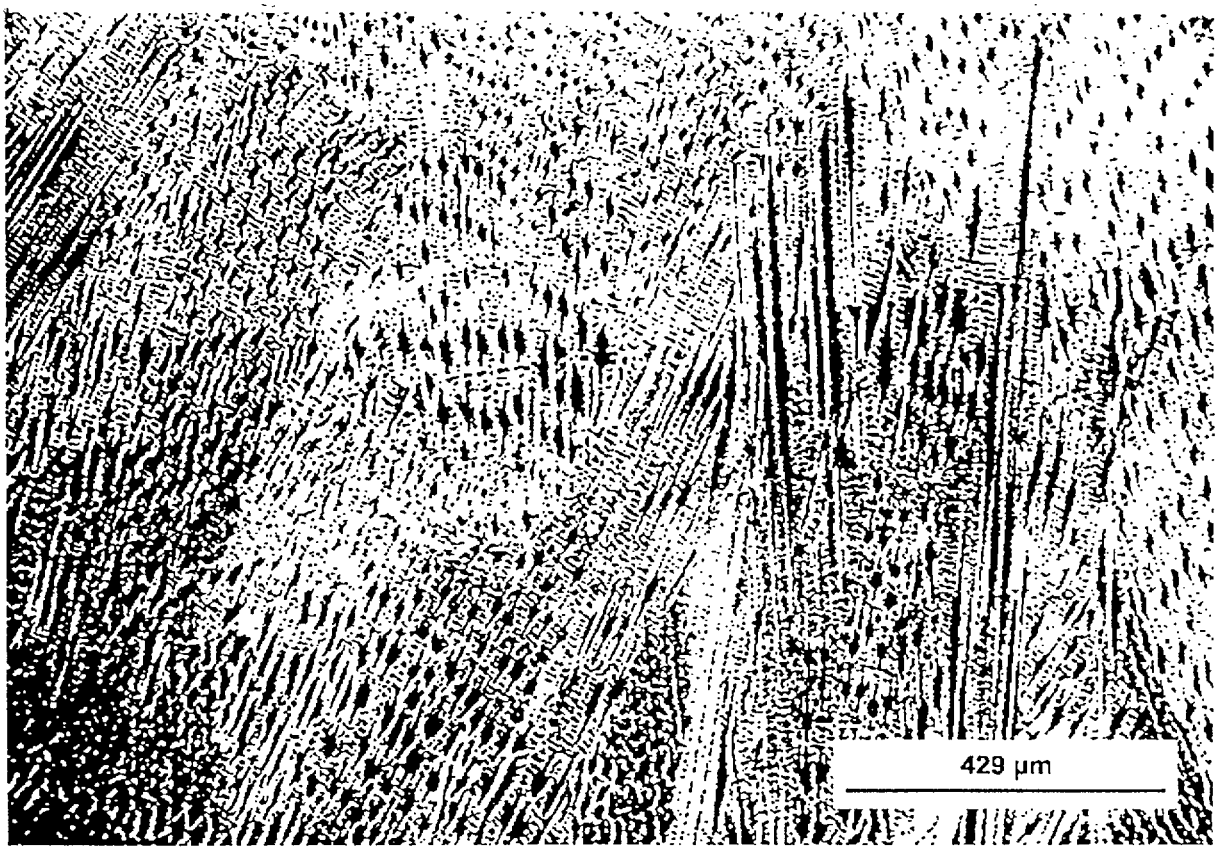


TS_AMR_fig4-62

NOTE: (TS393-019, 8/28/98, SN #393, p. 10)

Figure 65. SEM Micrograph of the Alloy 22 Weld Shown in Figure 58 Showing the Dendritic Structure Typical of Welds [DTN # LL000115905924.113]

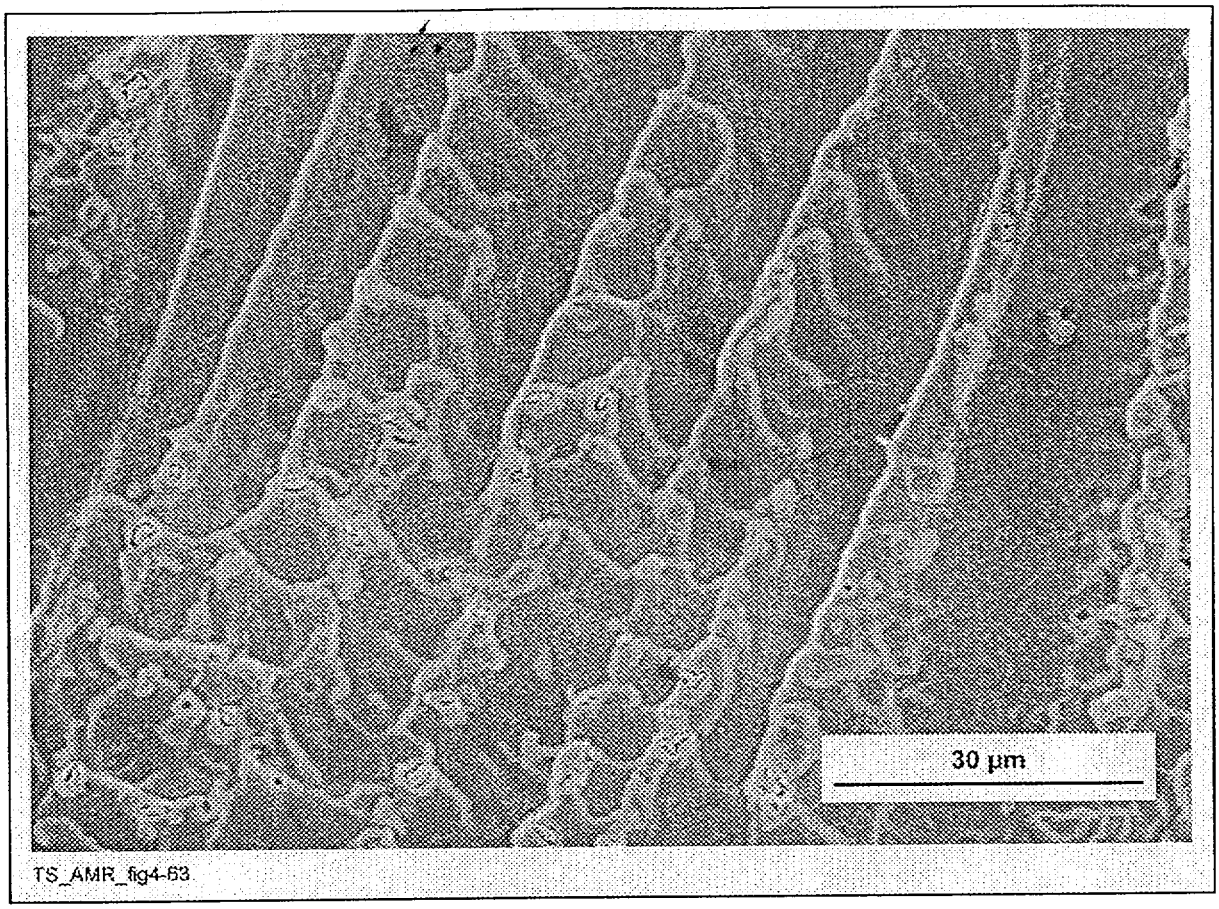


NOTE: Intermetallic particles are seen to form in the interdendritic regions. (TS393-019, 8/28/98, SN #393, p. 10)

Figure 66. SEM Micrograph of the Alloy 22 Weld Shown in Figure 58 Showing the Dendritic Structure Typical of Welds [DTN # LL000115905924.113]

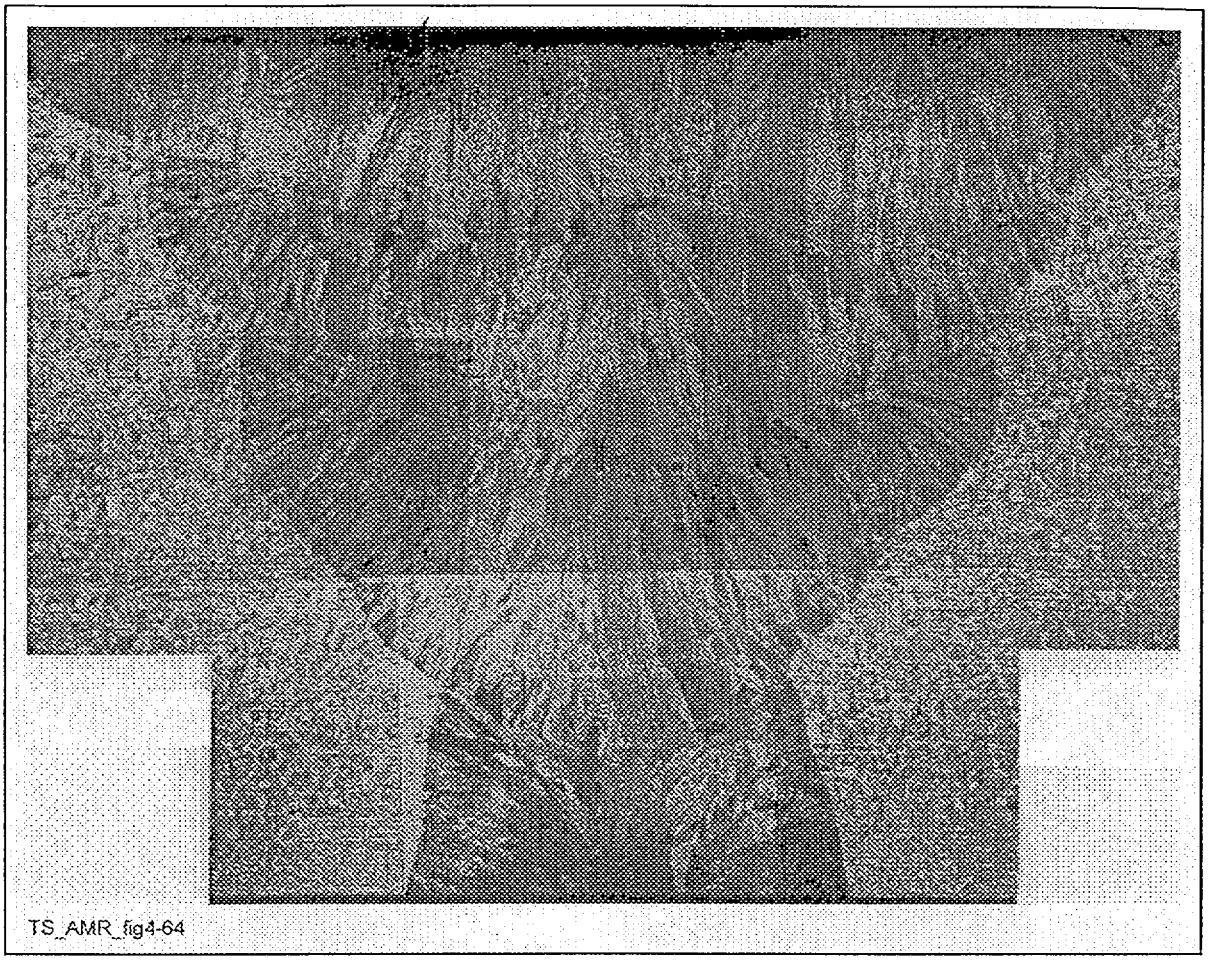


NOTE: Only approximately one-half of the half-inch plate is shown. (TS393-005b, 5/12/98, SN #369, p. 20)

Figure 67. Low-Magnification Optical Micrograph of an Alloy 22 Weld Similar to that Shown in Figure 64, but Aged for 40,000 hr at 427°C [DTN # LL000115905924.113]


NOTE: The white intermetallic particles are distributed nonuniformly throughout the weld. (TS393-005b, 5/12/98, SN #369, p. 20)

Figure 68. SEM Micrograph of the Alloy 22 Weld Shown in Figure 67 at the Junction of Two Weld Passes [DTN # LL000115905924.113]

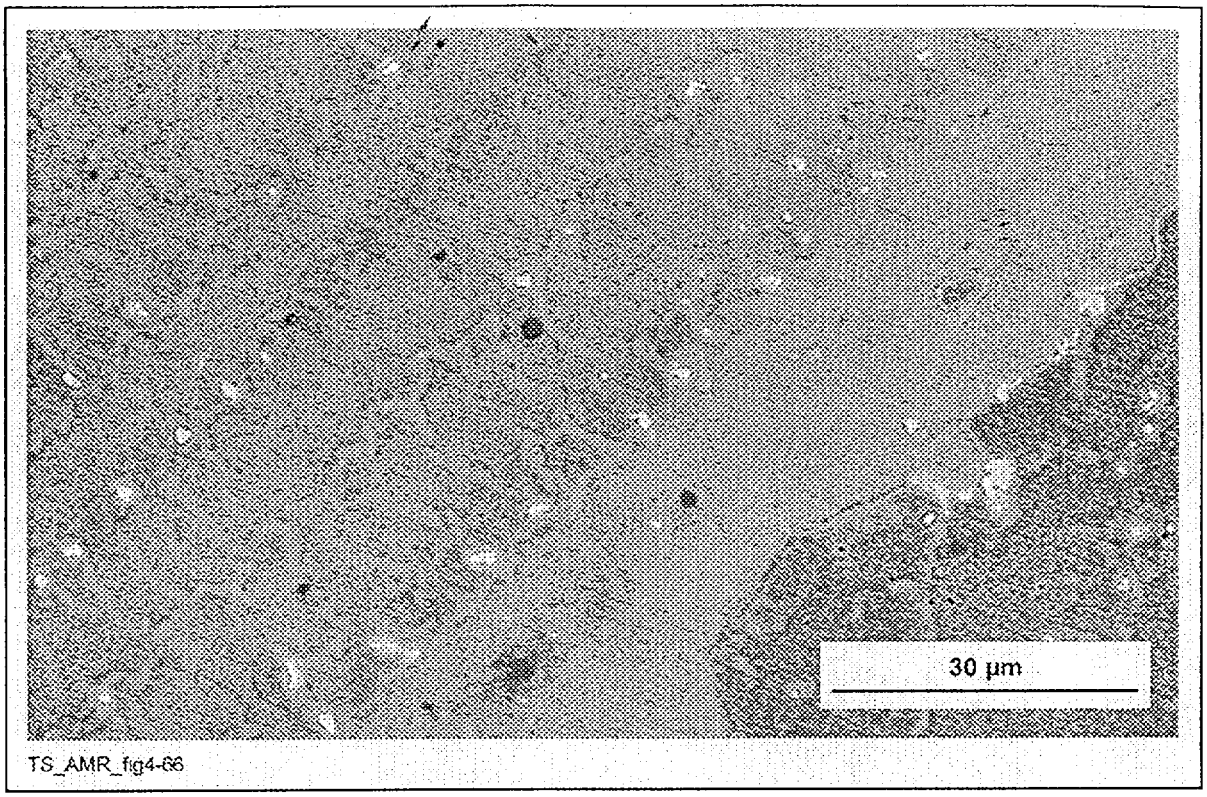


NOTE: Intermetallic particles are seen to form in the interdendritic regions, as was seen in the unaged weld of Figure 60. (TS393-005b, 5/12/98, SN #369, p. 20)

Figure 69. SEM Micrograph of the Alloy 22 Weld Shown in Figure 67 Showing the Dendritic Structure Typical of Welds [DTN # LL000115905924.113]

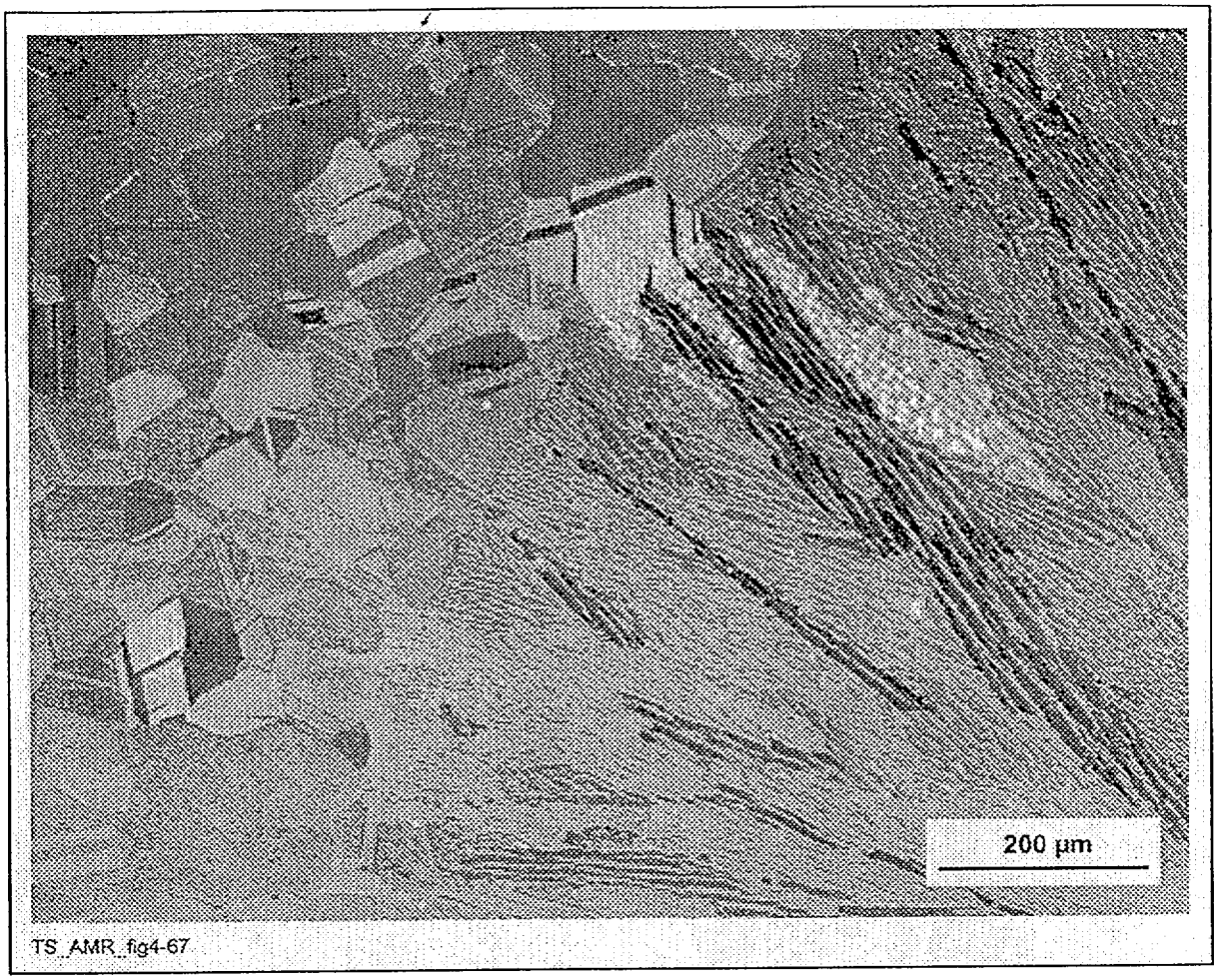


NOTE: Very few precipitates are seen in the HAZ of the aged weld. (TS393-005b, 5/12/98, SN #369, p. 20)

Figure 70. Optical Micrograph at the Fusion Line of the Alloy 22 Weld Shown in Figure 67 [DTN # LL000115905924.113]

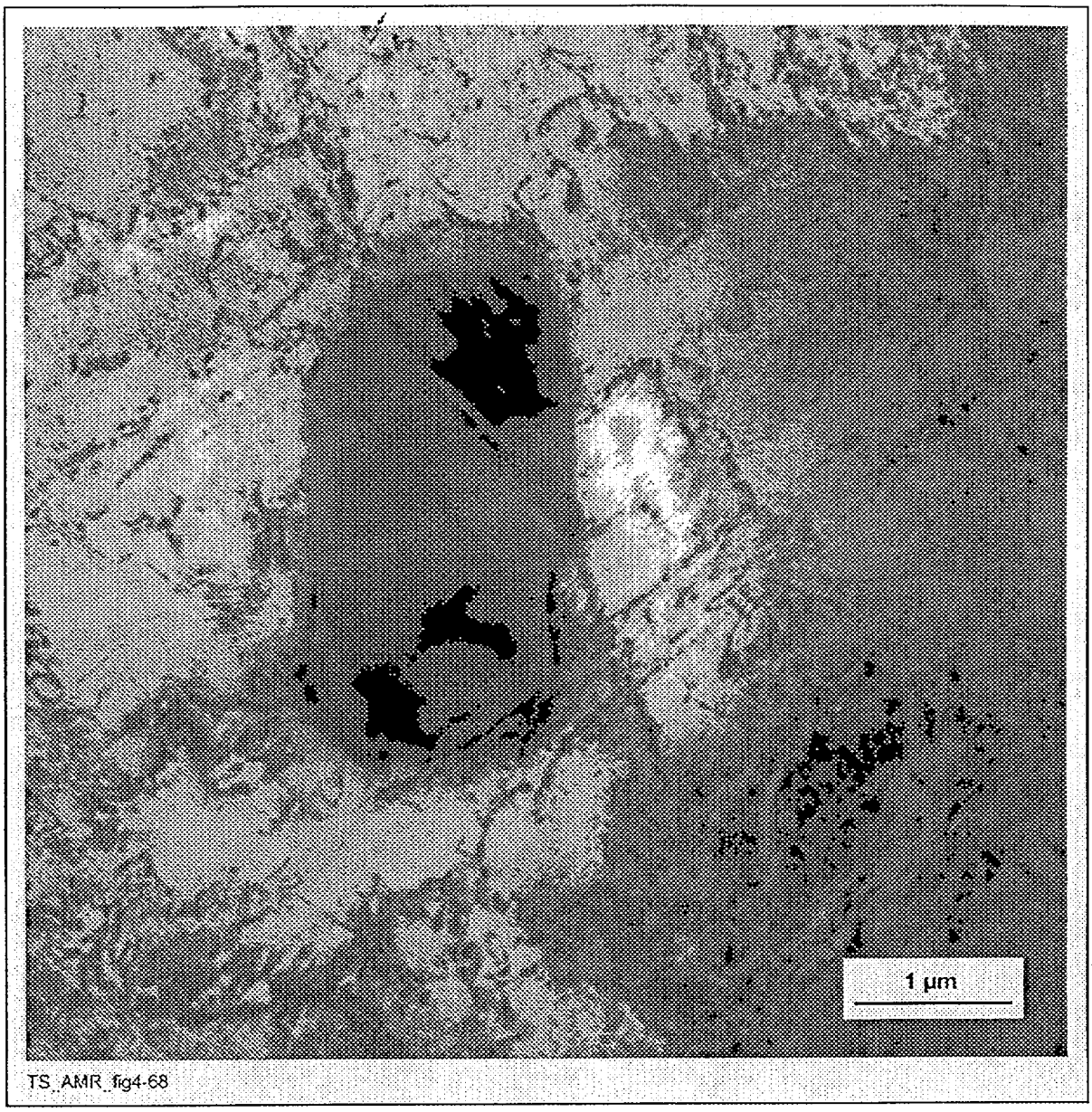


NOTE: This particle was not conclusively identified, but could be either P or σ. (TS369-005a, Image 1373, 5/21/98, SN #393, p. 27)

Figure 71. One of Few Precipitates Seen in the Alloy 22 Weld of Figure 67 Aged for 40,000 hr at 427°C [DTN # LL000115905924.113]

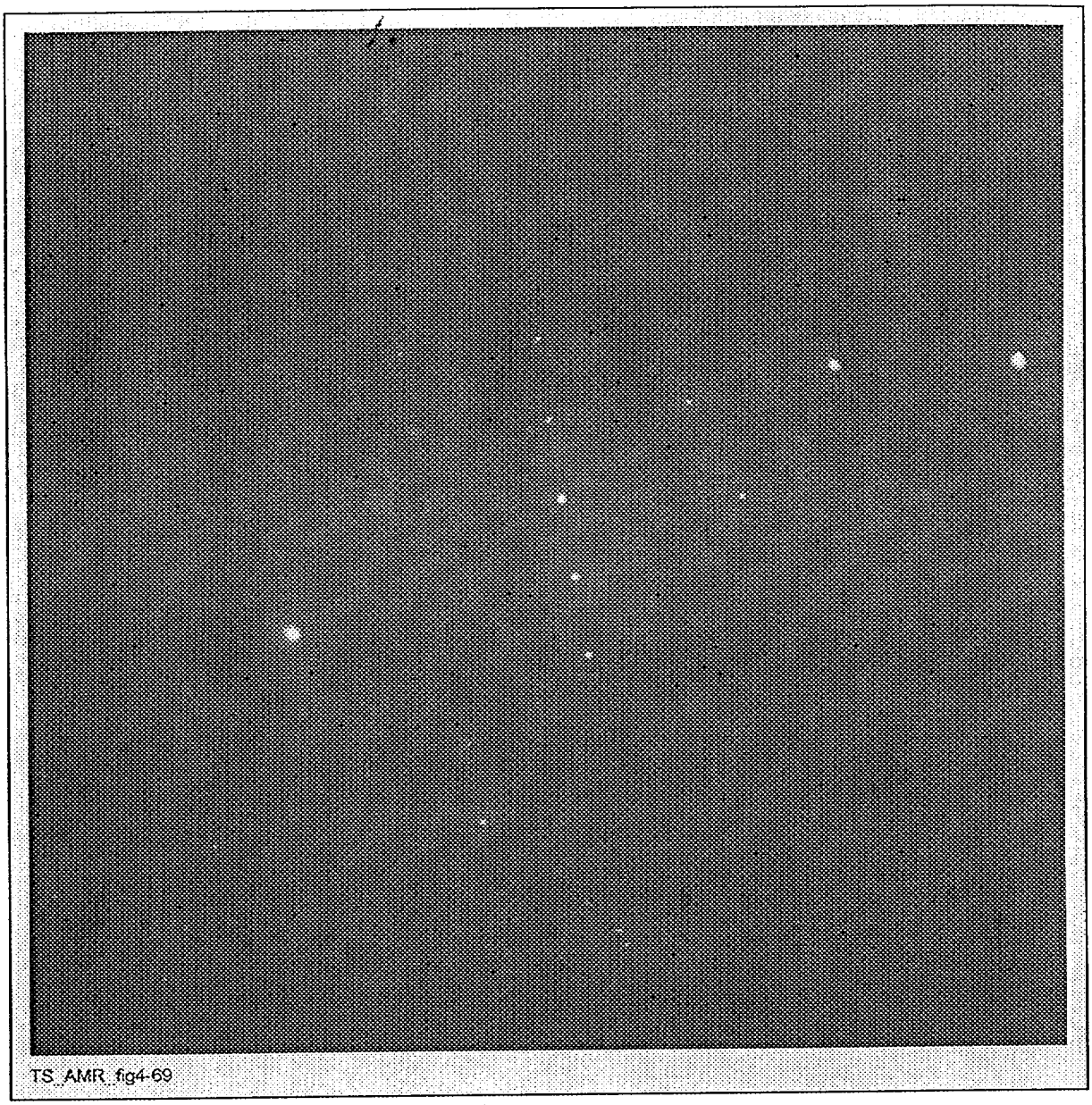


NOTE: This pattern could be indexed as either P phase or σ. (TS369-005a, Image 1374, 5/21/98, SN #393, p. 27)

Figure 72. SAD Pattern from the Precipitate Shown in Figure 71 [DTN # LL000115905924.113]

TS_AMR_fig4-70

NOTE: This pattern could be indexed as either P phase or σ. (TS369-005a, Image 1375, 5/21/98, SN #393, p. 31)

Figure 73. SAD Pattern from the Precipitate Shown in Figure 71 [DTN # LL000115905924.113]

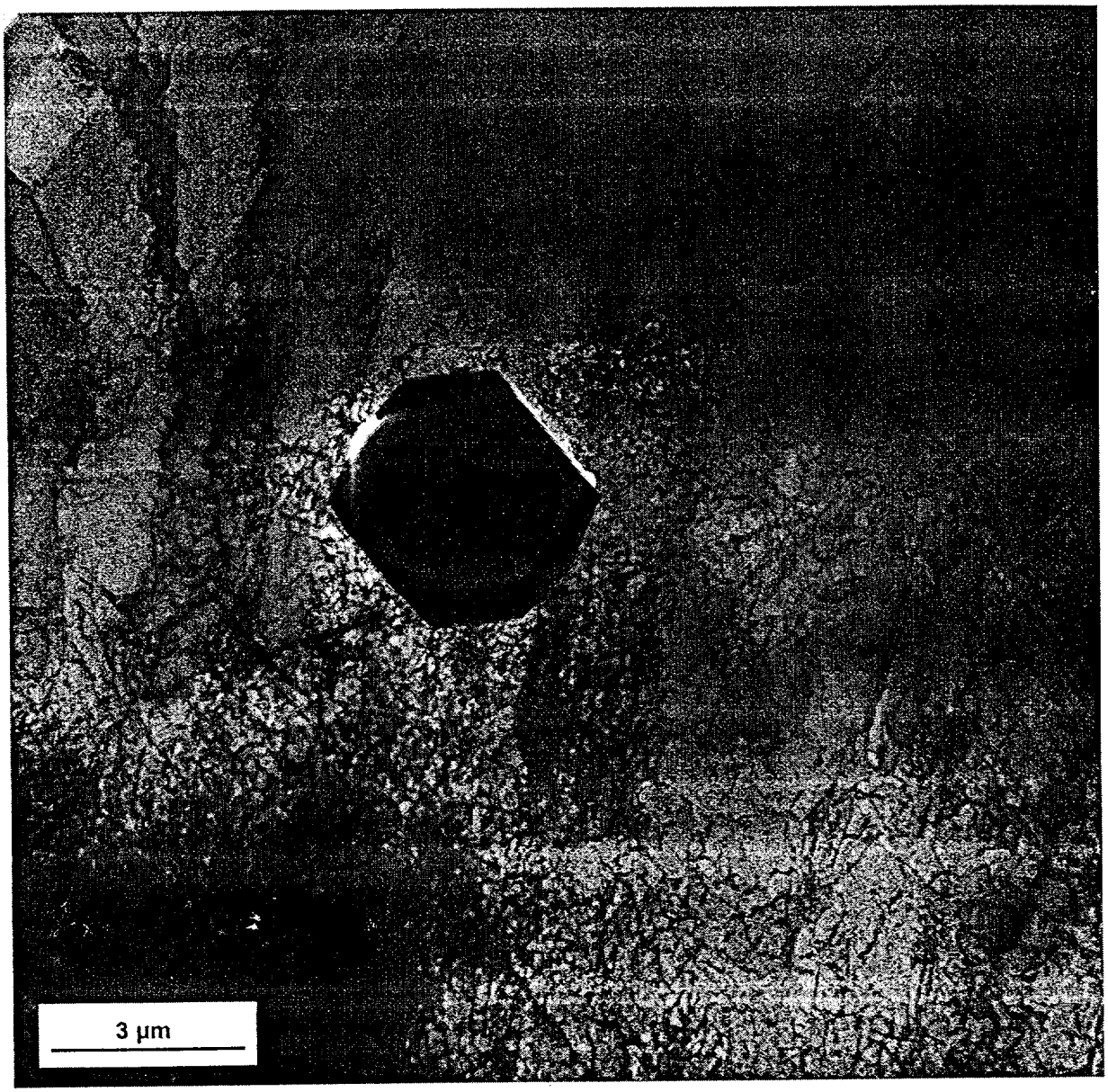


TS_AMR_fig4-71

NOTE: A SAD pattern was not taken from this particle, but it appears to be a carbide and was probably present in the base metal prior to welding. (TS369-005a, Image 1378, 5/22/98, SN #393, p. 37)

Figure 74. TEM Micrograph Showing One of Few Precipitates Seen in the HAZ of the Aged Alloy 22 Weld of Figure 67 [DTN # LL000115905924.113]

### 4.1.4 TEM Micrographs Showing When LRO Has Been Observed

LRO occurs in Ni-Cr-Mo alloys such as Alloy 22 at temperatures less than approximately 600°C. This ordering has been linked to an increased susceptibility of Ni-Cr-Mo alloys to SCC and hydrogen embrittlement. This section contains TEM micrographs (Figures 75 to 95) showing instances when LRO has been observed in aged Alloy 22 samples. Long-range order has been observed in Alloy 22 base metal after aging for 1000 hr and 16,000 hrs at 593°C, for 1000 hr at 538°C, and for 30,000 hr and 40,000 hr at 427°C. LRO has also been observed in Alloy 22 welds after aging for 40,000 hr at 427°C.


NOTE: (TS369-003a, Image 1484, 12/16/98, SN #393, p. 61)

Figure 75. TEM Micrograph Showing LRO Domains in an Alloy 22 Base Metal Sample Aged for 16,000 hr at 593°C [DTN # LL000115905924.113]

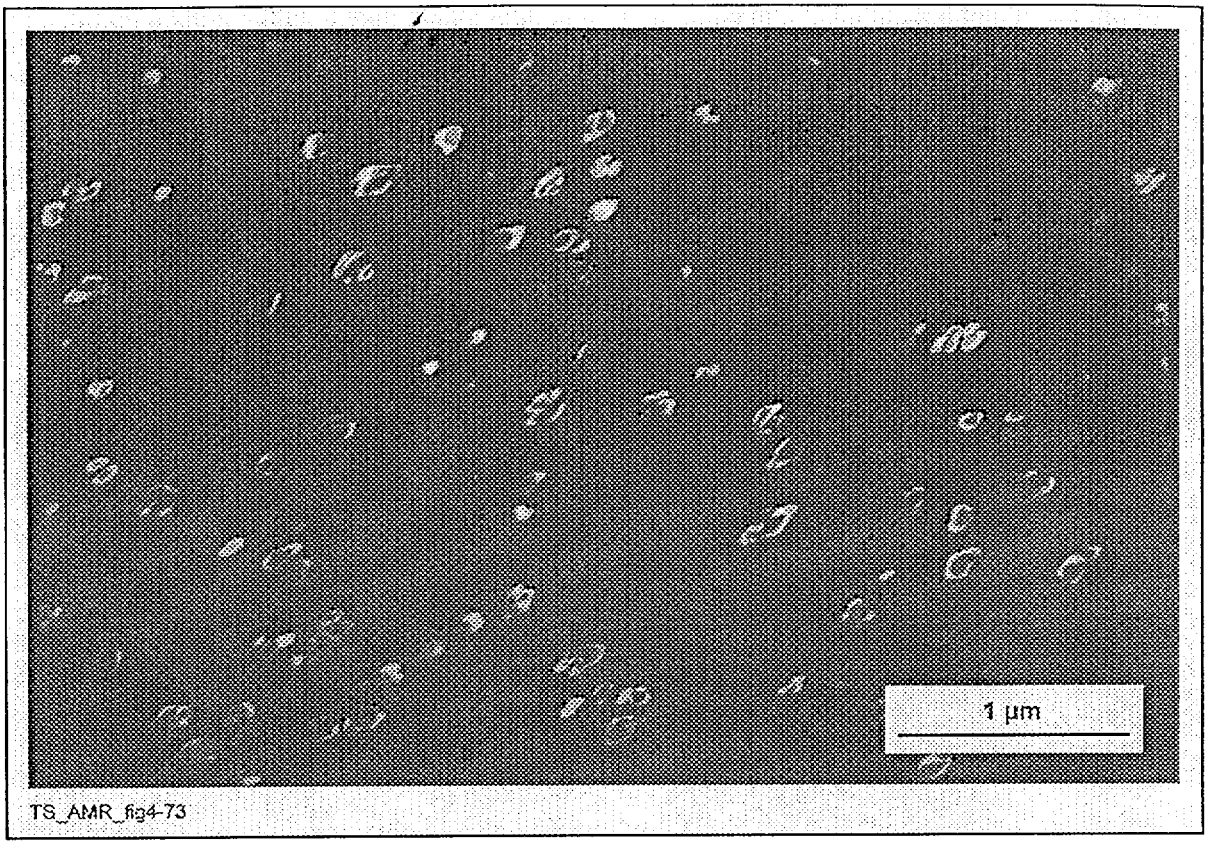


NOTE: One or more variants of the ordered domains appears light. (TS369-003a, Image 1485, 12/16/98, SN #393, p. 61)

Figure 76. Dark-Field Image Corresponding to Figure 75 [DTN # LL000115905924.113]

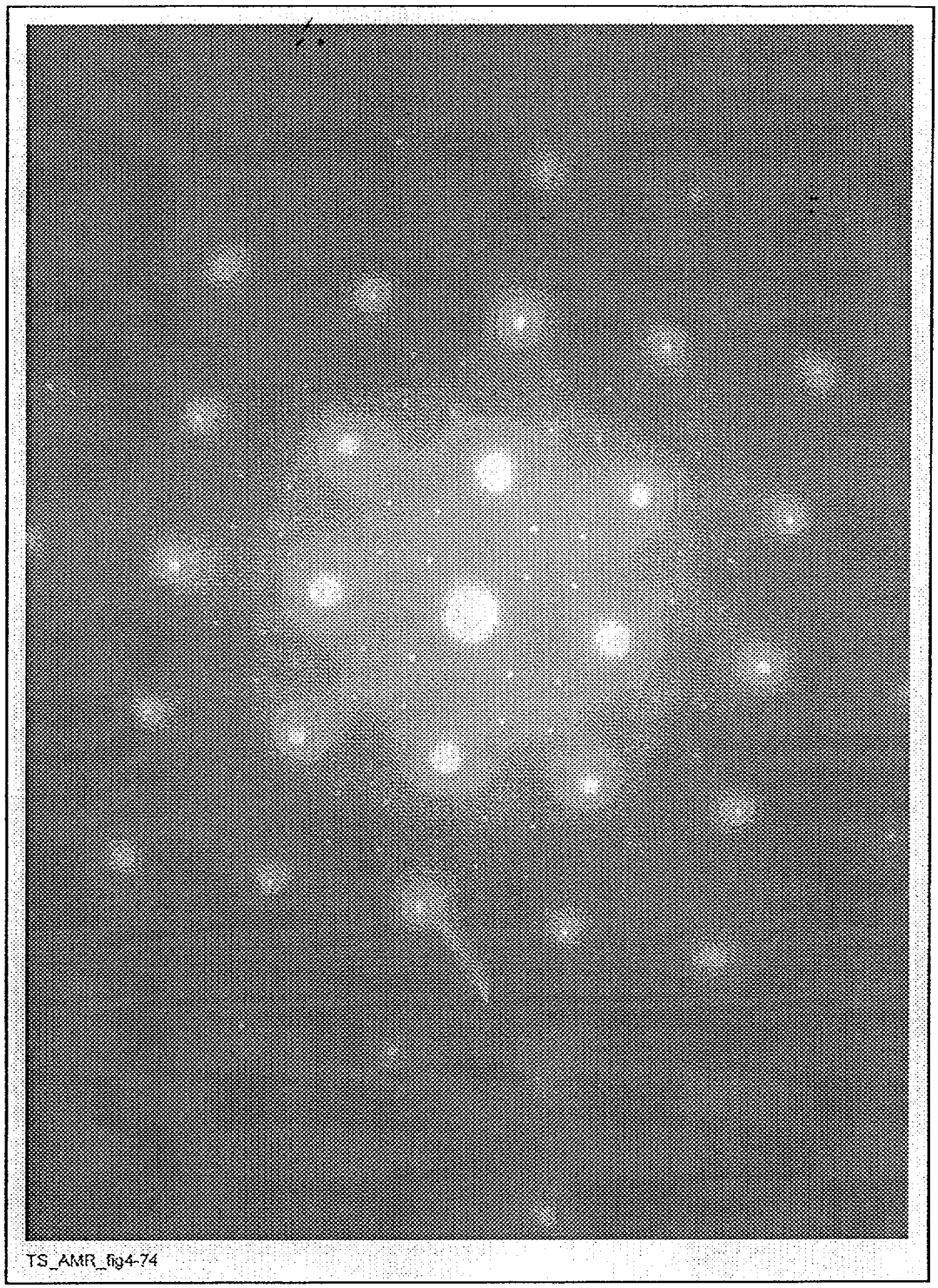


NOTE: The faint superlattice reflections are due to LRO. (TS369-003a, Image 1483, 12/16/98, SN #393, pp. 61.-.65)

Figure 77. SAD Pattern from the Area Shown in Figure 75 [DTN # LL000115905924.113]

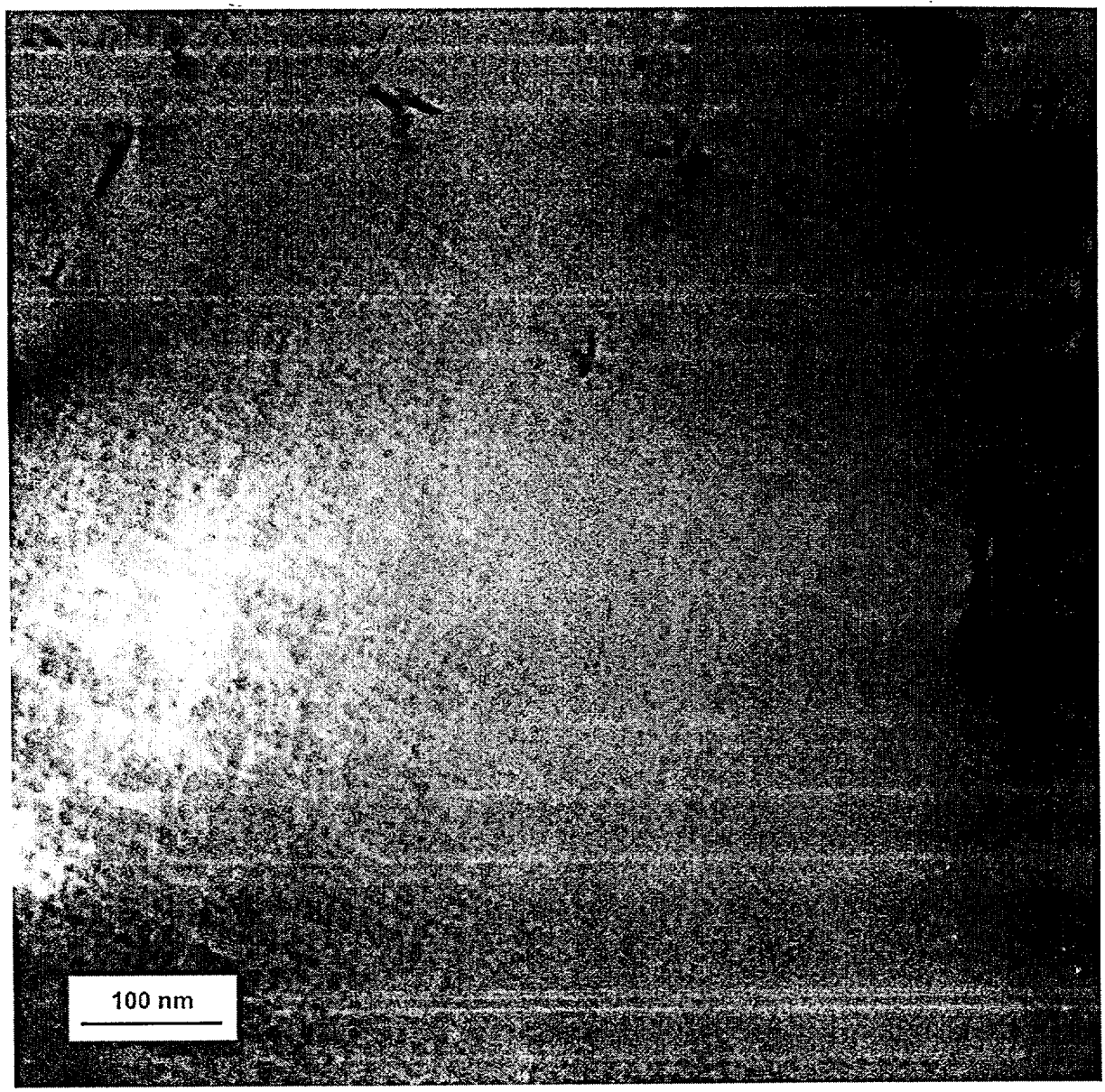


TS_AMR_fig4-75

NOTE: (TS369-005a base metal, Image 1354, 3/20/98, SN #369, p. 132)

Figure 78. TEM Micrograph from the Base Metal of an Alloy 22 Weld Sample Aged for 40,000 hr at 427°C [DTN # LL000115905924.113]

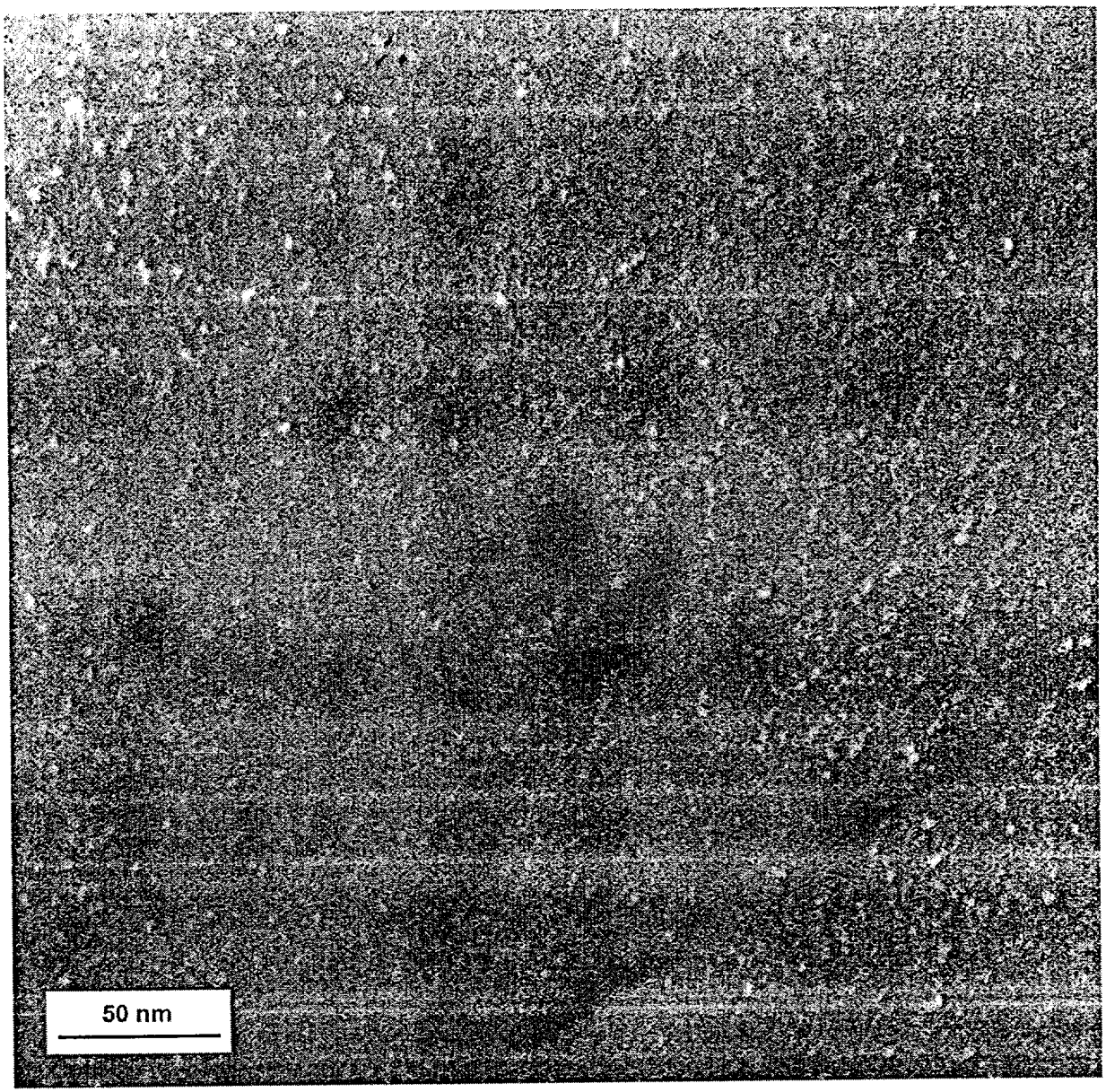


NOTE: One or more variants of the ordered domains appears light. (TS369-005a base metal, Image 1356, 3/20/98, SN #369, p. 133)

Figure 79. Dark-Field Image Corresponding to Figure 78 [DTN # LL000115905924.113]

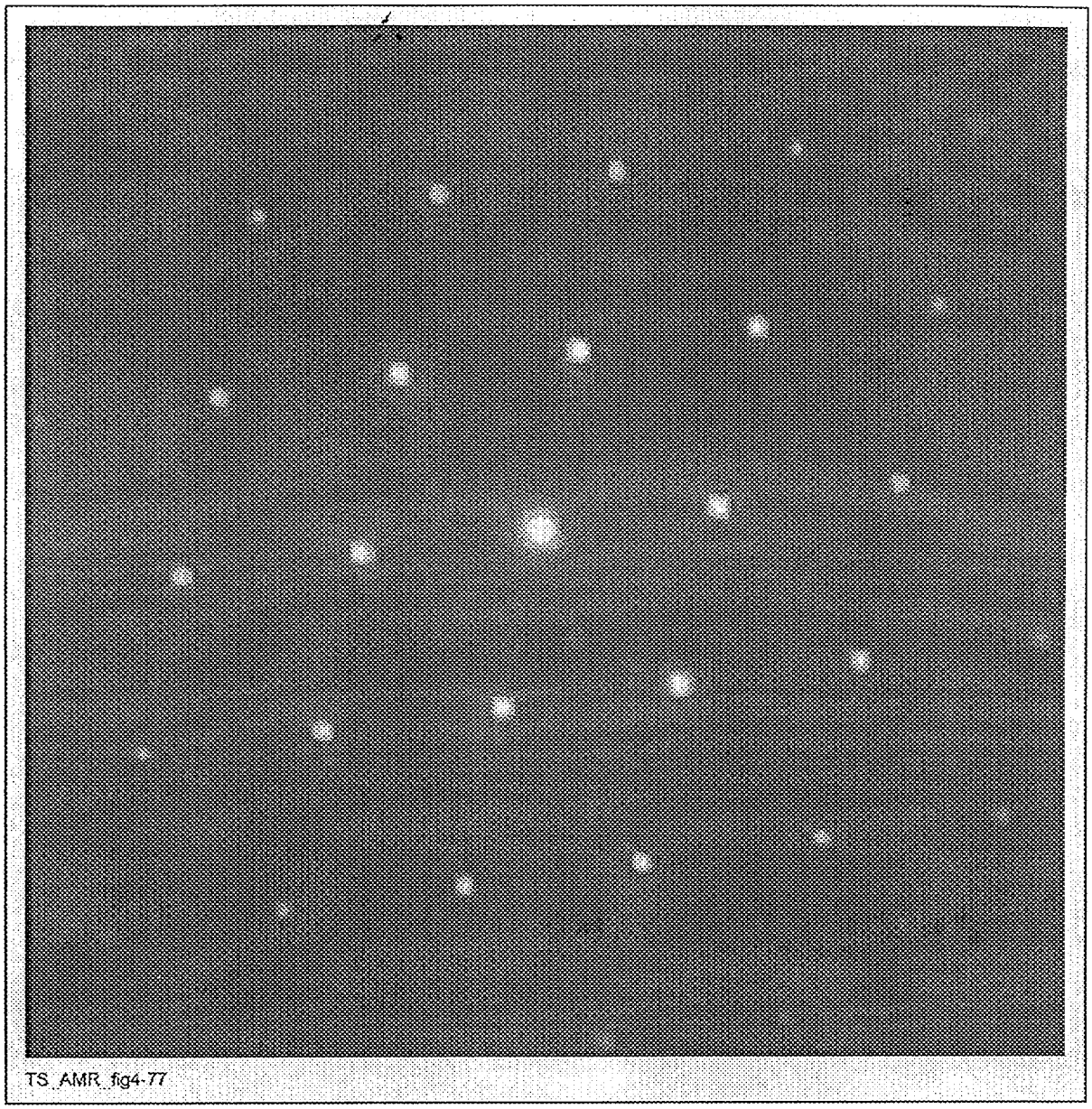


NOTE: The faint superlattice reflections are due to LRO. (TS369-005a base metal, Image 1353, 3/20/98, SN #369, p. 131)

Figure 80. SAD Pattern from the Area Shown in Figure 78 [DTN # LL000115905924.113]

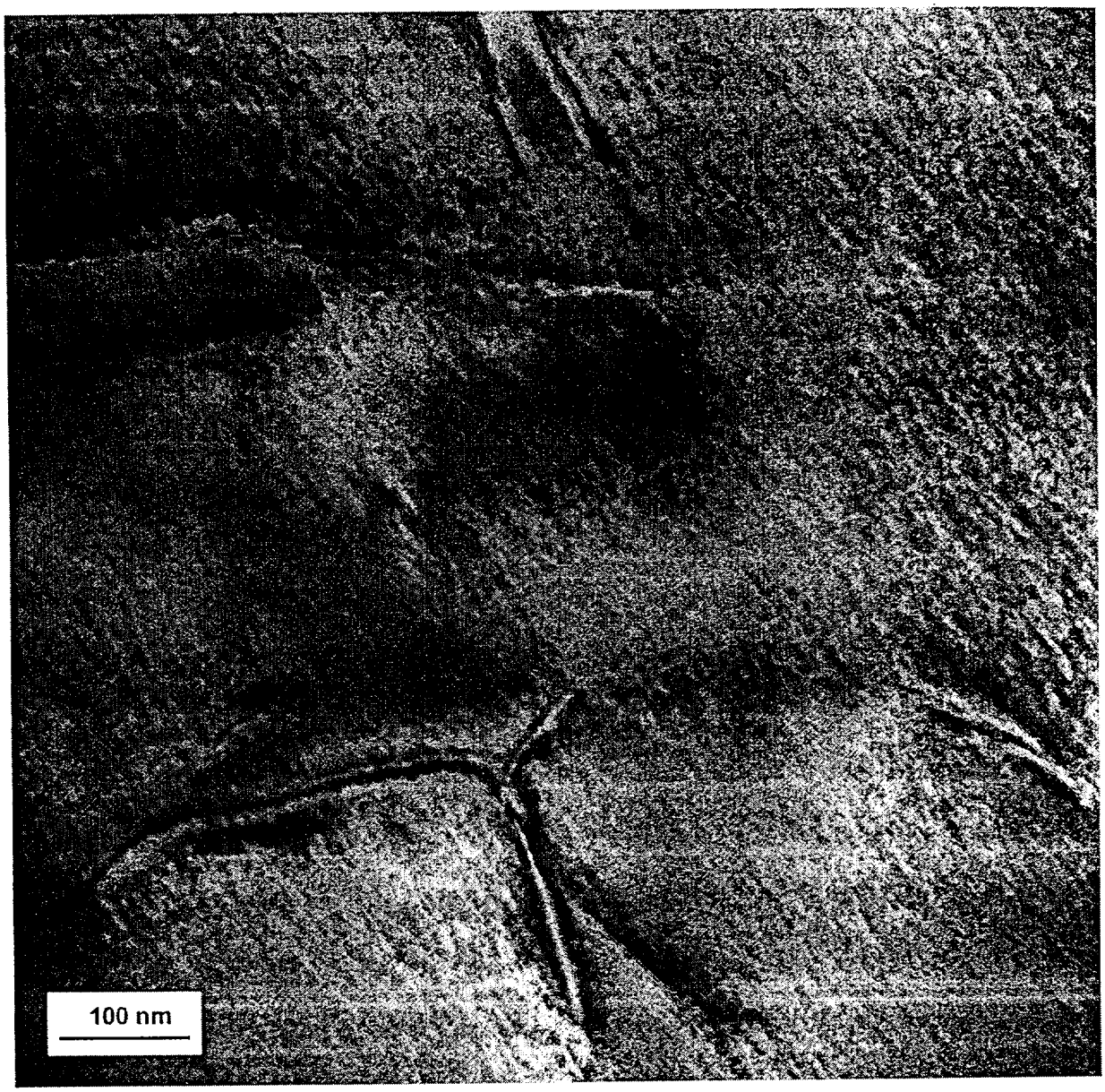


NOTE: (TS369-005a weld metal, Image 1371, 5/21/98, SN #393, p. 26)

Figure 81. TEM Micrograph from the Weld Metal of an Alloy 22 Multipass, Double-V GTAW Weld with Matching Filler Metal Aged for 40,000 hr at 427°C [DTN # LL000115905924.113]

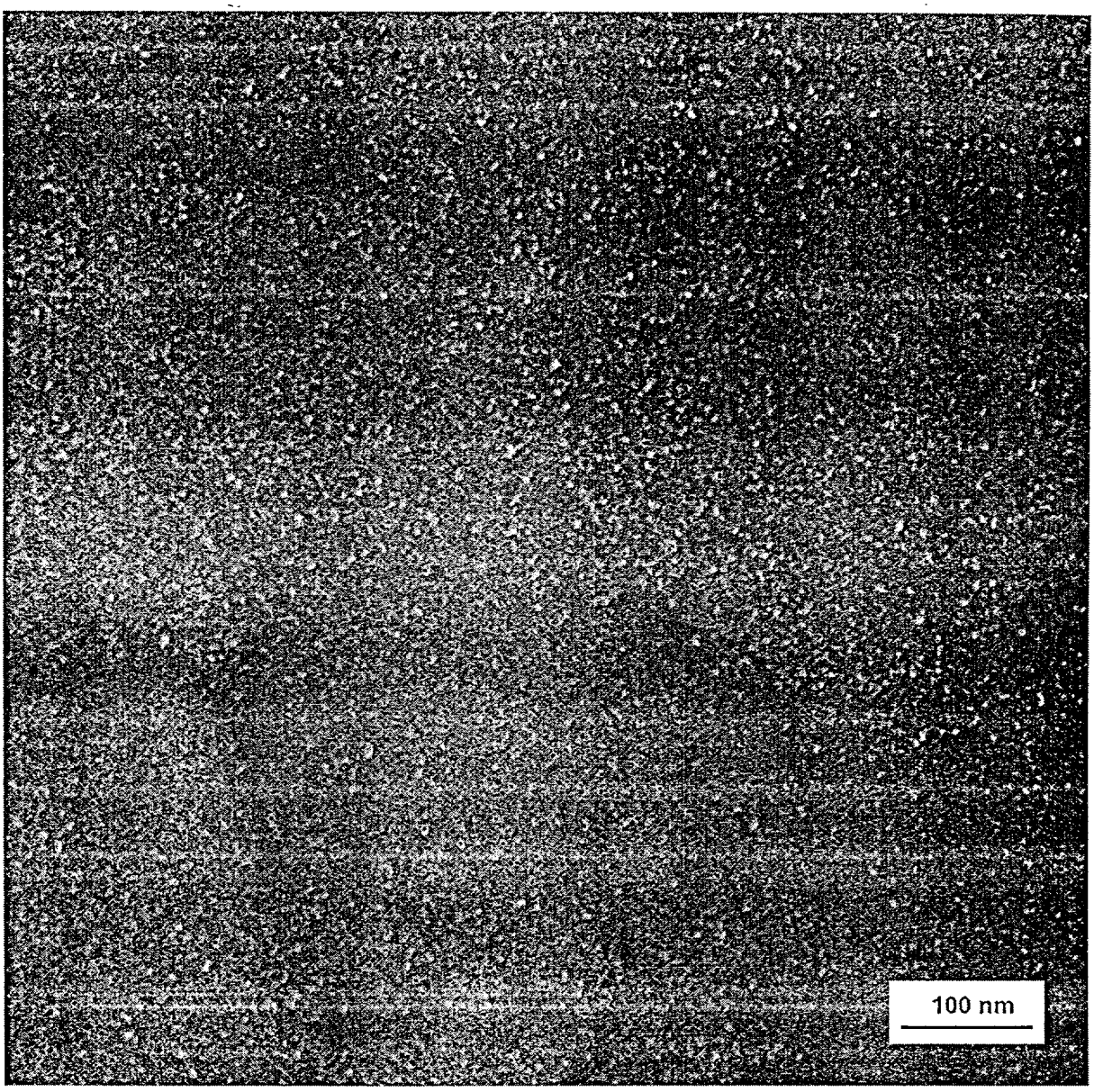


NOTE: The faint white regions are ordered domains. (TS369-005a weld metal, Image 1372, 5/21/98, SN #393, p. 26)

Figure 82. Dark-Field Image Corresponding to Figure 81 [DTN # LL000115905924.113]

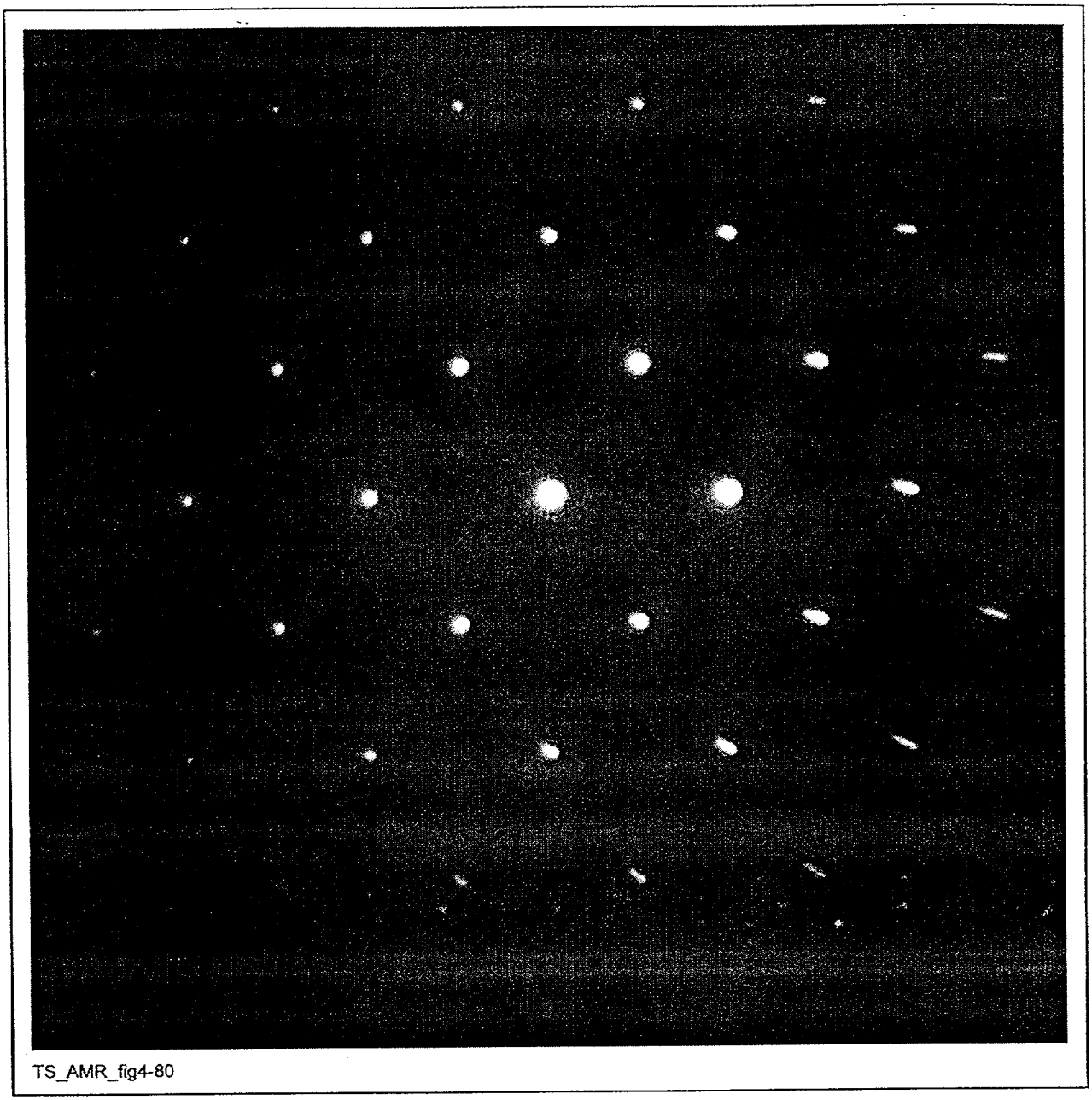


NOTE: The faint superlattice reflections are due to LRO. (TS369-005a weld metal, Image 1370, 5/21/98, SN #393, p. 25)

Figure 83. SAD Pattern from the Area Shown in Figure 81 [DTN # LL000115905924.113]

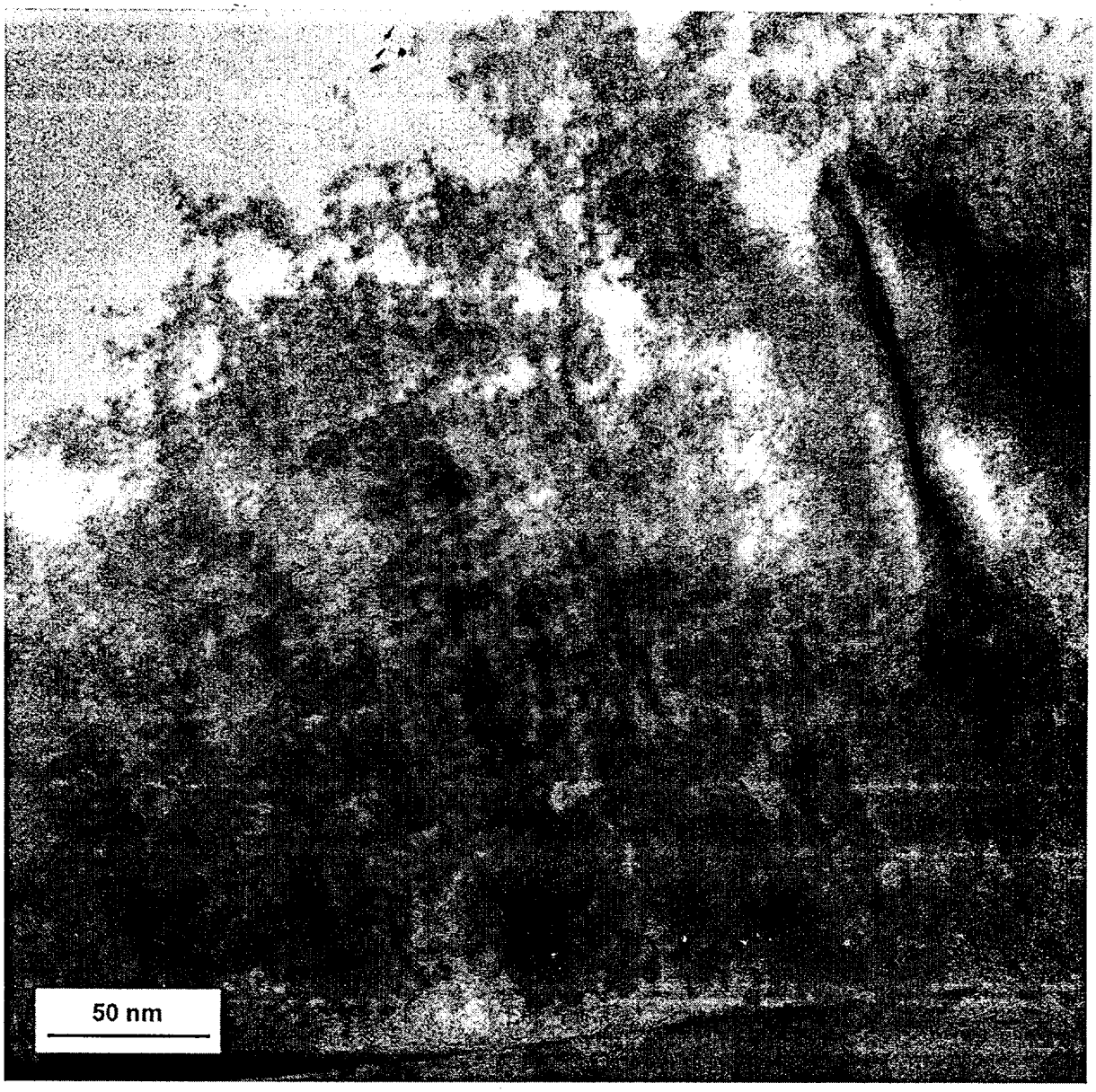


TS_AMR_fig4-81

NOTE: (TS369-005a HAZ, Image 1379, 5/22/98, SN #393, p. 38)

Figure 84. TEM Micrograph from the HAZ of the Alloy 22 Multipass, Double-V GTAW Weld with Matching Filler Metal Aged for 40,000 hr at 427°C [DTN # LL000115905924.113]

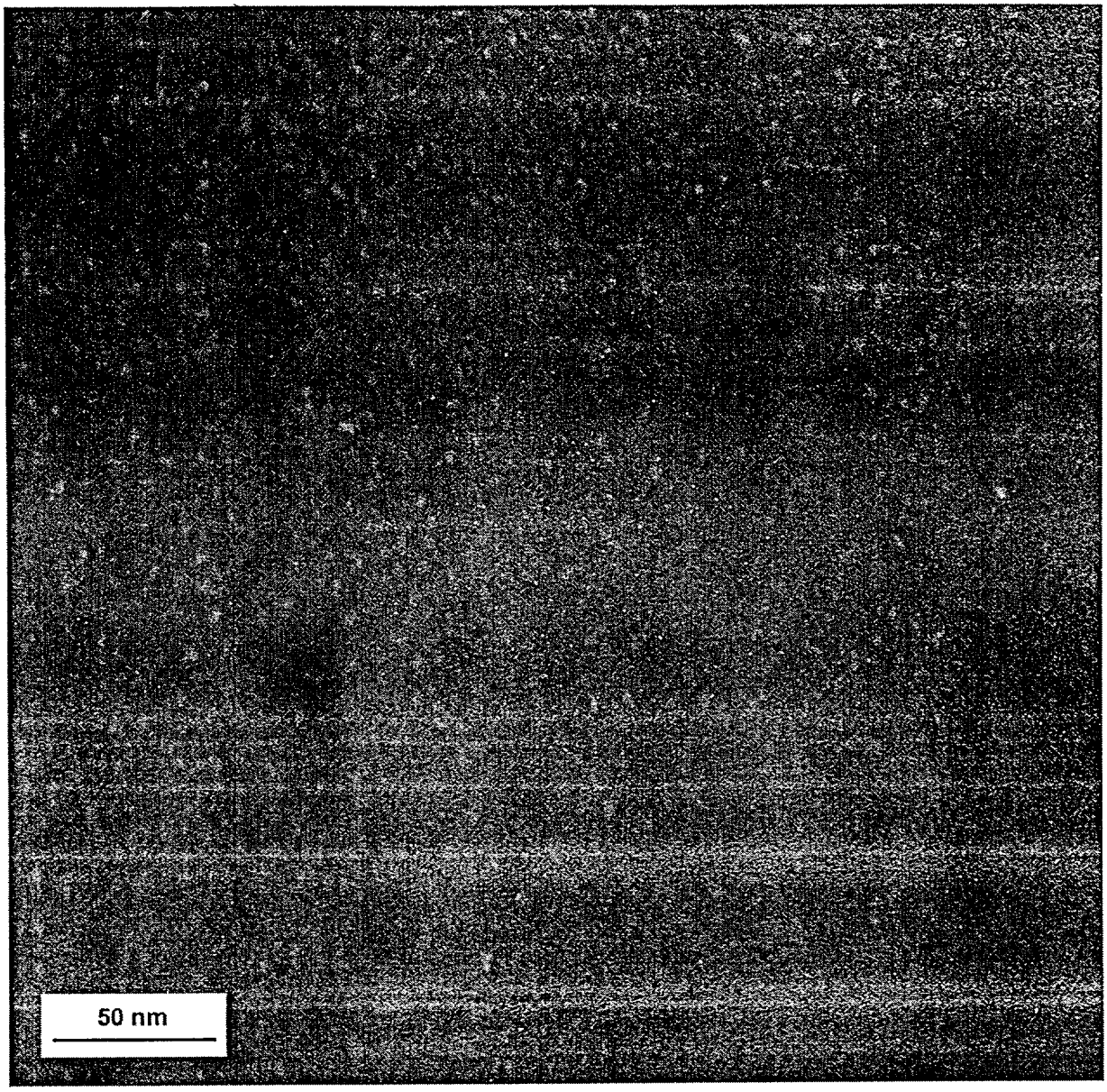


NOTE: The faint white regions are ordered domains. (TS369-005a HAZ, Image 1380, 5/22/98, SN #393, p. 39)

Figure 85. Dark-Field Image Corresponding to Figure 84 [DTN # LL000115905924.113]

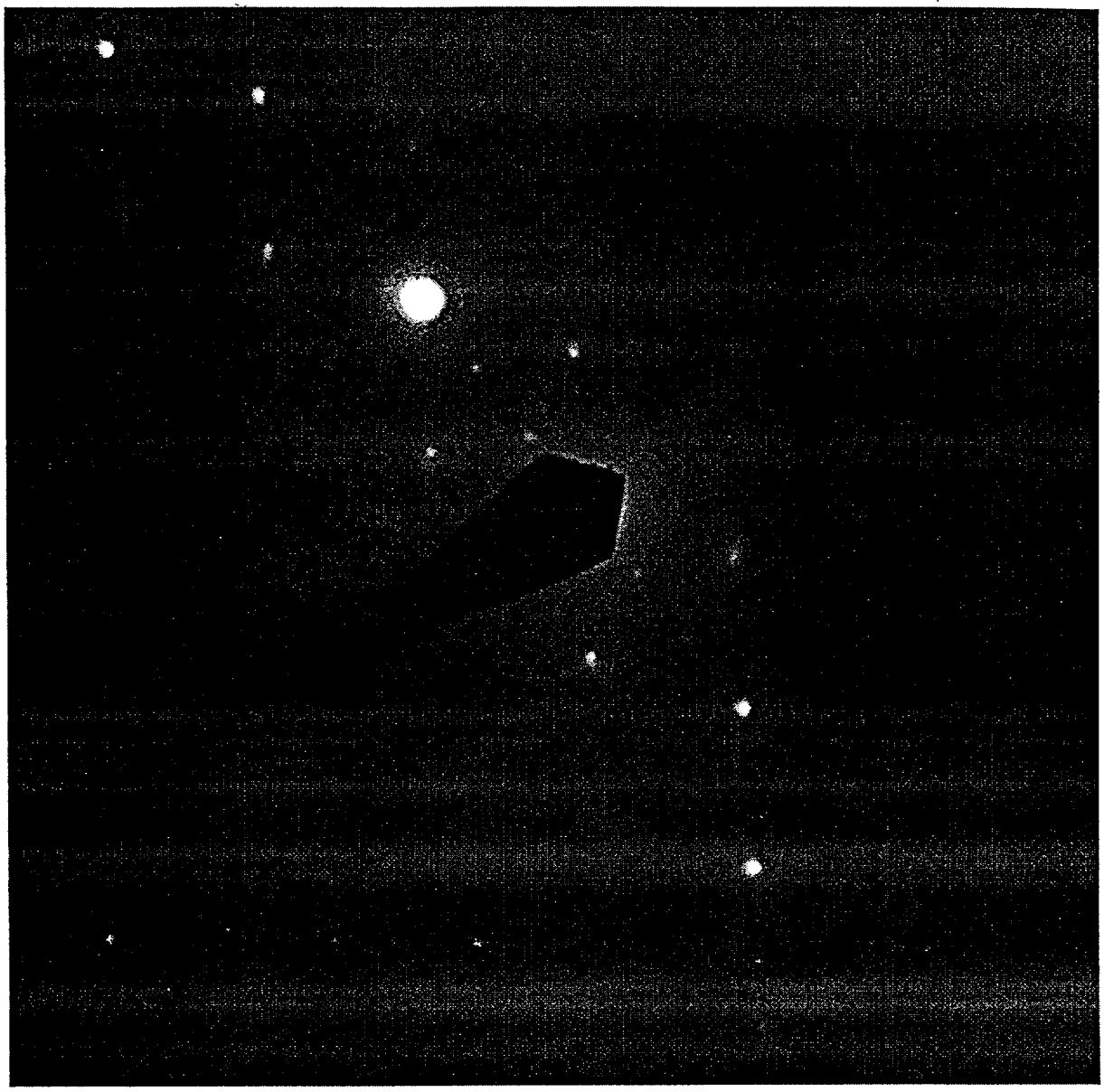

TS_AMR_fig4-83

NOTE: The faint superlattice reflections are due to LRO. (TS369-005a HAZ, Image 1381, 5/22/98, SN #393, p. 39)

Figure 86. SAD Pattern from the Area Shown in Figure 84 [DTN # LL000115905924.113]

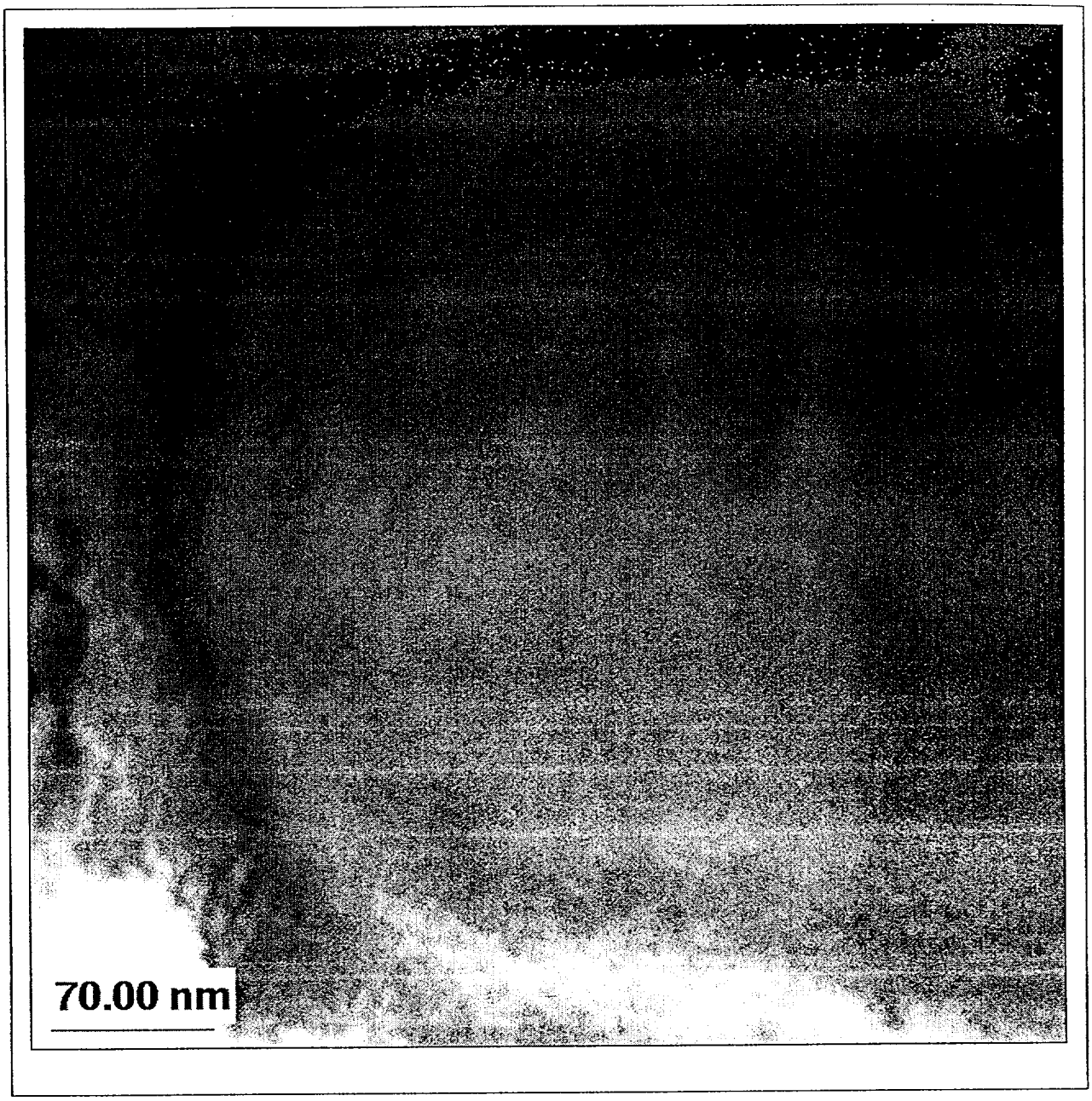


NOTE: The LRO domains are very small and are more easily seen in the dark-field image of Figure 88. (TS393-045b, Image S0274, 8/25/99, SN #442, p. 25)

Figure 87. TEM Micrograph of an Alloy 22 Base Metal Sample Aged for 30,000 hr at 427°C [DTN # LL000115905924.113]

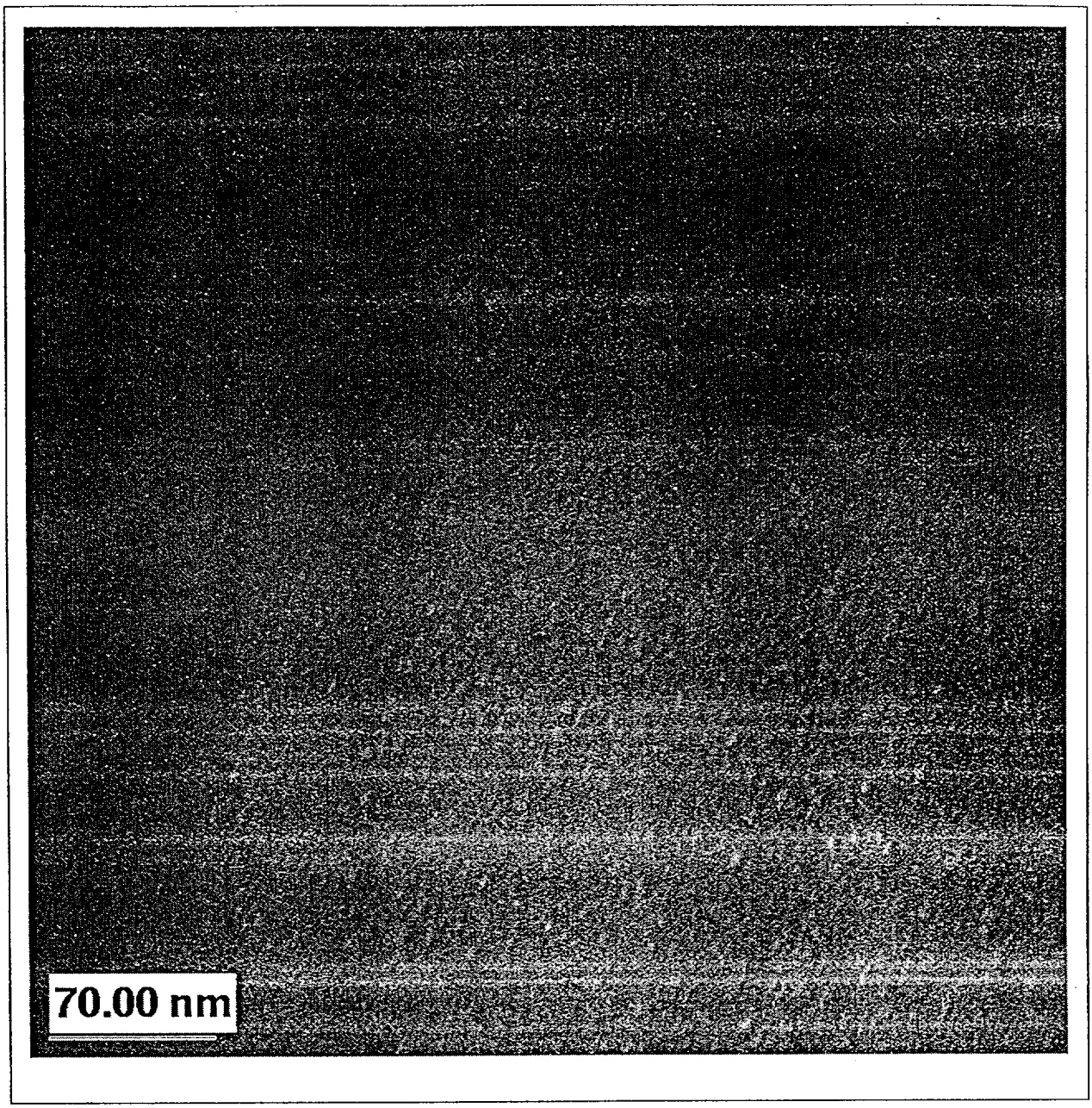


NOTE: The faint white spots are the LRO domains. (TS393-045b, Image S0272, 8/25/99, SN #442, p. 26)

Figure 88. Dark-Field Image Corresponding to Figure 87 [DTN # LL000115905924.113]

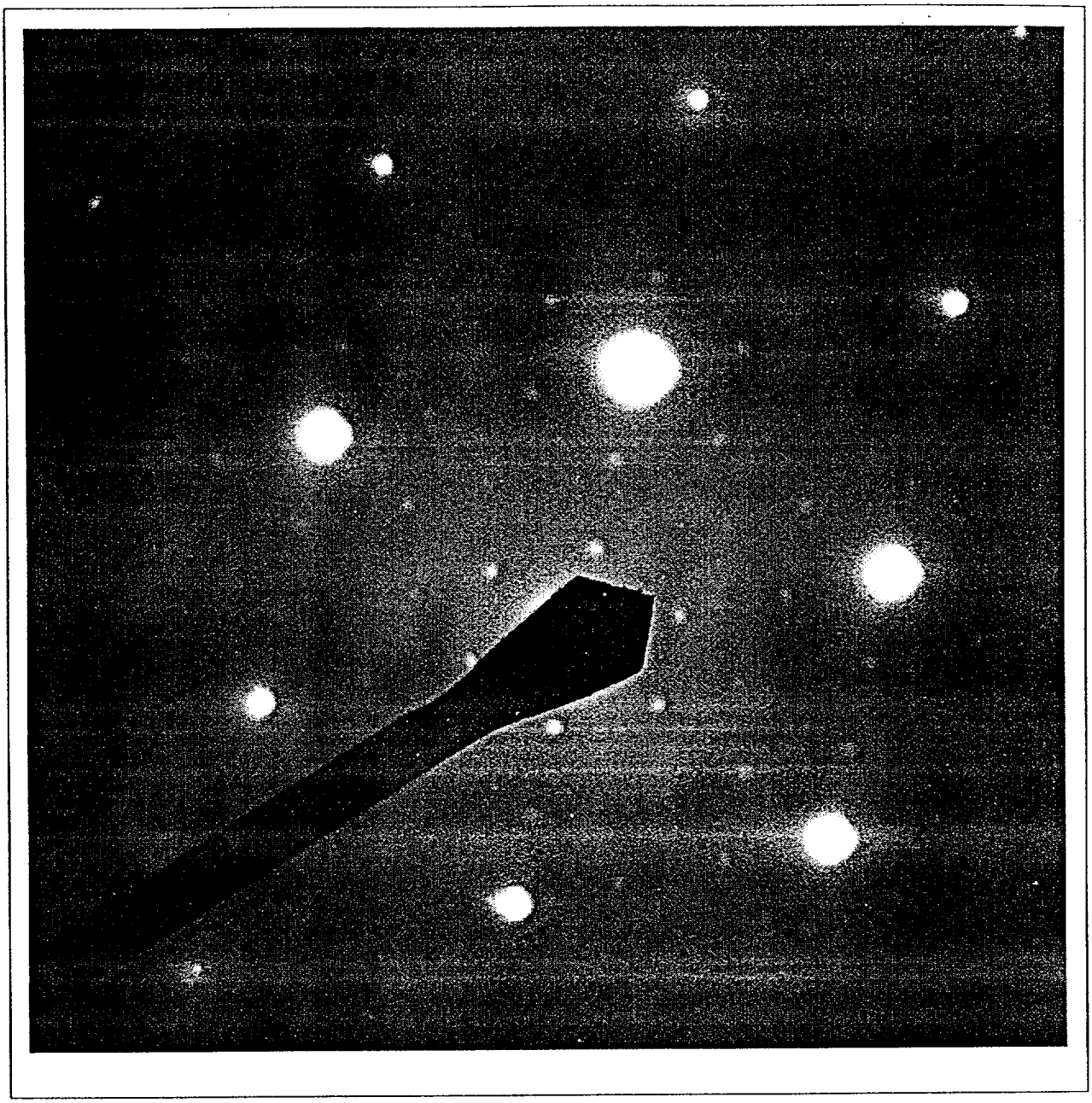

NOTE: (TS393-045b, Image S0271, 8/25/99, SN #442, p. 26)

Figure 89. SAD Pattern from the Area Shown in Figure 87 [DTN # LL000115905924.113]

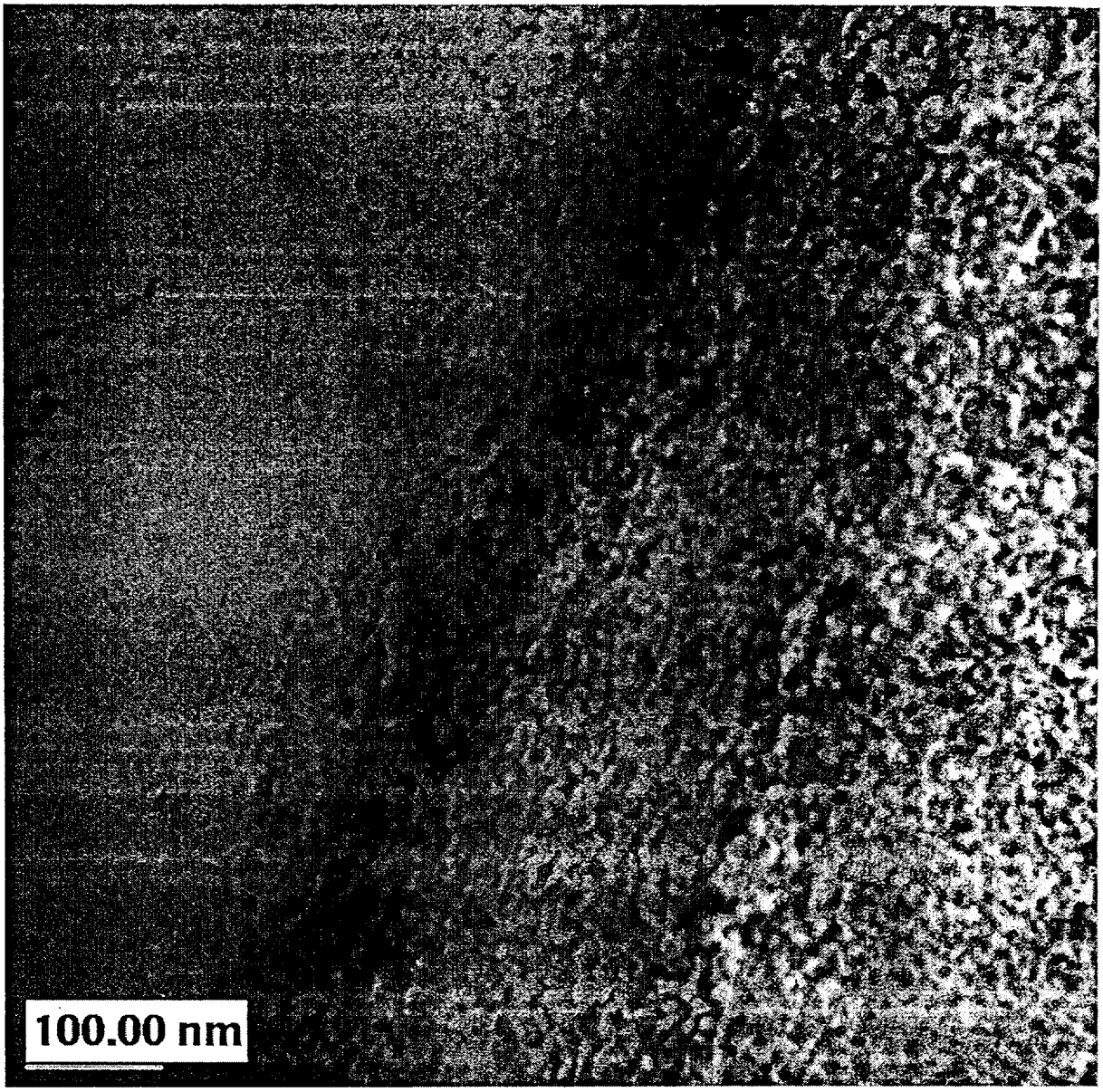


NOTE: (TS393-048b, Image S0251, 8/23/99, SN #442, p. 27)

Figure 90. TEM Micrograph Showing LRO Domains in an Alloy 22 Base Metal Sample Aged for 1000 hr at 538°C [DTN # LL000115905924.113]

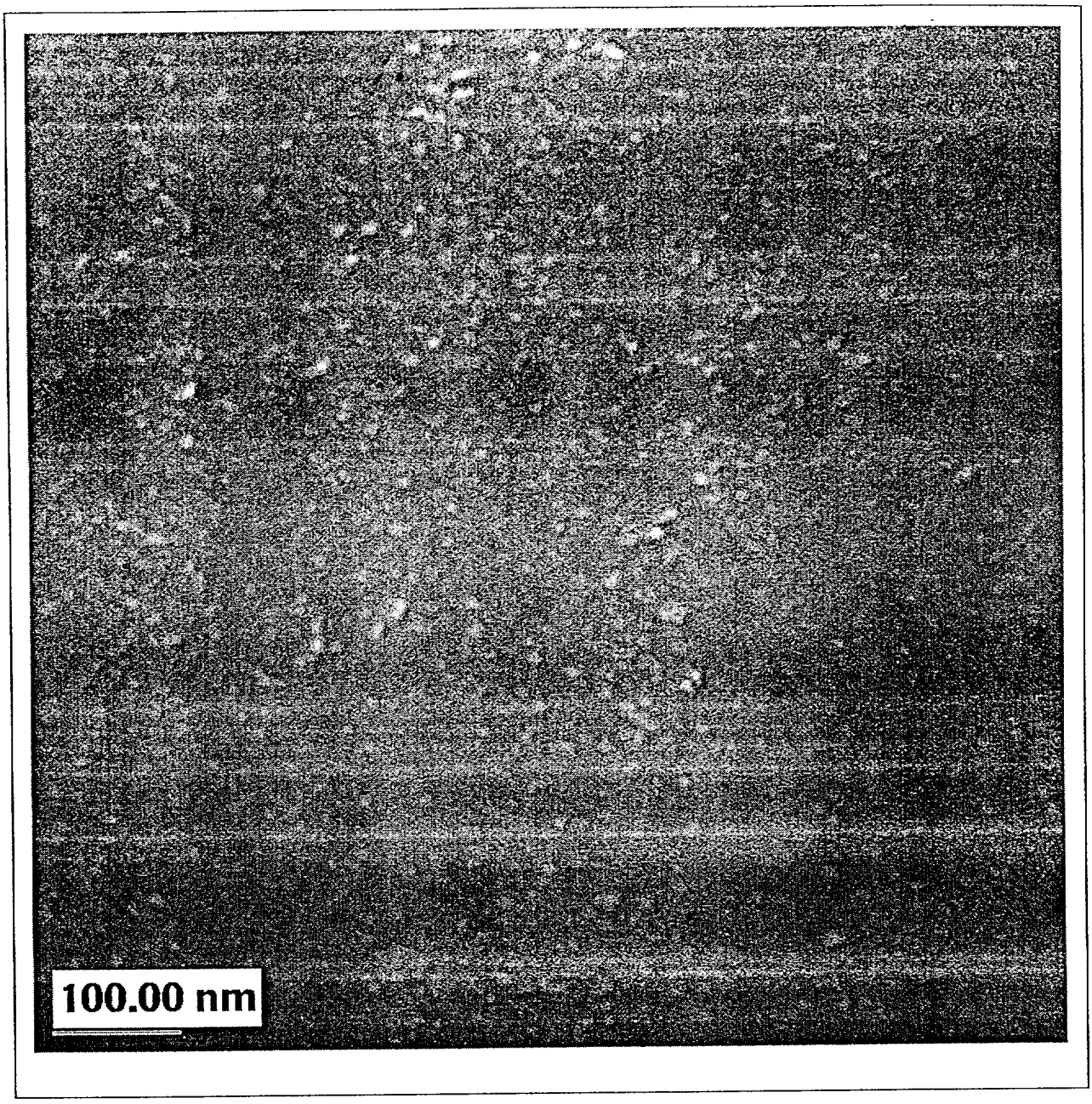


NOTE: The white spots are LRO domains. (TS393-048b, Image S0250, 8/23/99, SN #442, p. 28)

Figure 91. Dark-Field Image Corresponding to Figure 90 [DTN # LL000115905924.113]

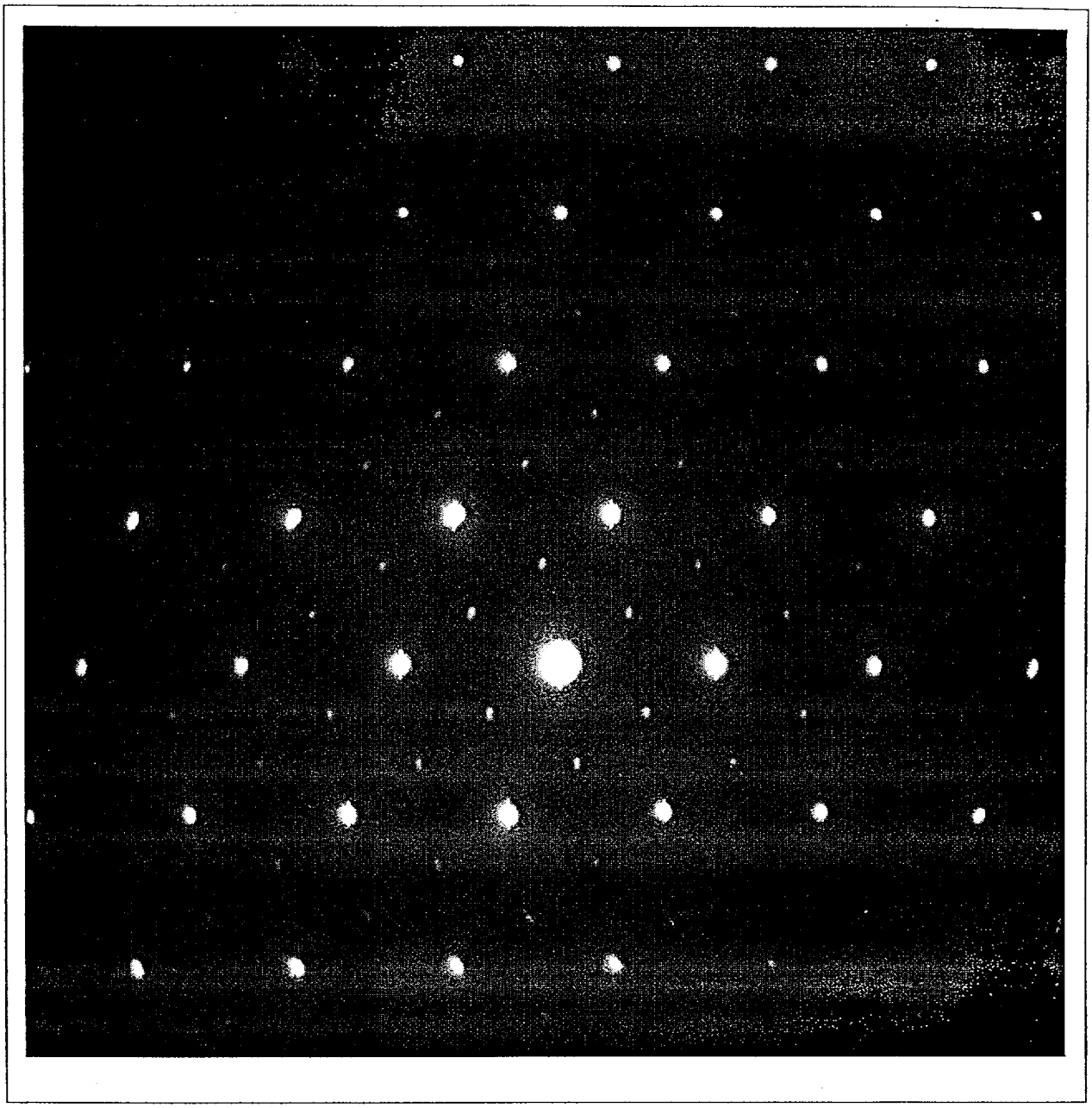

NOTE: (TS393-048b, Image S0252, 8/23/99, SN #442, p. 28)

Figure 92. SAD Pattern from the Area Shown in Figure 90 [DTN # LL000115905924.113]

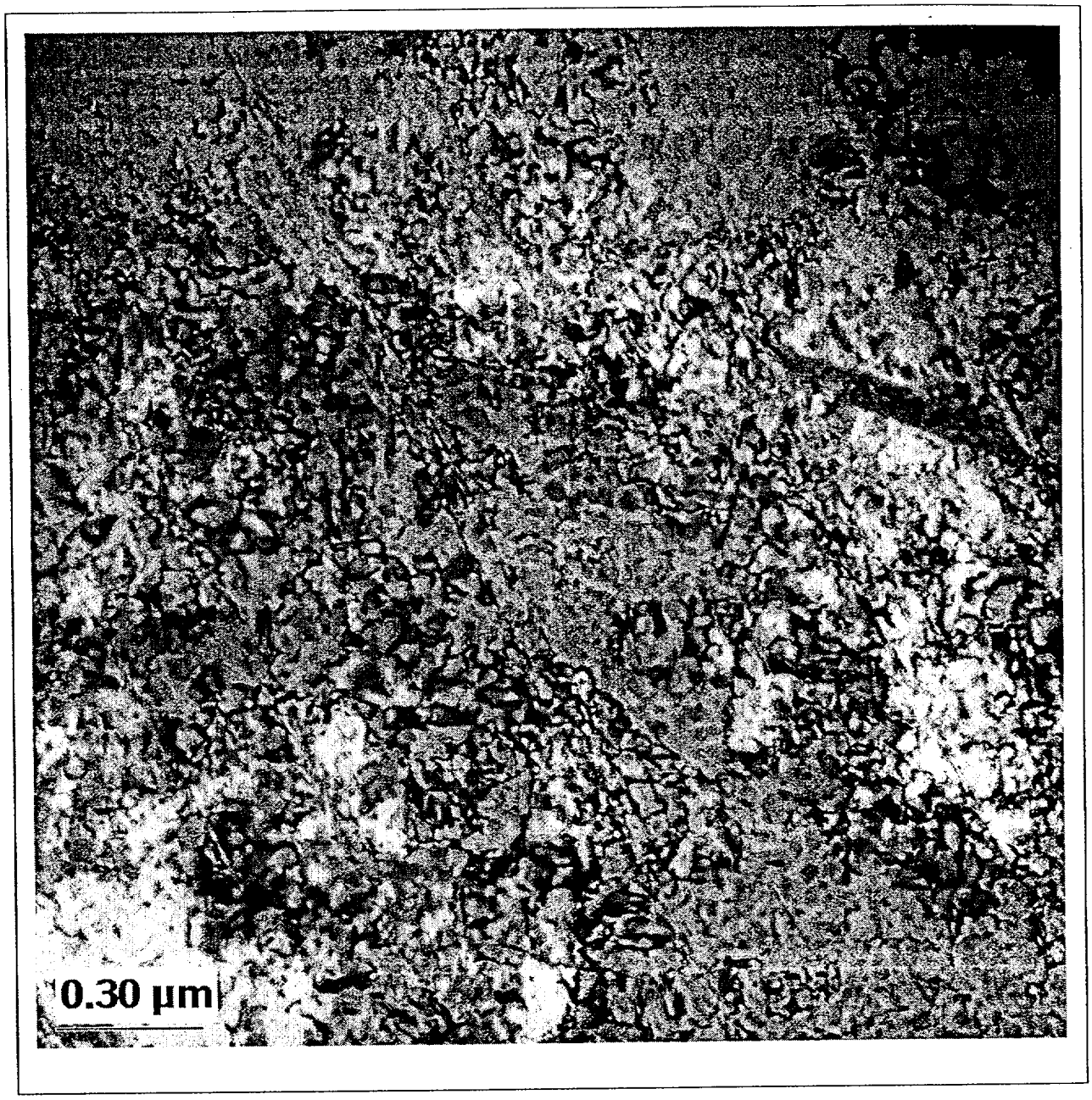


NOTE: (TS393-049b, Image S0243, 8/23/99, SN #442,p. 29)

Figure 93. TEM Micrograph Showing LRO Domains in an Alloy 22 Base Metal Sample Aged for 1000 hr at 593°C [DTN # LL000115905924.113]

NOTE: The white spots are LRO domains. (TS393-049b, Image S0240, 8/23/99, SN #442, p. 30)

Figure 94. Dark-Field Image Corresponding to Figure 93 [DTN # LL000115905924.113]

NOTE: (TS393-049b, Image S0238, 8/23/99, SN #442, p. 30)

Figure 95. SAD Pattern from the Area Shown in Figure 93 [DTN # LL000115905924.113]

## 4.2 CRITERIA

The following criterion applies to phase stability studies of the WPOB:

The disposal container/waste package shall be designed, in conjunction with the Emplacement Drift System and the natural barrier, such that the expected annual dose to the average member of the critical group shall not exceed 25 mrem total effective dose equivalent at any time during the first 10,000 years after permanent closure, as a result of radioactive materials released from the geologic repository. (CRWMS M&O 1999e, Section 1.2.1.3).

## 4.3 CODES AND STANDARDS

There are no codes or standards used in this document.

# 5. ASSUMPTIONS

## 5.1 KINETICS THE SAME FOR THE INTERMETALLIC AND CARBIDE PHASES IN ALLOY 22 (TBV-3045)

The relative amounts of μ, P, σ, and carbide phases have not been quantified; therefore, the kinetics of formation of these phases cannot be calculated independently at this time. It is probably reasonable to assume that their rates of formation are similar. This assumption is based on the following arguments. The amount of carbide and σ phases tends to be low in the samples examined thus far. Therefore, the rates of formation of these phases are not likely to contribute significantly to the overall performance of the WPOB nor are they likely to affect the transformation rates calculated based on volume fraction measurements which include these phases in the total precipitate volume. The μ and P phases are very similar (Leonard 1969, p. 225, ¶ 4; Raghavan et al. 1982, p. 983, Conclusions section, point 2), and the rate at which they form is likely to be similar. It also appears that P phase is a precursor to μ phase (Leonard 1969, p. 223, Figure 1). This would also explain why more P phase (relative to the amount of μ phase) has been observed at the lower temperatures than at the higher temperatures. If P phase is a precursor to μ phase, including the total amount of P + μ as input to the kinetic model is appropriate. A procedure for the quantification of the individual amounts of μ, P, σ, and carbide is currently being developed. Once this procedure is developed, this assumption can be tested directly. This assumption is used in the preliminary kinetic calculations discussed in Section 6.2.

## 5.2 TRANSFORMATION MECHANISMS OPERATING AT THE HIGHER TEMPERATURES INVESTIGATED ALSO OPERATE AT THE LOWER EXPECTED REPOSITORY TEMPERATURES (TBV-3046)

For a WP lifetime of 10,000 years, it is impossible to test directly in the laboratory the behavior of WPOB materials under expected repository conditions. The changes that may occur in these materials must be accelerated. For phase stability studies, phase transformations are accelerated by increasing the temperature. Extrapolation to low temperatures of kinetic data taken at high temperatures assumes two things: (1) the phases that are thermodynamically stable at high temperatures are also stable at the lower temperatures and (2) the mechanism by which the phases form at high temperatures also operates at the lower temperatures. The lower the temperature from which the extrapolation is made, the more likely the validity of these assumptions. This assumption will be based on both experimental and theoretical data. Long-term aging studies, which are currently under way, will allow measurements to be made at temperatures as low as 260°C. Also, theoretical modeling aimed at calculating the Alloy 22 phase diagram and precipitation kinetics has just been started. These calculations will further support the use of this assumption or provide means of calculating WPOB lifetime in the absence of this assumption. This assumption is used in Sections 6.2 and 6.5.

## 5.3 MINOR CHEMISTRY CHANGES WITHIN ASTM SPECIFICATION B575 (HEAT-TO-HEAT VARIABILITY) DO NOT SIGNIFICANTLY AFFECT THE PHASE STABILITY OF ALLOY 22 (TBV-3047)

It is assumed, in this version of the phase-stability analysis, that compositional changes falling within the range acceptable according to ASTM specification B575 (ASTM B 575-94 1994, p. 410, Table 1) for Alloy 22 do not significantly affect the precipitation kinetics. This assumption is based on the similarity of data collected from different heats of Alloy 22. Compare, for example, the time-temperature-transformation (TTT) diagram produced in this study (Section 6.2, Figure 96) and that published by Heubner et al. (1989, p. 252, Figure 4). This assumption is used throughout the model.

Very little data which would allow comparison of results from different heats of Alloy 22 exists. Eventually, work will need to be done to investigate heat-to-heat variability and confirm this assumption. There is some evidence that varying W and/or Fe within the range allowed by ASTM specification B575 (ASTM B 575-94 1994, p. 410, Table 1) may impact phase stability of alloy 22 (Heubner et al. 1989, p. 251, Figure 3). Thus, any heat-to-heat variability studies done to lift the TBV on this assumption will have to investigate the full range of values for these elements allowed by ASTM B575 (ASTM B 575-94 1994, p. 410, Table 1). If this assumption turns out not to be valid, the effect of minor compositional changes on phase stability will be evaluated. If necessary, the composition can be limited to smaller ranges than allowed by ASTM specification B575 (ASTM B 575-94 1994, p. 410, Table 1).

# 6. MODEL

## 6.1 PHASE IDENTIFICATION IN ALLOY 22

Alloy 22 samples were aged for 40,000 hr at 260, 343, and 427°C; for 30,000 hr at 427°C; for 1000 hr at 482, 538 and 593°C; and for 16,000 hr at 593, 649, 704, and 760°C and examined in TEM. A weld sample aged at 427°C for 40,000 hr was also observed in the weld metal, in the HAZ, and in the base metal removed from the weld. The other samples used for the subsequent kinetic arguments were not examined in TEM. Several phases were observed to form in Alloy 22: P, μ, σ, carbide, and $Ni_2(Cr,Mo)$ LRO. At 593°C, P phase was observed only on the grain boundaries. This is shown in Figures 1 through 6. At the higher aging temperatures (649, 704, and 760°C), both μ and P phase precipitated on grain boundaries (see Figures 9 through 14, 18, 21, 22, 25, 27, and 37 through 39). As the aging temperature increased, more μ and P phase precipitation occurred within the grains (see Figures 15 through 17, 28 through 30, 35, and 36). Grain boundary carbide precipitation was observed in samples aged at 593 and 704°C (see Figures 7, 8, 18 through 20, 23, and 24). Because of the small amount of carbide present in these samples and the small volume examined in TEM, it is likely that carbides also form at 649°C. They may or may not form at 760°C. Because of the similarity between the $M_6C$, the $M_{12}C$, and the $M_{23}C_6$-type carbide crystal structures, the specific carbide forming in these samples was not identified; however, it is a cubic carbide with lattice parameter of 10-11 Å. A σ phase was observed in the samples aged at 704 and 760°C (see Figures 25, 26, and 31 through 34). The amount of σ observed in these samples was small compared to the amount of μ and P. LRO was observed in the samples aged at 593°C for 16,000 hr (see Figures 75 through 77) and for 1000 hr (see Figures 93 through 95), in the sample aged at 538°C for 1000 hr (see Figures 90 through 92), and in the samples aged at 427°C for 40,000 hr (see Figures 78 through 86) and for 30,000 hr (see Figures 87 through 89). These observations are summarized in Table 1.

The results of this section are preliminary and extensive model validation has not yet been done. However, these data have been published in the open literature (Summers et al. 1999) and are consistent with other published results. For example, in Hastelloy Alloy C-276, an alloy in the same class as Alloy 22, mostly μ and P phases were seen after aging above about 650°C (Leonard 1969, p.228, Conclusions Section, point 5). Also, more μ relative to P was seen in C-276 as aging temperature was increased (Leonard 1969, p. 224, Table 2; Raghavan et al. 1982, Conclusions Section). In the earlier papers, μ phase had not been named; it was called the $Ni_7Mo_6$-type phase. By the time of the Raghavan et al. (1982) paper, this phase had been identified as μ. The presence of carbides is also consistent with previously published results for C-276 (Raghavan et al. 1982, Conclusions Section). The observance of LRO after aging between 427°C and 593°C is consistent with previously published occurrences of LRO in C-276 and in Alloy 22 (Tawancy et al. 1983, p.40, ¶ 4; Rebak and Koon 1998, Figure 9 and Conclusions Section, point 5). The presence of σ phase after aging above 700°C has not been previously reported in Alloy 22. There is not a lot of σ in these samples, and its presence is currently ignored (see Section 5.1).

The TEM micrographs from the samples in Section 4.1.1 were taken from samples aged for 16,000 hr at 593, 649, 704, and 760°C and for 1000 hr at 593°C. Samples aged for shorter time intervals have not been examined in TEM; therefore, evolution of the phases during aging is not known. Also, when a large number of precipitates is involved, TEM diffraction analysis is a cumbersome method of phase identification. This is especially true when the crystal structures of the various phases are similar. A single SAD pattern is often not enough to distinguish the phases that form in Alloy 22. Two patterns with a known tilt between them frequently must be analyzed. For this reason, little quantitative data exist for the relative amounts of each phase as a function of temperature. Chemical phase extraction and x-ray diffraction techniques might yield more quantitative results.

Table 1. Phases Observed in Alloy 22 in TEM [DTN # LL000115905924.113]

| Aging Condition | Phases Observed to Form in Alloy 22 |
|---|---|
| 260°C for 40,000 hr | No LRO<br>No signs of grain boundary precipitation in base metal |
| 343°C for 40,000 hr | No LRO<br>No signs of grain boundary precipitation in base metal |
| 427°C for 30,000 hr | LRO<br>No signs of grain boundary precipitation in base metal |
| 427°C for 40,000 hr | LRO<br>No signs of grain boundary precipitation in base metal |
| 482°C for 1000 hr | No LRO<br>No signs of grain boundary precipitation in base metal |
| 538°C for 1000 hr | LRO<br>No signs of grain boundary precipitation in base metal |
| 593°C for 1000 hr | LRO<br>Grain boundary films of P phase |
| 593°C for 16,000 hr | LRO<br>Grain boundary films of P phase<br>Carbide precipitates at grain boundaries |
| 649°C for 16,000 hr | No LRO<br>Precipitation of P and μ phase mainly at grain boundaries |
| 704°C for 16,000 hr | No LRO<br>Precipitation of P and μ phase at grain boundaries and within the grains<br>Carbide and σ precipitation at grain boundaries |
| 760°C for 16,000 hr | No LRO<br>Precipitation of P and μ phase at grain boundaries and within the grains<br>σ precipitation at grain boundaries |

## 6.2 KINETICS OF INTERMETALLIC PRECIPITATION IN ALLOY 22 BASE METAL

For this preliminary investigation, no distinction has been made between the various intermetallic and carbide phases that form. It is very difficult to distinguish these phases in SEM. Instead, it is assumed that the P and μ phases are kinetically similar and that there is only a small amount of carbide and σ phase. It is generally accepted that P and μ are similar (Leonard 1969, p. 225, ¶ 4; Raghavan et al. 1982, p. 983, Conclusions section, point 2), and, therefore, the kinetics of their

formation is expected to be similar. The validity of these assumptions will be verified as discussed in Section 5.2.

Table 2 lists the approximate times for the noted stages of intermetallic precipitation in Alloy 22 base metal as a function of temperature. These times were approximated from the images in Figures 40 through 63. Aged samples were observed after approximately 1, 10, 100, 1,000, and in some cases 16,000 hr. The errors noted are due to the uncertainty associated with the coarse time intervals of examination and not with any measurement and test equipment uncertainties, which are much smaller. For example, if precipitation was observed on twin boundaries at 100 hr, it could have begun at any time between 10 and 100 hr. In that case, the time noted for the start of precipitation on the twin boundaries would be 55 hr (halfway between 10 and 100), with upper and lower error bars of 45 hr. Because of the coarse examination intervals, there is some judgment involved in choosing the times noted in Table 2. These measurements are only intended as an initial estimate of the precipitation kinetics. The preceding observations were also used to generate the isothermal TTT diagram for Alloy 22 base metal shown in Figure 96. The curve associated with LRO came from TEM observations. Only a limited number of samples were examined in TEM; therefore, it is likely that ordering occurs at shorter times than indicated in Figure 96.

Table 2. Time for Intermetallic and Carbide Precipitation in Alloy 22 Base Metal to Begin on and Cover Grain Boundaries, Begin on Twin Boundaries, and Begin within the Grains as a Function of Temperature [DTN # LL000116005924.114]

| Temp | Time to Start on Grain Boundaries | | | Time to Cover Grain Boundaries | | |
|---|---|---|---|---|---|---|
| (°C) | Lower Error | Time (hr) | Upper Error | Lower Error | Time (hr) | Upper Error |
| 593 | 0 | 10 | 90 | 7500 | 8500 | 7500 |
| 649 | 1 | 1 | 9 | 450 | 550 | 450 |
| 704 | 0.5 | 0.5 | 0.5 | 90 | 100 | 900 |
| 760 | 0.5 | 0.5 | 0.5 | 9 | 10 | 109 |
| 800 | 0.5 | 0.5 | 0.5 | 9 | 10 | 90 |
| **Temp** | **Time to Start on Twin Boundaries** | | | **Time to Start Within Grains** | | |
| **(°C)** | **Lower Error** | **Time (hr)** | **Upper Error** | **Lower Error** | **Time (hr)** | **Upper Error** |
| 593 | | | | | | |
| 649 | 450 | 550 | 450 | 7500 | 8500 | 7500 |
| 704 | 90 | 100 | 900 | 450 | 550 | 450 |
| 760 | 54.5 | 64.5 | 54.5 | 54.5 | 64.5 | 54.5 |
| 800 | 45 | 55 | 45 | 45 | 55 | 45 |

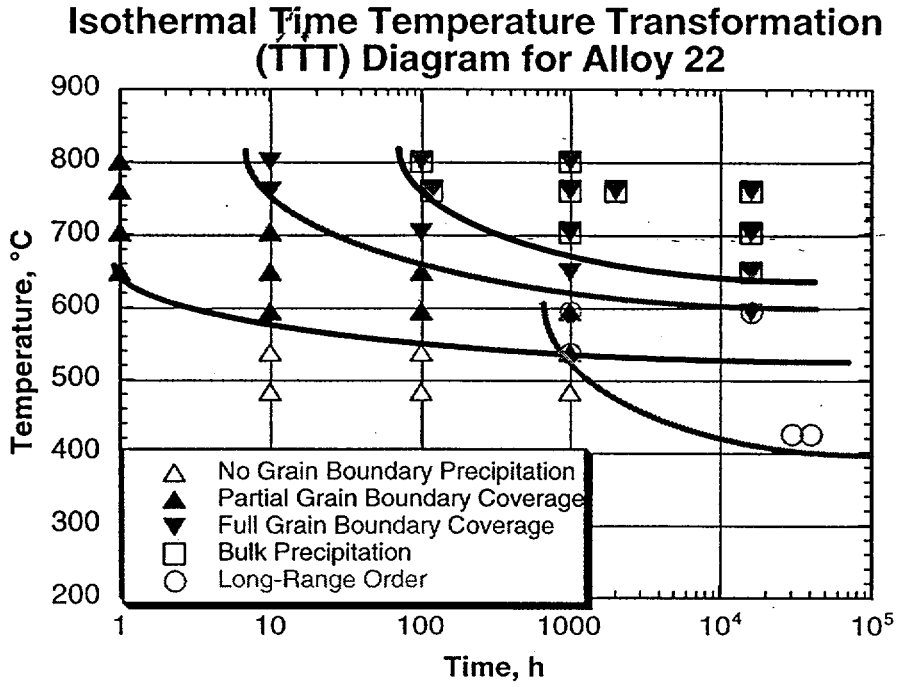


Figure 96. Isothermal TTT Diagram for Alloy 22 Base Metal [DTN # LL000116005924.114]

Nucleation and growth kinetics can often be represented by an equation of the form:

$$f = 1 - \exp(-kt^n) \qquad \text{(Eq. 1)}$$

where $f$ is the volume fraction of the precipitating phase, $t$ is time at the aging temperature, and $k$ and $n$ are constants (Christian 1981, p. 19, Eq. 4.11). The value of $k$ depends on nucleation and growth rates and therefore depends very strongly on temperature, usually of the form:

$$k = C_1 \exp(-C_2 / T) \qquad \text{(Eq. 2)}$$

where $C_1$ and $C_2$ are constants, and $T$ is the temperature (e.g., Christian 1981, p. 438, Eq. 49.2). Ideally, the volume fraction of precipitation would be measured as a function of time and temperature and fit to Eq. 1. The times in Table 2 can be fit to Eq.1 if it is modified for a constant volume fraction. Combining Eq. 1 and Eq. 2 at constant volume fraction yields:

$$\ln(t_f) = \frac{C_2}{n} \cdot \frac{1}{T} + C_f \qquad \text{(Eq. 3)}$$

The times in Table 2 can be fit to Eq. 3 because complete grain boundary coverage, for example, occurs at a constant volume fraction at different temperatures if the grain size and the thickness of the precipitation layer at the boundaries are the same. Plots of log(time) versus reciprocal temperature for the various precipitation stages in Alloy 22 base metal are given in Figure 97.

higher temperatures, grain boundary precipitation was seen to have already begun after 1 hr, which is the shortest aging time investigated thus far. Because precipitation on grain boundaries actually began at shorter times, these times were not plotted. The time at 649°C, however, was plotted because precipitation had only just started at a few sites on the grain boundaries in that sample.

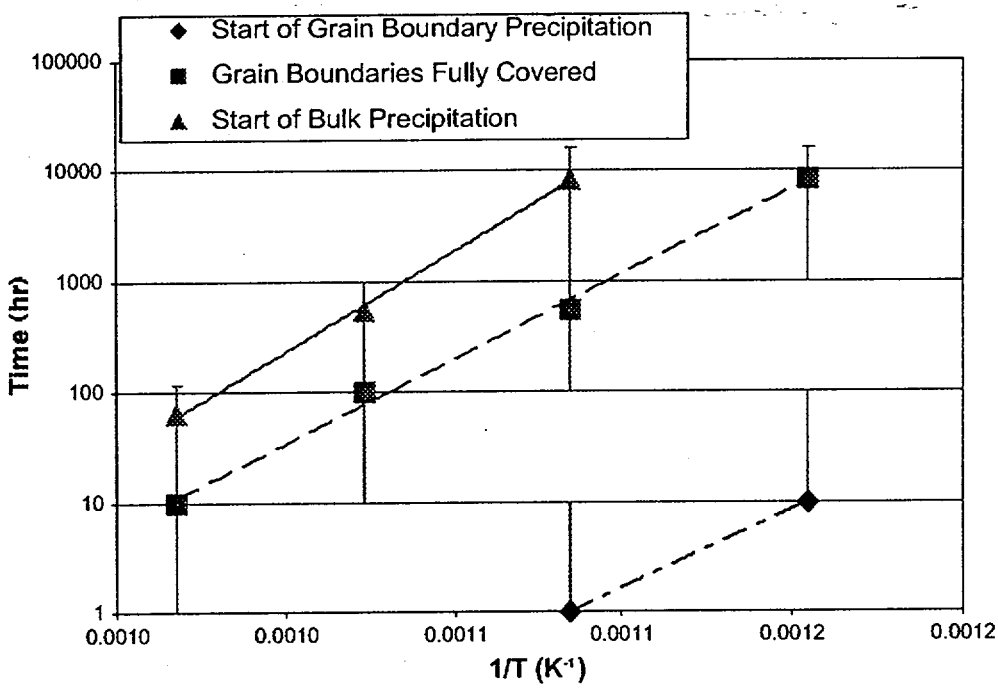


Figure 97. Time to Reach Various Stages of Precipitation in Aged Alloy 22 Base Metal Plotted on a Log Scale as a Function of Reciprocal Temperature (see Eq. 3). The temperatures in Table 2 were converted to Kelvin (K) by adding 273 and the reciprocals were taken in Microsoft Excel. These calculations were verified by hand before plotting. [DTN # LL000116005924.114]

If it can be assumed that the precipitation mechanism does not change, the lines in Figure 97 can be extrapolated to give the times that can be expected for the various stages of precipitation at lower temperatures. These data, however, are very preliminary. The times were estimated from examination of micrographs from samples with widely spaced aging times. Extrapolation to lower temperatures is difficult because the precipitation rate is quite sensitive to temperature; small changes in slope make a very large change in the time obtained from extrapolation to lower temperatures. In order to make a bounding argument, however, the curves associated with grain boundary coverage and bulk precipitation in Figure 97 are graphically extrapolated to 10,000 yr in Figure 98. The start of grain boundary precipitation is not plotted because of the limited amount of available data.

The horizontal axes in Figure 98 are reciprocal temperature; temperature increases to the left. If an extrapolation of the data intersects the horizontal line corresponding to 10,000 years to the left of the vertical line corresponding to 300°C, then the temperature must be held higher than 300°C

to get failure in 10,000 yr. In both cases, the data indicate that intermetallic precipitation will not occur in less than 10,000 years even if the temperature is held at 300°C. This temperature constraint is consistent with current estimates of waste package temperatures especially considering that calculated temperature profiles peak near 300°C in the worst cases with temperature decreasing to much lower values over time (CRWMS M&O 1999f) rather than remaining at 300°C for the 10,000-year lifetime.

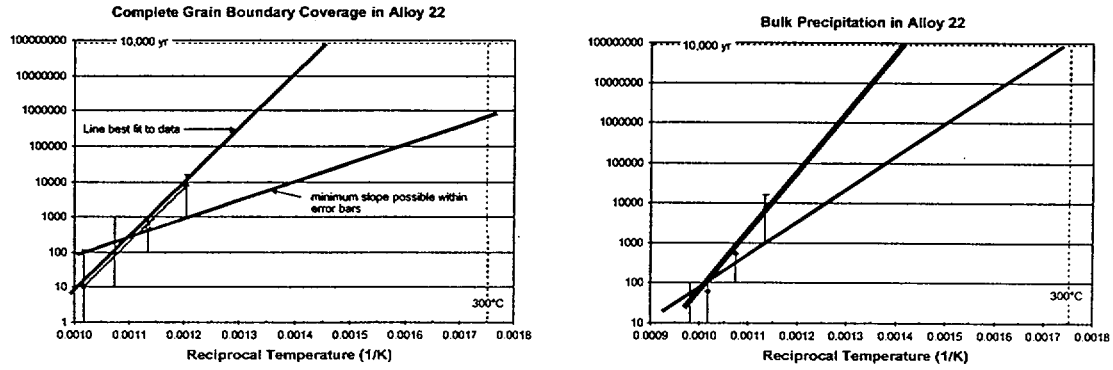


Figure 98. Graphical extrapolation of the curves in Figure 97 to repository-relevant temperatures. The temperatures in Table 2 were converted to Kelvin (K) by adding 273 and the reciprocals were taken in Microsoft Excel. These calculations were verified by hand before plotting. [DTN # LL000116005924.114]

Also plotted in Figure 98 are lines with the minimum possible slope allowed by the error bars on the data. Even accounting for the rather large uncertainty, bulk precipitation does not appear likely in 10,000 yr at 300°C. Grain boundary precipitation might, however, occur (left graph in Figure 98). Therefore, a good bounding argument would be to assume that precipitation covers the grain boundaries. As can be seen in the TTT diagram of Figure 96, laboratory samples aged for more than 100 hr at 700°C would produce a microstructure with precipitation covering the grain boundaries. Corrosion data obtained from alloy 22 base metal samples aged in such a way would represent a worse case situation from a phase stability point of view.

### 6.2.1 Basis for Confidence that Bounding Case is Conservative

As a measure of the reasonableness of the data plotted in Figure 97, the activation energy can be calculated. The slopes of the lines in Figure 97 (after accounting for the log(e) factor) are equal to C2/n in Eq. 3. If these slopes are averaged and n is assumed to be equal to one, which is a reasonable value for n (Christian 1981, p. 542, Table IX), then the activation energy is 280 kJ/mol (68 kcal/mol using a gas constant R=1.987 cal/mol·K). This is fairly close to the value of 62 kcal/mol obtained by Hodge (1973, p. 378 ¶ 1) for precipitation in alloy C-276. This value is also fairly typical for diffusion of relevant elements in nickel (Ni) (Brandes and Brook 1992, Ch. 13, p. 13-23). For example, the activation energy for diffusion of chromium in Ni is 272.6 kJ/mol, that of iron is 253 - 270 kJ/mol, and that of tungsten in Ni is 299 - 308 kJ/mol. These reasonable slopes are for the curves that best fit the actual data in Figure 98. The curves with the minimum slopes allowed by the large error bars are therefore likely to be conservative.

These reasonable slopes are for the curves that best fit the actual data in Figure 98. The curves with the minimum slopes allowed by the large error bars are therefore likely to be conservative.

No bulk precipitation was observed in the sample aged 16,000 hours at 593°C. This time at 593°C corresponds to a point that, although below the curve fit through the actual data, is above the line with the minimum slope used for the bounding argument in the right hand figure of Figure 98. At 649°C, grain boundary precipitation starts at about one hour, but bulk precipitation is not seen until after 1000 hours. At 593°C, grain boundary precipitation starts before 10 hours, but no bulk precipitation is seen even after 16,000 hours. These observations suggest that bulk precipitation does not occur until over three orders of magnitude in time after grain boundary precipitation starts. At 427°C, no intermetallic precipitation is seen even after 40,000 hours. Based on the above argument, it is unlikely that bulk precipitation would occur at 427°C before 10,000 years which is well above the bounding curve for bulk precipitation in Figure 98. Therefore, the available data for aging temperatures where no bulk precipitation is observed indicate that the bounding argument is conservative.

The data in Figure 97 represent the precipitation kinetics during an isothermal anneal. The repository temperature is not expected to remain constant. Instead, it will peak at some temperature and slowly decrease over time (CRWMS M&O 1999f). Therefore, the actual waste package temperatures are likely to be well below 300°C for a significant fraction of their required service life. Since the rate of these intermetallic precipitation reactions is strongly dependent on temperature and since it decreases with temperature, the above bounding case where temperature is assumed to be constant at its peak value is conservative.

### 6.2.2 Limitations on the Bounding Argument and the Need for Quantitative Data

The microstructural observations used to determine the time at certain stages of precipitation are subjective. Also, the time between these observations is large. Both of these factors lead to large uncertainties in time. Extrapolation of this type of data over several orders of magnitude carries with it some risk. Small changes in slope when extrapolated over several orders of magnitude can have significant effects on the predicted outcome. Quantitative data such as volume fraction measurements taken as a function of aging time and temperature are needed. These types of measurements can be made objectively and can be curve fitted which would lessen the error associated with the times in Table 2 and Figure 97 even if the time between microstructural observations were not decreased. Also, a more quantitative model based on Eq. 1 that can be integrated over a variable temperature profile would provide more accurate results.

Cold work, which might be present in or around welds or might result from rock fall, is known to accelerate precipitation reactions. The effect of cold work on the kinetics of these transformations has not yet been investigated. Also, the effects of compositional variation (heat-to-heat variability) have not been investigated as stated in Section 5.3.

The samples examined to create the data in Table 2 from which this bounding argument is made are not confirmed. All data (DTN #LL000115905924.113 and DTN # LL000116005924.114) associated with this bounding argument are TBV (TBV-4159 and TBV-4158). Some of these samples have already been found acceptable by the Office of Quality Assurance pending

chemical analysis by a qualified vendor. Therefore, it is unlikely that a significant number of these samples will be designated as unqualified. If some samples cannot be qualified, then the bounding argument will be reevaluated using only qualified samples. It is likely that the uncertainty in the bounding argument will increase if some of the available samples cannot be used. An aging study has been initiated. Qualified data from this study will be available for future revisions of this report.

## 6.3 EFFECT OF INTERMETALLIC AND CARBIDE PRECIPITATION ON MECHANICAL PROPERTIES OF ALLOY 22 BASE METAL

Intermetallic and carbide phases, especially those forming at grain boundaries, are known to embrittle Ni-Cr-Mo alloys such as Alloy 22 (Matthews 1976, p. 219). Mechanical property data of aged samples that would allow the determination of the effect of any precipitation that is predicted to form on the mechanical properties are not available at this time.

## 6.4 KINETICS OF INTERMETALLIC PRECIPITATION IN ALLOY 22 WELDS

The HAZ of a weld is the region of the base metal near the weld that is subjected to a significant thermal pulse during the welding process. Intermetallic precipitation kinetics in the HAZ will be similar to that in the base metal, discussed in Section 6.2, but actual rates of precipitation may be different. The high temperatures, approaching the melting point, seen in the HAZ of welds might trigger nucleation of intermetallic and/or carbide precipitates. If nuclei are already present, precipitation will proceed much faster than in the base metal where they are not present.

Very few precipitates have been observed in the HAZ of weld samples thus far (Figures 70 and 74), but only two weld samples have been examined: one in the as-welded condition and one after aging at 427°C for 40,000 hr. These precipitates may simply be carbides that were present in the mill-annealed (i.e., as-received) condition. Carbides are known to be present in Ni-base alloys similar to Alloy 22, but they are usually within the grains and are generally called primary carbides to distinguish them from other secondary phases that form, often on grain boundaries, after an aging treatment (Tawancy et al. 1983, p. 40, ¶ 3). The particle in Figure 74 was not identified but could be one of these primary carbides.

Welding causes melting of the alloy and the development of an as-cast structure upon cooling. The dendritic structure typical of welds can be seen in Figures 64 through 69. As an Alloy 22 weld solidifies, Mo and Cr are rejected from the solid phase causing their concentration to increase in the liquid. Therefore, the interdendritic regions, which are the last solid to form in a weld, tend to have high concentrations of these elements relative to typical values for Alloy 22 (Cieslak et al. 1986, p. 2039, Figure 7). Because formation of the intermetallic phases, which are also enriched in Mo and/or Cr, is favored by higher Mo and Cr concentrations, these phases are present in the interdendritic regions of Alloy 22 welds.. Intermetallic particles can be seen in Figure 66. Primarily P phase is seen in the as-welded condition of Alloy 22 welds, but $\sigma$ and $\mu$ phase are also seen (Cieslak et al. 1986, p. 2041, ¶ 2). Only one particle was seen in TEM in an Alloy 22 weld (Figures 71 through 73); this particle could be indexed as either P or $\sigma$ phase.

Because precipitates are present in Alloy 22 welds from the beginning, kinetics of precipitation is not an issue as it is in the base metal and HAZ. Instead, it must be verified that the weld's mechanical and corrosion properties are not degraded by this precipitation. Whether these precipitates are stable and grow or unstable and dissolve with aging at repository-relevant temperatures must also be determined.

## 6.5 KINETICS OF LRO REACTIONS IN ALLOY 22

The kinetics of LRO are treated in a manner similar to that discussed for intermetallic and carbide precipitation in Section 6.2. However, very little kinetic data exists for LRO in alloy 22. Thus far, LRO has been observed in five samples. A very fine dispersion of ordered domains was seen after aging for 30,000 and 40,000 hr at 427°C in Alloy 22 base metal (Figures 78 through 80) and in a weld similarly aged (Figures 81 through 86). The ordering in these cases is so fine that it would be difficult to measure the volume fraction of the ordered domains. LRO was also observed in Alloy 22 base metal aged at 593°C for 16,000 hr (Figures 75 through 77) and at 538 and 593°C for 1000 hr (Figures 87 through 95). The volume fraction of ordered domains has not been measured in these samples. Alloy 22 base metal samples aged for 40,000 hr at 260 and 343°C and for 1000 hr at 482°C were also examined in TEM, but no LRO was observed. These observations are summarized in Figure 96.

The kinetics of ordering in Alloy 22 can be estimated by looking at the earliest times where LRO is seen. From the TTT diagram in Figure 96, the earliest times where LRO is observed are 1000 hours at 538°C and 30,000 hours at 427°C. These two points are plotted in Figure 99. This graph was generated and the data curve fit with an exponential function in Microsoft Excel. Extrapolation of this curve fit in Figure 99, in a manner that was done for intermetallic precipitation in Figure 98, indicates that LRO may occur in less than 10,000 yr at 300°C. Taking the natural logarithm of both sides of this equation yields:

$$\ln(t) = \ln(5x10^{-7}) + \frac{17395}{T} \qquad \text{(Eq. 4)}$$

Solving for temperature T:

$$T = \frac{17395}{\ln(t) - \ln(5x10^{-7})} \qquad \text{(Eq. 5)}$$

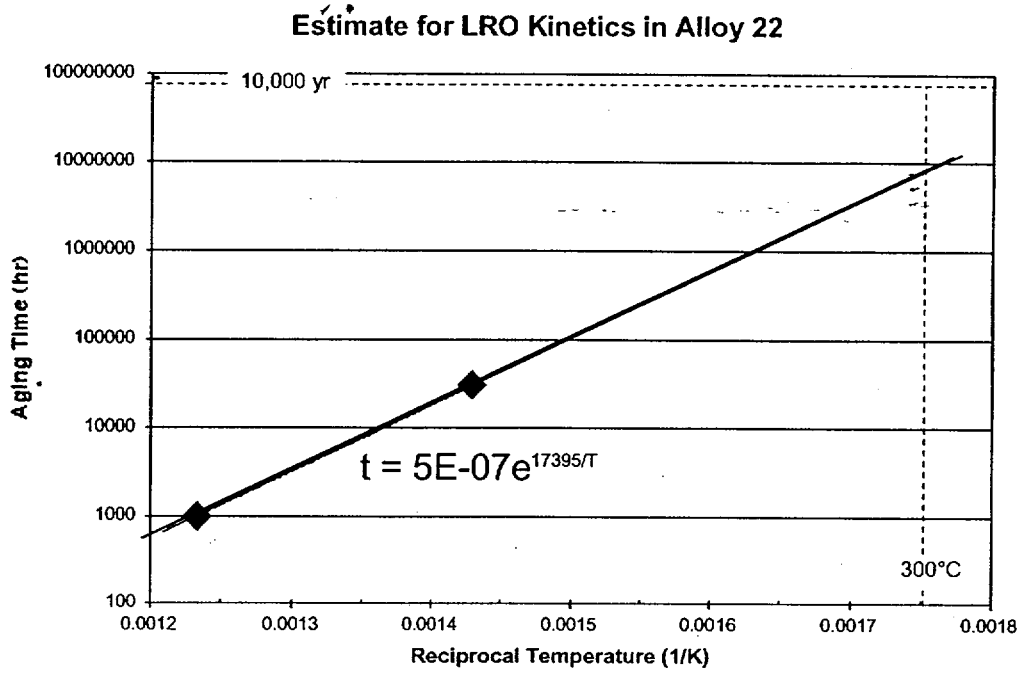


Figure 99. Graphical extrapolation of the limited kinetic data for LRO in Alloy 22 base metal. The points in this graph correspond to aging at 538°C for 1000 hours and at 427°C for 30,000 hours. These temperatures were converted to Kelvin (K) by adding 273 and the reciprocals were taken in Microsoft Excel. These calculations were verified by hand before plotting. [DTN # LL000116005924.114]

### 6.5.1 Basis for Confidence that Bounding Case is Conservative

The points in Figure 99 were chosen because the amount of ordering observed after aging under those conditions was relatively small. The amount of ordering in the sample aged at 538°C (the point at the higher temperature on the left in Figure 99) is greater than that in the sample aged at 427°C. To get the same amount of ordering at 427°C, a longer time would be needed (i.e. the point on the right in Figure 99 would shift up). This shift would increase the slope of the curve which would result in a higher extrapolated time at 300°C. There are not a lot of corrosion or mechanical property data for samples aged at relatively low temperatures, but available data do not indicate that the amount of ordering present after aging at 538°C for 1000 hours significantly affects the properties of alloy 22 base metal (Rebak et al. 2000, Tables 2 and 3).

Other published data (Rebak and Koon 1998, Figure 9) indicate that the curve in Figure 99 is conservative. According to Rebak and Koon (1998, Figure 9) ordering in C-276 occurs after 550 hours at 500°C. This point falls well below the curve in Figure 99. According to the same reference, ordering begins at 427°C at nearly the same time as in Figure 99. Thus, the slope of the line drawn through this data would be considerably greater (and thus, less conservative) than that used for the above bounding argument.

The data in Figure 99 represent the precipitation kinetics during an isothermal anneal. The repository temperature is not expected to remain constant. Instead, it will peak at some

the line drawn through this data would be considerably greater (and thus, less conservative) than that used for the above bounding argument.

The data in Figure 99 represent the precipitation kinetics during an isothermal anneal. The repository temperature is not expected to remain constant. Instead, it will peak at some temperature and slowly decrease over time (CRWMS M&O 1999f). Therefore, the actual waste package temperatures are likely to be well below 300°C for a significant fraction of their required service life. Since the rate of these intermetallic precipitation reactions is strongly dependent on temperature and since it decreases with temperature, the above bounding case where temperature is assumed to be constant at its peak value is conservative.

### 6.5.2 Limitations on the Bounding Argument and the Need for Quantitative Data

The two data points plotted in Figure 99 are tentative. Samples aged for shorter times at 427 and 538°C have not been examined in TEM. The curve in Figure 99 may shift down (to shorter times) after more data are collected. Unless the shift down is also accompanied by an increase in slope, the temperature limit for the bounding case would be lower than predicted above.

The extrapolation above is based on two data points which themselves are not certain. As more samples are examined and more quantitative data (e.g. volume fraction measurements) obtained, the curve fit to the data could easily change. Because small changes in the slope of a line such as that in Figure 99 can produce large changes in predictions obtained by extrapolating out over several orders of magnitude, it is somewhat risky to extrapolate over three orders of magnitude in time from only two data points. It is crucial that more data for LRO be obtained.

Cold work, which might be present in or around welds or might result from rock fall, is known to accelerate precipitation reactions. The effect of cold work on the kinetics of LRO has not yet been investigated. Also, the effects of compositional variation (heat-to-heat variability) have not been investigated as stated in Section 5.3.

The samples examined to create the data plotted in Figure 99 from which this bounding argument is made are not confirmed. All data (DTN #LL000115905924.113 and DTN # LL000116005924.114) associated with this bounding argument are TBV (TBV-4159 and TBV-4158). Some of these samples have already been found acceptable by the Office of Quality Assurance pending chemical analysis by a qualified vendor. Therefore, it is unlikely that a significant number of these samples will be designated as unqualified. If some samples cannot be qualified, then the bounding argument will be reevaluated using only qualified samples. It is likely that the uncertainty in the bounding argument will increase if some of the available samples cannot be used. An aging study has been initiated. Qualified data from this study will be available for future revisions of this report.

INTENTIONALLY LEFT BLANK

# 7. CONCLUSIONS

After aging for 16,000 hr at 593°C, P phase was found at Alloy 22 grain boundaries. At higher temperatures (as much as 760°C for the same aging time), both μ and P phase formed on grain boundaries and within the grains. Grain boundary carbides also form at 593°C and higher, but the amount of carbide is small compared to the μ and P phases. A small amount of σ phase forms in Alloy 22 after 16,000 hr at 704 and 760°C. LRO was seen after aging for 1000 hr at 538 and 593°C and for 30,000 hr at 427°C, but ordering most likely begins at shorter times. More work must be done in phase identification. Samples aged at times less than 16,000 hr must be examined so that the phase evolution during aging can be determined. Phase extraction and x-ray diffraction would make phase identification and quantification of the relative amounts of each phase easier.

The times at which various stages of intermetallic precipitation occur in Alloy 22 base metal displayed an exponential (Arrhenius-type) temperature dependence. The activation energy was determined to be 280 kJ/mol. It is important to note that while this data is linear as plotted, it is preliminary and should not be extrapolated to determine the precipitation times at the lower repository temperatures. The method used to obtain the data in Table 2 is considerably subjective, and the uncertainty in time is rather large due to the coarse time intervals examined. Because the Arrhenius plot of Figure 97 is a semilog plot, small changes in the slopes of the lines drawn for the different stages of precipitation would project to a considerable variation in times at the repository relevant temperatures. Looking at lines with a minimum slope allowed within the error bars, it was concluded that alloy 22 base metal samples with grain boundaries completely covered by intermetallic precipitation such as that which would be obtained by aging at 700°C for more than 100 hr would represent a bounding microstructure representative of repository conditions.

A more quantitative model based on precipitate volume fraction measurements that can be integrated over a variable temperature profile must be developed before a quantitative prediction of the phase stability of Alloy 22 base metal under repository conditions can be made. In addition, the effect of intermetallic and carbide precipitation on Alloy 22 properties must be determined.

Precipitation kinetics in weld heat-affected zones, as well as in the base metal, must be studied because the thermal pulse given the HAZ during the welding process may alter nucleation of intermetallics and, therefore, the precipitation kinetics. Intermetallic and carbide precipitates form in Alloy 22 welds during the welding process. It must be verified that these phases do not have a detrimental effect on the relevant weld properties. The effect of aging on the precipitate volume fraction and average size and on weld properties must also be determined.

Long-range order has been observed in a sample aged at 593°C for 1000 hr and in a sample aged at 427°C for 30,000 hr. These observations are not sufficient to evaluate the possibility of LRO occurring in Alloy 22 under repository conditions. Alloy 22 samples must be aged for various times at temperatures less than approximately 600°C. The volume fraction of ordered domains

in these aged samples must be measured and fit to nucleation and growth theory. Using only the above two data points, a bounding argument was made, and it was concluded that LRO would probably not occur in fully annealed alloy 22 base metal provided the temperature was kept below about 260°C. More work is necessary to confirm this conclusion.

The bounding arguments presented in this report are based on a very limited amount of data. Also, the effects of heat-to-heat variability and cold work on the precipitation kinetics have not been accounted for. It is intended that more data be generated and incorporated into future revisions of this report.

The Input data (DTN #LL000115905924.113 and DTN #LL000116005924.114) have TBV-4159 and TBV-4158 associated with them which is due to the source of the samples. These samples are currently being verified. It is unlikely that none of the samples will be qualified leaving the model without input data. There should be enough samples qualified to support the bounding case of this model as it stands now, although if some samples cannot be qualified, then confidence in the bounding arguments made will likely decrease. More data is currently being generated that can be used in future versions of this model.

The experimental analyses previously discussed assume that the kinetics of formation of the μ and P phases are similar and that the amount of carbide and σ phase present is too small to affect the measured rates of precipitation (TBV-3045). This assumption will be verified through the direct measurement of the amounts of each phase forming as a function of aging time and temperature. Should this assumption prove to be invalid, the analyses for intermetallic and carbide precipitation will be modified to account for the different phases precipitating. Minor compositional changes in Alloy 22 are also assumed to have little or no effect on the rate of precipitation (TBV-3047). Heat-to-heat variability studies will have to be done to verify this assumption. Should this assumption turn out to be invalid, then the acceptable composition limits can be made tighter than that permitted by ASTM B 575 (ASTM B 575-94 1994, p. 410, Table 1).

The experimental analyses previously discussed also assume that the precipitation mechanism operating at the high temperatures studied also operates at the lower temperatures expected in the potential repository and that the phases seen at the higher temperatures are stable at the lower temperatures (TBV-3046). Theoretical modeling, currently in the planning stages, will be done to verify these assumptions and to aid the extrapolation of experimental data to the long times associated with the WP container lifetime.

This AMR summarizes work in progress aimed at addressing the phase stability and mechanical property portions of the Issues Resolution Status Report (NRC 1999) Subissue 2. Insufficient data exist for a quantitative evaluation of the potential for materials instability in Alloy 22, but bounding cases have been made for intermetallic precipitation and LRO in the base metal. Further work is planned for quantifying the kinetics of these transformations in Alloy 22. Corrosion data in relevant environments has been obtained for aged samples, and these data are discussed in the AMR covering corrosion of the WPOB (CRWMS M&O 2000b). Samples are

currently being aged for the determination of the effect of aging on the mechanical properties, but these data do not yet exist. The effects of chemical composition and fabrication processes such as thermal treatments and cold work have not yet been addressed.

INTENTIONALLY LEFT BLANK

# 8. INPUTS AND REFERENCES


ASTM B 575-94. 1994. *Standard Specification for Low-Carbon Nickel-Molybdenum-Chromium, Low-Carbon Nickel-Chromium-Molybdenum, and Low-Carbon Nickel-Chromium-Molybdenum-Tungsten Alloy Plate, Sheet, and Strip.* Philadelphia, Pennsylvania: American Society for Testing and Materials. TIC: 237683.

Brandes, E.A. and Brook, G.B., eds. 1992. *Smithells Metals Reference Book.* 7th Edition. Oxford, United Kingdom: Butterworth-Heinemann. TIC: 246620.

Christian, J.W. 1981. "Equilibrium and General Kinetic Theory." Part I of *The Theory of Transformations in Metals and Alloys.* 2nd Edition. Pages 19, 438, 542. New York, New York: Pergamon Press. TIC: 245378.

Cieslak, M.J.; Headley, T.J.; and Romig, A.D., Jr. 1986. "The Welding Metallurgy of Hastelloy Alloys C-4, C-22, and C-276." *Metallurgical and Materials Transactions A, 17A,* (11), 2035-2047. Warrendale, Pennsylvania: Metallurgical Society of AIME and American Society for Metals. TIC: 233952.

CRWMS(Civilian Radioactive Waste Management System) M&O (Management and Operating Contractor) 1999a. *Aging and Phase Stability of Waste Package Outer Barrier.* Work Direction and Planning Document. Las Vegas, Nevada: CRWMS M&O. ACC: MOL.19990708.0233.

CRWMS M&O 1999b. *License Application Design Selection Report.* B00000000-01717-4600-00123 REV 01 ICN 01. Las Vegas, Nevada: CRWMS M&O. ACC: MOL.19990908.0319.

CRWMS M&O 1999c. *Classification of the MGR Uncanistered Spent Nuclear Fuel Disposal Container System.* ANL-UDC-SE-000001 REV 00. Las Vegas, Nevada: CRWMS M&O. ACC: MOL.19990928.0216.

CRWMS M&O 1999d. *11012113PM Waste Package Testing and Data Generation (All Except M6, M7, and MB).* Activity Evaluation, September 21, 1999. Las Vegas, Nevada: CRWMS M&O. ACC: MOL.19991012.0218.

CRWMS M&O 1999e. *Uncanistered Spent Nuclear Fuel Disposal Container System Description Document.* SDD-UDC-SE-000001 REV 00. Las Vegas, Nevada: CRWMS M&O. ACC: MOL. 19991217.0512.

CRWMS M&O 1999f. *3-D Repository Scale Thermal Evaluations for EDA Selection.* BBA000000-01717-0210-00061 REV00. Las Vegas, Nevada: CRWMS M&O. ACC: MOL. 19990618.0230.

CRWMS M&O 2000a. *Repository Safety Strategy: Plan to Prepare the Postclosure Safety Case to Support Yucca Mountain Site Recommendation and Licensing Considerations.* TDR-WIS-RL-000001, REV 03. Las Vegas, Nevada: CRWMS M&O. ACC: MOL.20000119.0189.

CRWMS M&O 2000b. *General Corrosion and Localized Corrosion of Waste Package Outer Barrier.* ANL-EBS-MD-000003 REV 00. Las Vegas, Nevada: CRWMS M&O. ACC: MOL.20000202.0172.

DOE (U.S. Department of Energy) 2000. *Quality Assurance Requirements and Description.* DOE/RW-0333P, REV 9. Washington, D.C.: U.S. Department of Energy, Office of Civilian Radioactive Waste Management. ACC: MOL.19991028.0012.

Heubner, U.L.; Altpeter, E.; Rockel, M.B.; and Wallis, E. 1989. "Electrochemical Behavior and Its Relation to Composition and Sensitization of NiCrMo Alloys in ASTM G-28 Solution." *Corrosion, 45*, (3), 249-259. Houston, Texas: National Association of Corrosion Engineers. TIC: 240169.

Hodge, F.G. 1973. "Effect of Aging on the Anodic Behavior of Ni-Cr-Mo Alloys." *Corrosion, 29*, (10), 375-383. Houston, Texas: National Association of Corrosion Engineers. TIC: 240167.

Leonard, R.B. 1969. "Thermal Stability of Hastelloy Alloy C-276." *Corrosion, 25*, (5), 222-228. Houston, Texas: National Association of Corrosion Engineers. TIC: 240456.

LL000115905924.113. Transmission Electron Microscopy (TEM), Scanning Electron Microscopy (SEM), and Optical Microscopy Micrographs of Aged Alloy 22 Samples. Submittal date: 2/4/2000.

LL000116005924.114. Analysis of Transmission Electron Microscopy (TEM) and Scanning Electron Microscopy (SEM). Submittal date: 2/23/2000.

Matthews, S.J. 1976. "Thermal Stability of Solid Solution Strengthened High Performance Alloys." *Superalloys: Metallurgy and Manufacture. Proceedings of the Third International Symposium, September 12-15, 1976, Seven Springs, Pennsylvania.* 215-226. Baton Rouge, Louisiana: Claitor's Publishing Division. TIC: 245098.

NRC (U.S. Nuclear Regulatory Commission) 1999. *Issue Resolution Status Report Key Technical Issue: Container Life and Source Term.* Rev. 2. Washington, D.C.: U.S Nuclear Regulatory Commission. TIC: 245538.

Raghavan, M.; Berkowitz, B.J.; and Scanlon, J.C. 1982. "Electron Microscopic Analysis of Heterogeneous Precipitates in Hastelloy C-276." *Metallurgical and Materials Transactions A, 13A*, 979-984. Warrendale, Pennsylvania: Metallurgical Society of AIME and American Society for Metals. TIC: 240058.

Rebak, R.B. and Koon, N.E. 1998. "Localized Corrosion Resistance of High Nickel Alloys As Candidate Materials for Nuclear Waste Repository. Effect of Alloy and Weldment Aging at 427°C For Up To 40,000 H. Paper No. 153." *Corrosion98.* Houston, Texas: National Association of Corrosion Engineers. TIC: 245068.

Rebak, R.B.; Koon, N.E.; Dillman, J.R.; Crook, P.; and Summers, T.S.E. 2000. "Influence of Aging on Microstructure, Mechanical Properties, and Corrosion Resistance of a Ni-22Cr-13Mo-3W Alloy." *Corrosion 2000.* Pages 00181/1-00181/16. Houston, Texas: National Association of Corrosion Engineers. TIC: 247157.

Summers, T.S.E.; Wall, M.A.; Kumar, M.; Matthews, S.J.; and Rebak R.B. 1999. "Phase Stability and Mechanical Properties of C-22 Alloy Aged in the Temperature Range 590 to 760°C for 16,000 Hours." *Scientific Basis for Nuclear Waste Management XXII, Symposium held November 30-December 4, 1998, Boston, Massachusetts, U.S.A.* Wronkiewicz, D.J. and Lee, J.H., eds. *556*, 919-926. Warrendale, Pennsylvania: Materials Research Society. TIC: 247156.

Tawancy, H.M.; Herchenroeder, R.B.; and Asphahani, A.I. 1983. "High Performance Ni-Cr-Mo-W Alloys." *Journal of Metals*, *35*, (6), 37 - 43. Warrendale, Pennsylvania: The Minerals, Metals & Materials Society. TIC: 245100.